THE UNIVERSITY OF ADELAIDE
AUSTRALIA

Guiding Light in Low-Index Media via Multilayer Waveguides

by

Kristopher J. Rowland

Supervisors:
Prof. Tanya M. Monro
Dr Shahraam Afshar Vahid

A thesis submitted in fulfillment of the degree of Doctor of Philosophy

in the
Faculty of Sciences
School of Chemistry & Physics

December 2010

Appendix A

Electromagnetic Wave Propagation Theory

The majority of the content in this appendix is not original to this Thesis, but has been re-derived and expressed in a consistent nomenclature for completeness and ease of discussion in the body of the work. Those parts that *are* original are highlighted as such below. The theoretical and numerical results derived in the body of this thesis, based on the theory below, are to the best of my knowledge all original by the hand of the author.

A.1 Wave Equations

This review of the electromagnetic wave equations and their use is adopted from various texts [14, 34, 146, 178, 179, 211, 212], brought together here in a manner consistent with the remainder of this thesis and as a means of explaining the techniques used.

A.1.1 Maxwell's Equations

First, begin by considering Maxwell's equations within an arbitrary material:

$$\nabla \times \mathbf{E} = -\frac{\partial}{\partial t}\mathbf{B}, \tag{A.1}$$

$$\nabla \times \mathbf{H} = \frac{\partial}{\partial t}\mathbf{D} + \mathbf{J}, \tag{A.2}$$

$$\nabla \cdot \mathbf{D} = \rho, \tag{A.3}$$

$$\nabla \cdot \mathbf{B} = 0, \tag{A.4}$$

where $\mathbf{D} = \epsilon\mathbf{E}$ (called the electric displacement) and $\mathbf{H} = \mathbf{B}/\mu$ are the *constitutive relations* relating the $\mathbf{E}$ and $\mathbf{B}$ fields to the 'auxiliary' [212] $\mathbf{D}$ and $\mathbf{H}$ fields, respectively.

ρ is the free charge density and $\mathbf{J}$ is the free current within the material. In general one can write the permittivity and permeability as the product of their vacuum and relative values as $\epsilon \equiv \epsilon(\mathbf{r}) = \epsilon_r(\mathbf{r})\epsilon_0$ and $\mu \equiv \mu(\mathbf{r}) = \mu_r(\mathbf{r})\mu_0$, respectively.

While metals in waveguides used to be only practical for the microwave regime, there is a significant resurgence of interest in metal waveguides in the area of *plasmonics.* Nonetheless, here only *dielectric* materials are considered: non-magnetic materials with zero charge density; such as glass or polymer. Thus we can set relative permeability $\mu_r(\mathbf{r}) = 1$ and charge density $\rho(\mathbf{r}) = 0$. This simplifies things considerably and is used below in the derivation of the wave equations for propagation in dielectric media.

A.1.2 Time-Dependent Wave Equations in Simple Media

Wave equations for arbitrary electric and magnetic fields in *homogeneous* dielectric media will now be derived.

Taking the curl of Eq. A.1 and substituting in Eq. A.2 with $\mathbf{J} = 0$ (no currents in the dielectric):

$$\begin{aligned} \nabla \times (\nabla \times \mathbf{E}) &= -\mu \frac{\partial}{\partial t} \nabla \times \mathbf{H} \\ \text{(by Eq. A.2)} &= -\mu\epsilon \frac{\partial^2 \mathbf{E}}{\partial t^2}. \end{aligned} \tag{A.5}$$

Since only homogeneous media are being considered here, the permittivity ϵ is assumed constant over all space. Eq. A.3 then implies $\nabla \cdot \mathbf{E} = 0$. Using this together with the identity Eq. B.1, Eq. A.5 then implies:

$$\nabla^2 \mathbf{E} - \mu\epsilon \frac{\partial^2 \mathbf{E}}{\partial t^2} = 0 \tag{A.6}$$

Similarly, taking the curl of Eq. A.2 (again setting $\mathbf{J} = 0$), and substituting in Eq. A.1:

$$\begin{aligned} \nabla \times (\nabla \times \mathbf{H}) &= \epsilon \frac{\partial}{\partial t} \nabla \times \mathbf{E} \\ \text{(by Eq. A.1)} &= -\mu\epsilon \frac{\partial^2 \mathbf{H}}{\partial t^2}. \end{aligned}$$

Since only homogeneous media are being considered here, the permeability μ is assumed constant over all space. Eq. A.4 then implies $\nabla \cdot \mathbf{H} = 0$. Using this together with the identity Eq. B.1, Eq. A.7 then implies:

$$\nabla^2 \mathbf{H} - \mu\epsilon \frac{\partial^2 \mathbf{H}}{\partial t^2} = 0 \tag{A.7}$$

The solutions of Eqs. A.6 and A.7, for propagation in the direction of a unit vector $\hat{\mathbf{k}}$, are of the form (generalised from [178]):

$$\mathbf{E} = \mathbf{E}_0 g(t \pm \mathbf{r} \cdot \hat{\mathbf{k}}/v), \tag{A.8}$$

$$\mathbf{H} = \mathbf{H}_0 g(t \pm \mathbf{r} \cdot \hat{\mathbf{k}}/v), \tag{A.9}$$

respectively, where g is any well-defined function and v is the wave velocity[1]. Taking the positive value in the argument of g corresponds to wave propagation in the negative $\hat{\mathbf{k}}$ direction, while taking the negative value corresponds to propagation in the positive $\hat{\mathbf{k}}$ direction (assuming $v > 0$). By substituting Eqs. A.8 and A.9 back into Eqs. A.8 and A.9, respectively, the wave velocity is found to be $v = \frac{1}{\sqrt{\mu\epsilon}} = \frac{c}{\sqrt{\mu_r\epsilon_r}}$ [14, 178].

An important special case of the solutions Eqs. A.8 and A.9 is when $g(t) = e^{i\omega t}$ (the real part of g is taken when the physical fields are desired, as discussed in detail in the next section). Assuming propagation in the z-direction, the waveform then becomes $g(t \pm z/v) = e^{i\omega(t \pm z/v)} = e^{i(\omega t \pm \beta z)}$, where the *phase constant* is defined as $\beta = \omega/v$: the phase shift per unit length along the propagation direction. Since the wave is sinusoidal, it only has a singular frequency component, seeing v referred to as the *phase velocity* [178].

A.1.3 Time Harmonic Wave Equations in Inhomogeneous Media

Here *inhomogeneous* dielectric media are considered but the time-dependence is dropped. First, consider a time-harmonic (single angular frequency, ω) wave,

$$\mathbf{A}(\mathbf{r}, t) = \mathrm{Re}\{\overline{\mathbf{A}}(\mathbf{r}) \exp(-i\omega t)\}, \tag{A.10}$$

where $\mathbf{A}$ represents any of the fields $\mathbf{E}$, $\mathbf{B}$, $\mathbf{D}$, or $\mathbf{H}$. $\overline{\mathbf{A}}$ is the *complex* amplitude of the wave's phasors. Here we shall relabel $\overline{\mathbf{A}}(\mathbf{r}) \to \mathbf{A}(\mathbf{r})$, but it should still be understood that we take the *real* part when finally evaluating the fields.

Note that the time-dependent oscillatory term $\exp(-i\omega t)$ is the complex conjugate of the $\exp(i\omega t)$ term typically used throughout the other sections of this thesis. Since the real part of the fields are to be eventually taken, as per Eq. A.10, the choice is somewhat arbitrary. The $\exp(-i\omega t)$ convention is adopted here in order to stay relatively close to the well-known treatments of Joannopoulos et al. [34] and Snyder and Love [146], which are combined here to an extent. Section A.1.4 also uses this sign convention. The conventions as used in each section do not affect the results presented throughout this thesis.

[1] This can be readily verified by substituting the solutions back into Eqs. A.6 and A.7

Substitute Eq. A.10 (for **E**, **H**, **D**, and **B**) into Eq. A.1 and Eq. A.2 and using our dielectric assumptions that $\mu_r(\mathbf{r}) = 1$ and $\rho(\mathbf{r}) = 0$:

$$\nabla \times \mathbf{E} = i\omega\mathbf{B} = i\omega\mu_0\mathbf{H}, \tag{A.11}$$

$$\nabla \times \mathbf{H} = -i\omega\mathbf{D} = -i\omega\epsilon\mathbf{E}, \tag{A.12}$$

$$\nabla \cdot \mathbf{H} = 0, \tag{A.13}$$

$$\nabla \cdot (\epsilon_{\mathrm{r}}\mathbf{E}) = 0, \tag{A.14}$$

These are the chromatic wave equations in a dielectric medium of arbitrary relative permittivity $\epsilon_r \equiv \epsilon_r(\mathbf{r}) = \epsilon(\mathbf{r})/\epsilon_0$. Recall that in a dielectric medium, the relative permittivity is related to the refractive index n by $\epsilon_{\mathrm{r}} = n^2$.

The **E** and **H** fields can be decoupled into individual wave equations as follows. We will begin with the magnetic field. Divide each side of Eq. A.12 by $\epsilon_r \equiv \epsilon_r(\mathbf{r})$ and then take the curl [34]:

$$\nabla \times \left(\frac{1}{\epsilon_r}\nabla \times \mathbf{H}\right) = -i\omega\epsilon_0\nabla \times \mathbf{E}. \tag{A.15}$$

Then substitute in the expression for $\nabla \times \mathbf{E}$ from Eq. A.11:

$$\nabla \times \left(\frac{1}{\epsilon_r}\nabla \times \mathbf{H}\right) = \left(\frac{\omega}{c}\right)^2 \mathbf{H}, \tag{A.16}$$

This is clearly an eigenvalue equation as it can be re-written in the form $\Theta\mathbf{H} = (\omega/c)^2\mathbf{H}$, where the composite curl functions on the left side are represented by Θ. This is what is often called the "master equation" in photonic crystal analysis (Joannopoulos et al. [34] give a thorough account). Its namesake results from its versatility when used for the analysis of infinitely periodic dielectric structures since the operator Θ is hermitian.

The same can be done for the electric field. Taking the curl of both sides of Eq. A.11:

$$\nabla \times (\nabla \times \mathbf{E}) = i\omega\mu_0\nabla \times \mathbf{H}, \tag{A.17}$$

and then substituting Eq. A.12 into the right hand side:

$$\nabla \times (\nabla \times \mathbf{E}) = \epsilon_r \left(\frac{\omega}{c}\right)^2 \mathbf{E}, \tag{A.18}$$

This form is less useful for photonic crystal analysis since the equivalent eigen-operator to Eq. A.18 is not hermitian [34].

Eqs. A.16 and A.18 can be expanded into more manageable forms by using the vectorial calculus relations of Eqs. B.1 and B.2. Consider first the vectorial wave equation for **H**, Eq. A.16. Using Eq. B.2 then B.1, the left hand side can be written as:

$$\begin{aligned}
\nabla\times\left(\frac{1}{\epsilon_r}\nabla\times\mathbf{H}\right) &= \frac{1}{\epsilon_r}\nabla\times(\nabla\times\mathbf{H})+\left(\nabla\frac{1}{\epsilon_r}\right)\times(\nabla\times\mathbf{H})\\
\text{(by Eq. B.1)} &= \frac{1}{\epsilon_r}\left[\nabla(\nabla\cdot\mathbf{H})-\nabla^2\mathbf{H}\right]+\left(\nabla\frac{1}{\epsilon_r}\right)\times(\nabla\times\mathbf{H})\\
\text{(by Eq. A.13)} &= -\frac{1}{\epsilon_r}\nabla^2\mathbf{H}+\frac{1}{\epsilon_r^2}(\nabla\epsilon_r)\times(\nabla\times\mathbf{H})\\
&= \frac{1}{\epsilon_r}\left[(\nabla\ln\epsilon_r)\times(\nabla\times\mathbf{H})-\nabla^2\mathbf{H}\right].
\end{aligned}$$

Eq. A.16 can thus be written as:

$$\nabla^2\mathbf{H}+(nk)^2\,\mathbf{H}=(\nabla\ln\epsilon_r)\times(\nabla\times\mathbf{H}). \tag{A.19}$$

noting that $\nabla\ln\epsilon_r \to \nabla_\perp\ln\epsilon_r$ when $\partial\epsilon_r/\partial z=0$ as is typically the case for longitudinally invariant waveguides as considered throughout this thesis.

A similar approach is taken for the vectorial wave equation for **E**, Eq. A.18. First, note that Eq. A.14 can be expanded as:

$$\begin{aligned}
\nabla\cdot(\epsilon_{\mathrm{r}}\mathbf{E}) &= \nabla\epsilon_r\cdot\mathbf{E}+\epsilon_r\nabla\cdot\mathbf{E}=0,\\
\Rightarrow\quad \nabla\cdot\mathbf{E} &= -\frac{1}{\epsilon_r}\nabla\epsilon_r\cdot\mathbf{E}\\
&= -\nabla\ln\epsilon_r\cdot\mathbf{E}.
\end{aligned}$$

Using Eq. B.2, the left hand side of A.18 can be written as:

$$\begin{aligned}
\nabla\times(\nabla\times\mathbf{E}) &= -\nabla(\nabla\cdot\mathbf{E})-\nabla^2\mathbf{E}\\
&= -\nabla(\nabla\ln\epsilon_r\cdot\mathbf{E})-\nabla^2\mathbf{E},
\end{aligned}$$

Eq. A.18 can thus be written as:

$$\nabla^2\mathbf{E}+\nabla(\nabla\ln\epsilon_r\cdot\mathbf{E})+(nk)^2\,\mathbf{E}=0. \tag{A.20}$$

While their separability makes the fields possible to solve via an eigen-value analysis, it is at the cost of making the differential equations second-order[2]. Second order differential equations are harder to solve than first order, with many different ways to solve them; from analytical to numerical, depending on the system at hand.

[2]See comment of [212] p. 376.

A.1.4 Wave Equations of a Longitudinally Invariant System

Let the the z axis be aligned with the longitudinal axis of the waveguide. Light propagating within an *infinitely long* waveguide will always lend itself to be represented as a superposition of a set of eigenmodes [146]. When this is the case, these modes may be expressed as both time- *and* longitudinally-harmonic oscillating fields[3]:

$$\mathbf{E}(\mathbf{r}_\perp, z) = \mathbf{E}(\mathbf{r}_\perp) e^{i(\beta z - \omega t)}, \tag{A.21}$$

$$\mathbf{H}(\mathbf{r}_\perp, z) = \mathbf{H}(\mathbf{r}_\perp) e^{i(\beta z - \omega t)}, \tag{A.22}$$

where β is called the *propagation constant* of the wave. It is important to note that when β is complex, $\mathrm{Im}\{\beta\} > 0$ implies the existence of an inherent loss for the given mode, *i.e.*, $\beta \in \mathbb{C} \Rightarrow e^{i(\beta z - \omega t)} = e^{i(\mathrm{Re}\{\beta\} z - \omega t)} e^{-\mathrm{Im}\{\beta\} z}$, where the second exponential factor is an explicit length-dependent exponential decay. From this we can define the *confinement loss* (CL) of a mode. The oscillatory terms are only of concern when calculating the relative power after some propagation distance $\Delta z = z_2 - z_1$ since, for a given modal field distribution, $\mathbf{E}(\mathbf{r}_\perp, z_2) = \mathbf{E}(\mathbf{r}_\perp, z_1)$. Explicitly, the relative power of the propagated to the initial field is calculated as:

$$\begin{aligned} \Delta P &= \frac{|\mathbf{E}(\mathbf{r}_\perp, z_2) e^{i(\mathrm{Re}\{\beta\} z_2 - \omega t_2)} e^{-\mathrm{Im}\{\beta\} z_2}|^2}{|\mathbf{E}(\mathbf{r}_\perp, z_1) e^{i(\mathrm{Re}\{\beta\} z_1 - \omega t_1)} e^{-\mathrm{Im}\{\beta\} z_1}|^2} \\ (t \in \mathbb{R}) \quad &= \frac{|e^{-\mathrm{Im}\{\beta\} z_2}|^2}{|e^{-\mathrm{Im}\{\beta\} z_1}|^2} \\ &= e^{-2\mathrm{Im}\{\beta\} \Delta z}; \end{aligned} \tag{A.23}$$

an exponential power decrease with distance. Expressing this as a power loss in dB:

$$\begin{aligned} \Delta P[dB] &= 10 \log_{10}(\Delta P) \\ &= 10 \log_{10}(e^{-2\mathrm{Im}\{\beta\} \Delta z}) \\ &= 20 \mathrm{Im}\{\beta\} \Delta z \log_{10}(e) \\ &= \frac{20 \Delta z}{\ln(10)} \mathrm{Im}\{\beta\}, \end{aligned} \tag{A.24}$$

such that the loss, in dB, per unit length is:

$$\mathrm{CL} = \frac{20}{\ln(10)} \mathrm{Im}\{\beta\}, \tag{A.25}$$

and is called *Confinement Loss.*

[3]It is implicitly implied that the *real* part of these complex oscillatory fields is to be ultimately taken, producing real valued field amplitudes [14, 212].

β foremost describes how the wave amplitude oscillates longitudinally but it is also intimately related to the structure of the mode profiles, as well. In fact, β can be shown to be an explicit function of the modal fields $\mathbf{E}(\mathbf{r}_\perp)$ and $\mathbf{H}(\mathbf{r}_\perp)$ themselves (Ref. [146], Eq. 11-42):

$$\beta_j = \left(\frac{\mu_0}{\epsilon_0}\right)^{\frac{1}{2}} k \frac{\int_{A_\infty} n^2 \mathbf{E}_j \times \mathbf{H}_j^* \cdot \hat{\mathbf{z}} dA}{\int_{A_\infty} n^2 |\mathbf{E}_j|^2 dA} \tag{A.26}$$

Similarly, analytic solutions to the longitudinal wave equations typically produce field expressions that explicitly depend on β.

Also, the confinement loss can be calculated directly from the fields as per the integral form for the imaginary component of the effective mode index [213]:

$$\mathrm{Im}(\tilde{n}) = \frac{1}{2k} \frac{\oint_{\delta A} \mathbf{S} \cdot \hat{\mathbf{n}}\ dl}{\oint_A \mathbf{S} \cdot \hat{\mathbf{z}}\ dA}, \tag{A.27}$$

where $\mathbf{S} = \mathbf{E} \times \mathbf{H}$ is the Poynting vector and $\hat{\mathbf{n}}$ is the unit normal to an arbitrary contour δA which surround an area A.

This expression for the confinement loss reveals something about it's nature: the path integral in the numerator quantifies the power escaping the waveguide; the integral in the denominator quantifies the total axial power flow. Thus, the confinement loss is, true to its name, a measure of the power escaping the waveguide for a given mode.

In this longitudinally invariant regime, the wave Equations A.20 and A.19 simplify, via Eqs. A.21 and A.22, to:

$$\nabla_\perp^2 \mathbf{E} + \nabla\left(\frac{\nabla \epsilon_\mathrm{r}}{\epsilon_\mathrm{r}} \cdot \mathbf{E}\right) + k^2(\epsilon_\mathrm{r} - \tilde{n}^2)\mathbf{E} = 0, \tag{A.28}$$

$$\nabla_\perp^2 \mathbf{H} + \frac{\nabla \epsilon_\mathrm{r}}{\epsilon_\mathrm{r}} \times (\nabla \times \mathbf{H}) + k^2(\epsilon_\mathrm{r} - \tilde{n}^2)\mathbf{H} = 0. \tag{A.29}$$

These are the *full vectorial wave equations* for guided waves in dielectric media and are obviously eigenvalue equations, so their solutions will come in the form of spatial eigenvectors (for $\mathbf{E}(r,\theta)$ and $\mathbf{H}(r,\theta)$) coupled with scalar eigenvalues (the *effective mode index* $\tilde{n} = \beta/k$). One can consider either $\tilde{n}$ or β as the eigenvalue since $k = 2\pi/\lambda$ is a constant of the system. Eigen-solutions of a given system can form a *discrete* or *continuous* set. The modes with discrete eigenvalues are referred to as *bound* or *leaky* modes (see below) which, due to their discrete nature, means that the eigenvalues can be countably labelled and categorised in ways that prove useful when analysing the fibre's behaviour.

An important distinction should be made here between bound, leaky and radiation modes (*e.g.*, Snyder and Love [146]). Bound modes are discrete eigenvalues of a given waveguide system with a purely real propagation constant and hence no inherent confinement loss. Radiation modes are essentially the remainder of the complete set of discrete bound modes of the system and hence are not guided by the waveguide (in the bound sense) and typically form a continuum of states. Leaky modes, like the loss-less bound modes, are also discrete eigenvalues of a system but which exhibit a complex propagation constant and hence an inherent confinement loss. Such leaky modes can be shown to actually be a superposition of radiation modes which subsequently give rise to the leaky mode's quasi-bound nature [214]. This connection between the radiation and leaky modes is very subtle and, as argued and demonstrated by Hu and Menyuck [214], not presented comprehensively in the literature. Their work demonstrates that while this complex connection between the mode types is highly nontrivial, one can nonetheless analyse leaky structures by solving for the complex eigenvalues (as done in this thesis); while their interpretation is mathematically distinct to a radiation mode superposition, their physical interpretation is the same [214]. This is quite a remarkable feature of leaky mode systems and one that seems to be often under-appreciated.

The full vectorial wave equations will not be used directly here, since no continuous gradients appear in the considered refractive index distributions (which are ideally handled by the $\nabla\epsilon_r$ term). These forms of the wave equations are shown in order to show *why* this problem is essentially an eigenvalue problem in even the most general case.

Eqs. A.28 & A.29 can be reduced to the so called *Helmholtz equations* when ϵ_r (hence n) is approximately homogeneous in the medium[4]. Evaluating the curl function in cylindrical coordinates (Eq. B.3) for the first two of the chromatic wave equations (Eqs. A.11 and A.12) one finds:

$$\begin{aligned}
\frac{1}{r}\frac{\partial}{\partial\theta}E_z + i\beta E_\theta &= -i\omega\mu_0 H_r && \text{(A.30)}\\
-i\beta E_r - \frac{\partial}{\partial r}E_z &= -i\omega\mu_0 H_\theta && \text{(A.31)}\\
\frac{1}{r}\frac{\partial}{\partial r}(rE_\theta) - \frac{1}{r}\frac{\partial}{\partial\theta}E_r &= -i\omega\mu_0 H_z && \text{(A.32)}\\
\frac{1}{r}\frac{\partial}{\partial\theta}H_z + i\beta H_\theta &= i\omega\epsilon_0 n^2 E_r && \text{(A.33)}\\
-i\beta H_r - \frac{\partial}{\partial r}H_z &= i\omega\epsilon_0 n^2 E_\theta && \text{(A.34)}\\
\frac{1}{r}\frac{\partial}{\partial r}(rH_\theta) - \frac{1}{r}\frac{\partial}{\partial\theta}H_r &= i\omega\epsilon_0 n^2 E_z && \text{(A.35)}
\end{aligned}$$

keeping in mind that we're assuming the spatial dependence of all quantities, *i.e.*, all field components, $E_{r,\theta,z}(\mathbf{r}_\perp)$ and $H_{r,\theta,z}(\mathbf{r}_\perp)$, and the refractive index, n, are functions of

[4] See Kiwano and Kitoh Eqs. 2.146 & 2.147

the *transverse* coordinate vector $\mathbf{r}_\perp = (r, \theta)$, and ϵ_0 and μ_0 are scalars. Eqs. A.30→ A.35 are thus the chromatic wave equations in cylindrical component form.

We can rearrange Eqs. A.30 → A.35 to express the derivatives of the longitudinal (z) field components in terms of the transverse (r and θ) field components:

$$\begin{aligned} i\beta E_\theta - i\omega\mu_0 H_r &= \frac{1}{r}\frac{\partial}{\partial\theta}E_z & \text{(A.36)} \\ -i\beta E_r + i\omega\mu_0 H_\theta &= \frac{\partial}{\partial r}E_z & \text{(A.37)} \\ i\omega\epsilon_0 n^2 E_r - i\beta H_\theta &= \frac{1}{r}\frac{\partial}{\partial\theta}H_z & \text{(A.38)} \\ i\omega\epsilon_0 n^2 E_\theta + i\beta H_r &= -\frac{\partial}{\partial r}H_z & \text{(A.39)} \end{aligned}$$

By combining and rearranging Eqs. A.36 → A.39 we can express the transverse field components in terms of the longitudinal field components. Also note that we have used the relations: let the velocity of light in a vacuum be $c \equiv 1/\sqrt{\epsilon_0\mu_0}$ so $k \equiv \omega/c = \omega\sqrt{\epsilon_0\mu_0}$.

Eq.(A.37)$\times\beta$+Eq.(A.38)$\times\omega\mu_0 \Rightarrow$

$$E_r = -\frac{i}{k^2n^2 - \beta^2}\left(\beta\frac{\partial}{\partial r}E_z + \omega\mu_0\frac{1}{r}\frac{\partial}{\partial\theta}H_z\right) \tag{A.40}$$

Eq.(A.36)$\times\beta$+Eq.(A.39)$\times\omega\mu_0 \Rightarrow$

$$E_\theta = -\frac{i}{k^2n^2 - \beta^2}\left(\beta\frac{1}{r}\frac{\partial}{\partial\theta}E_z + \omega\mu_0\frac{\partial}{\partial r}H_z\right) \tag{A.41}$$

Eq.(A.36)$\times\omega\epsilon_0 n^2$+Eq.(A.39)$\times\beta \Rightarrow$

$$H_r = -\frac{i}{k^2n^2 - \beta^2}\left(\beta\frac{\partial}{\partial r}H_z + \omega\epsilon_0 n^2\frac{1}{r}\frac{\partial}{\partial\theta}E_z\right) \tag{A.42}$$

Eq.(A.37)$\times\omega\epsilon_0 n^2$+Eq.(A.38)$\times\beta \Rightarrow$

$$H_\theta = -\frac{i}{k^2n^2 - \beta^2}\left(\beta\frac{1}{r}\frac{\partial}{\partial\theta}H_z + \omega\epsilon_0 n^2\frac{\partial}{\partial r}E_z\right) \tag{A.43}$$

Thus, if one is able to find the longitudinal components, the transverse components can be evaluated directly.

Wave equations for these z-component fields can be derived by substituting these expressions into the general wave equations [Eqs. A.30 → A.35]. Substitute Eqs. A.42 and

A.43 into Eq. A.35 to get:

$$\left\{\frac{\partial^2}{\partial r^2}+\frac{1}{r}\frac{\partial}{\partial r}+\frac{1}{r^2}\frac{\partial^2}{\partial\theta^2}+k^2(n^2-\tilde{n}^2)\right\}E_z=0. \tag{A.44}$$

Substitute Eqs. A.40 & A.41 into Eq. A.32 to get:

$$\left\{\frac{\partial^2}{\partial r^2}+\frac{1}{r}\frac{\partial}{\partial r}+\frac{1}{r^2}\frac{\partial^2}{\partial\theta^2}+k^2(n^2-\tilde{n}^2)\right\}H_z=0. \tag{A.45}$$

Note that Eqs. A.44 & A.45 are essentially Helmoltz equations (in cylindrical coordinates)[5]:

$$\left[\nabla_\perp^2+k^2\left(n^2-\tilde{n}^2\right)\right]\left\{\begin{matrix}E_z\\ H_z\end{matrix}\right\}=0 \tag{A.46}$$

[5]The actual form of the Helmholtz equation is $(\nabla^2+k^2n^2)A_z=0$; The $\frac{\partial^2}{\partial z^2}$ term pulls down two $i\beta$ terms from the longitudinal variation of the fields, $\exp(i\beta z)$, producing the $-k^2\tilde{n}^2$ term given above, *i.e.*, $\nabla^2\rightarrow\nabla_\perp^2-\beta^2$ for guided modes.

A.2 Planar Waveguides

Much of the following analysis is adapted from Refs. [14, 153, 178]. Where novel results or comments have been made by the author, they are highlighted as such (*e.g.*, Corollaries A.1 and A.2).

The most structurally simple form waveguide is that of a single homogeneous planar layer embedded in another homogeneous medium. Figure A.1 shows a schematic of such a structure.

Consider first a *ray* picture of light propagation: the light wave is represented as a plane wave travelling in a specific direction. The layer (the *core*) guides light by reflecting the rays from each of the interfaces made with the surrounding medium (the *cladding*).

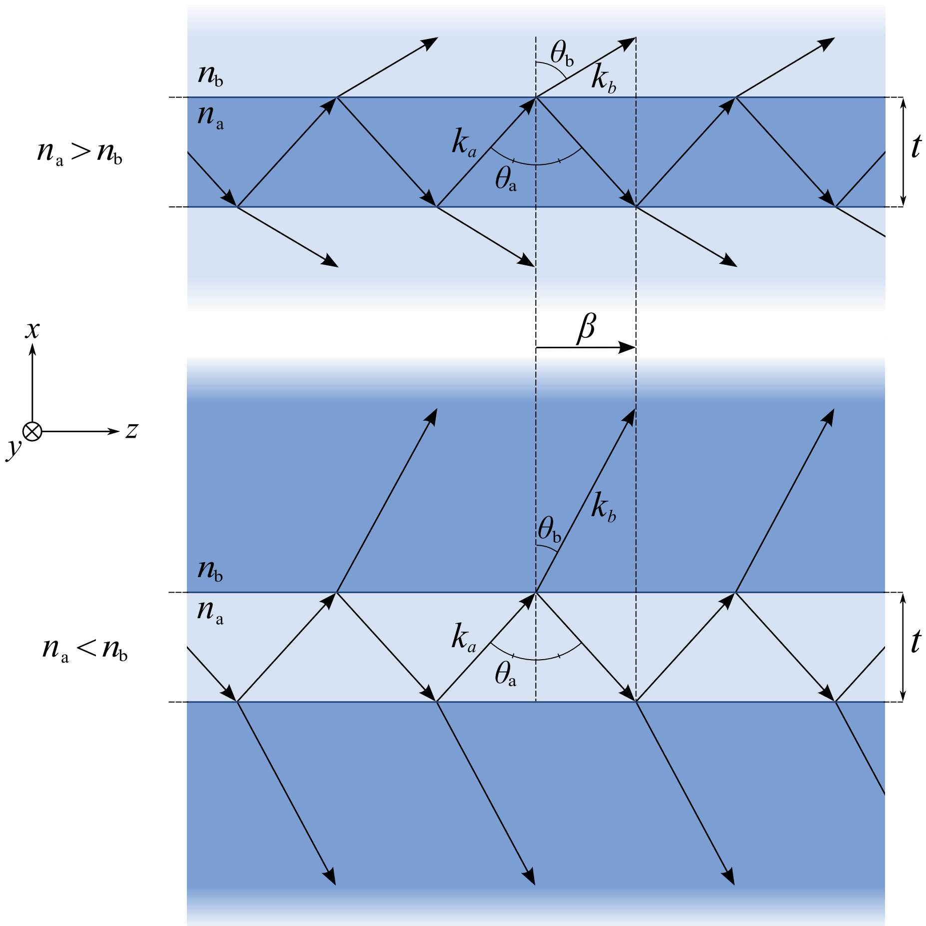

FIGURE A.1: Ray propagation within planar waveguides with either high- or low-index cores. *Top*: A layer with a *higher* core refractive index than the surrounding cladding. *Bottom*: The same waveguide but with a core index *lower* than the surrounding cladding. While each diagram represents the same guided longitudinal wavenumber β (the $\mathbf{k}_a$ vector is the same for each by design—this needn't be the case), the transmitted rays differ markedly depending on whether the ray penetrates into a higher or lower refractive index region. All vector labels represent their amplitudes.

Provided the index of refraction of the cladding is different to that of the core (*i.e.*, $n_a \neq n_b$), the light will be reflected back into the layer. Once the light reaches the other side of the core, it is again reflected back toward its centre. This trapping of the light as it travels down the core is referred to as *guidance* or *confinement*. Figure A.1 demonstrates this light-ray guidance concept.

The relative values of the layer and cladding refractive indices greatly influences the type of reflection undergone by the light as it interacts with the interface. If the core index is larger than the cladding index (*i.e.*, $n_a > n_b$), and the angle the guided ray makes with the interfaces is equal to or greater than a critical value (*i.e.*, $\theta \geq \theta_c$), the light will succumb to *total internal reflection* (TIR). In this regime, all light is confined to the core and none can escape into the cladding[6]. If, however, the ray is incident below the critical angle, only a portion of the power of the light is reflected back into the core, with the remainder escaping to the cladding, never to be recaptured. For propagation over a certain distance, then, a certain amount of guided light power will be lost from the guidance region by means purely due to the way the light is confined (such as inherent material losses, say). This effect is known as *confinement loss*. The waveguidance mechanisms behind confinement loss are not always as simple as the example just described.

Most important for the work considered herein, *light can also be guided within a core of lower refractive index than the surrounding cladding* (*i.e.*, when $n_a < n_b$). In this regime, confinement loss occurs for all incidence angles of the guided rays within the core. This is because no TIR regime exists for propagation from a low-index to a high-index medium, hence there will always be some fraction of the light allowed to escape the core guidance region. This is the precise reason why guiding light in low-index media can be troublesome. While some applications can make do with the high transmission losses that come with low-index guidance with a homogeneous cladding, there is a wealth of rich physics and a plethora of unique applications that flow from the various ways in which one can coerce light be guided within a region with a low refractive index. Before these interesting phenomena and techniques can be discussed, the aforementioned waveguidance fundamentals should be discussed in more detail.

[6]Although a portion of the light's field will penetrate into the cladding as an evanescent field, it is bound to the interface and cannot propagate away from the layer. This is discussed in more detail in § A.2.1.2

A.2.1 Geometric Optics and the Plane Wave Picture

The following sections are mostly adapted from the excellent texts Refs. [14, 153], with significant reworking by myself indicated where appropriate.

A.2.1.1 Plane Waves

The ray optics picture will now be extended to the case of *plane waves*; a regime closely related to ray optics, or *geometric optics*. The ray picture is derived from the plane wave picture: a ray is a linear path perpendicular to the phase fronts of a given plane wave, and must thus point in the direction of the wavevector. When a 'ray' is referred to here, one can typically assume it is interchangeable with the concept of a local plane wave[7]. It is the first analytic tool discussed here as it is comparatively simple, it highlights some important features of the waveguidance phenomena discussed later, and defines many fundamental concepts used throughout this work.

Wave optics as used here involves approximating the guided light within the waveguide as a multiply reflected plane wave. In a homogeneous medium of refractive index n_i, a plane wave will travel in the direction of its wave-vector [178]:

$$\mathbf{k}_i = k_i\widehat{\mathbf{k}_i} = n_i k\widehat{\mathbf{k}_i} = n_i k \left\{\cos\theta_i\hat{\mathbf{x}} + \sin\theta_i\hat{\mathbf{z}}\right\}, \tag{A.47}$$

where $\widehat{\mathbf{k}_i}$ is a unit vector in the direction of $\mathbf{k}_i$, λ is the free space wavelength of the light wave, and $k = 2\pi/\lambda$ is the free-space wavenumber. For a plane wave, the electric and magnetic fields, $\mathbf{E}$ and $\mathbf{H}$ as defined in Section A.1.1, will at any point in time have a constant amplitude on the infinite plane perpendicular to $\widehat{\mathbf{k}_i}$. These amplitudes sinusoidally oscillate between their maxima and minima at an angular frequency $\omega = kc$, where $c = 2.99792458 \times 10^8 ms^{-1}$ is the speed of light in vacuum [14, 178, 212]. This unidirectional plane-wave propagation behaviour constitutes a light *ray*. Following from the results of Section A.1.2, the fields of the plane wave can be represented as [14, 178, 212]:

$$\mathbf{A}(\omega, \mathbf{r}) = A_0 e^{i(\omega t - \mathbf{k}_i\cdot\mathbf{r})} = A_0 e^{i\omega t} e^{-i(k_{ix}x + k_{iy}y + k_{iz}z)}, \tag{A.48}$$

where $\mathbf{A} \equiv \{\mathbf{E}, \mathbf{H}\}$, A_0 is the field amplitude, and $\mathbf{r} = r\hat{\mathbf{r}}$ is the radial coordinate vector. Such waves indeed satisfy the wave equations in homogeneous media, as discussed in Section A.1.2.

Unlike general electromagnetic waves, plane waves have a very simple relationship between their $\mathbf{E}$ and $\mathbf{H}$ fields. Assuming propagation in the z-direction, an x-polarised

[7] 'Local' since, as discussed earlier, true plane waves are infinite in extent and can't exist in the present of inhomogeneities.

electric wave field is represented as $\mathbf{E} = E\hat{\mathbf{x}} = E_0 e^{i(\omega t - k_i z)}\hat{\mathbf{x}}$. By substituting this form of $\mathbf{E}$ into the first of Maxwell's Equations, Eq. A.1, only one of the curl term components survives, producing $\nabla \times \mathbf{E} = \frac{\partial}{\partial z} E\hat{\mathbf{y}} = -ik_i E\hat{\mathbf{y}}$. Equating this to the right hand side of Eq. A.1, one finds $\mathbf{H} = \frac{k_i}{\omega\mu} E_0 e^{i(\omega t - k_i z)}\hat{\mathbf{y}} = H_0 e^{i(\omega t - k_i z)}\hat{\mathbf{y}}$, where one defines $H_0 = \frac{k_i}{\omega\mu} E_0$. The ratio of the electric and magnetic field amplitudes is then $\frac{E_0}{H_0} = \frac{\omega\mu}{k_i} = \sqrt{\frac{\mu}{\epsilon}} = \eta$, where η is known as the *intrinsic impedance* of the medium. In a dielectric ($\mu = \mu_0$), as considered here, the intrinsic impedance can be expressed as $\eta = \sqrt{\frac{\mu_0}{\epsilon}} = \frac{1}{\sqrt{\epsilon_r}}\sqrt{\frac{\mu_0}{\epsilon_0}} = \frac{\eta_0}{n_i}$, where η_0 is the impedance of vacuum and n_i is the refractive index of the local medium.

To summarise:

- At any point in time, the $\mathbf{E}$ and $\mathbf{H}$ fields of the plane wave have a constant value on the infinite plane perpendicular to $\widehat{\mathbf{k}_i}$,
- The fields are linearly polarised in a specific direction within the plane perpendicular to $\mathbf{k}_i$: $\mathbf{E} \cdot \mathbf{k}$=0 and $\mathbf{H} \cdot \mathbf{k}$=0,
- The electric field is always in phase with and perpendicular in polarisation to the magnetic: $|\mathbf{E}(\mathbf{t})| = \frac{\eta_0}{n_i}|\mathbf{H}(\mathbf{t})|$, $\mathbf{E} \cdot \mathbf{H} = 0$.

While light propagation in more complicated structures, such as waveguides, sees these conditions deviate in some way or other, plane wave theory is very useful for the more complicated analyses required for the description of propagation within such structures.

A.2.1.2 Transmission and Reflection at an Interface

Figure A.2 depicts ray propagation across a planar interface made by two homogeneous dielectric media. Rays propagating from the medium with refractive index n_a into the medium with index n_b approach the interface with wave-vector k_a at an angle θ_a to the interface normal and exit with wave-vector k_b at an angle θ_b to the normal. The other possibility is that a fraction (possibly all) all of the light can be reflected from the interface, depicted by the $\mathbf{k}'_a$ wave-vector in Fig. A.2. Figure A.2 also shows the decomposition of the wave-vectors into Cartesian components: the x-component $k_{ix} = \mathbf{k}_i \cdot \hat{\mathbf{x}}$ and the z-component $k_{iz} = \beta = \mathbf{k}_i \cdot \hat{\mathbf{z}}$; no y-component exists by the orientation of the x-z-plane with the plane of incidence here. Integral to much of the following work is that the longitudinal component k_{iz} is conserved, as will be derived later, *i.e.*, the longitudinal component of the wave-vector has the same value before and after transmission and reflection, so that one may set $k_{az} = k'_{az} = k_{bz} = \beta$; a direct result of the Law of Refraction, Eq A.63. β thus becomes an important quantity when considering the propagation of light through multiple interfaces, or when considering

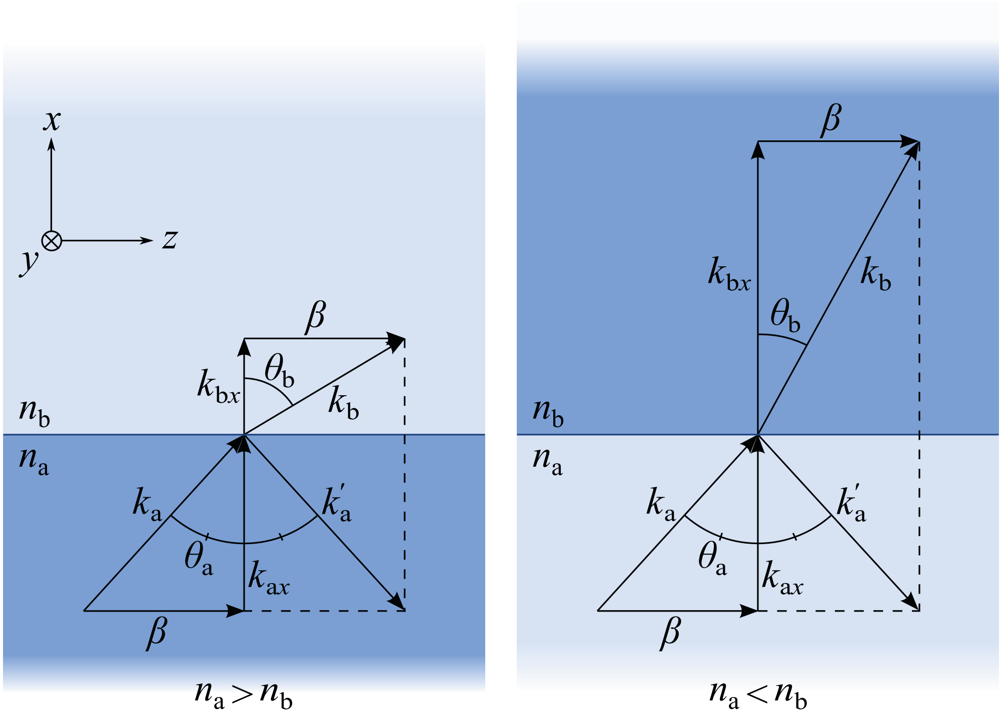

FIGURE A.2: Ray propagation across a plane interface from both a high to a low refractive index (*left*, $n_\mathrm{a} > n_\mathrm{b}$) and from a low to a high refractive index (*right*,$n_\mathrm{a} < n_\mathrm{b}$). Note how the longitudinal (z-dimension, here) component of $\mathbf{k}_i$, β, is conserved under transmission and reflection. All vector labels represent their amplitudes.

the propagation of light along the interface plane (*e.g.*, the z-axis). Such relationships between the incident and transmitted and/or reflected wave-vectors can be derived by considering the behaviour of the electric and magnetic fields at the interface, as will now be demonstrated.

There are two independent types of incident plane waves on an interface: *transverse electric* (TE) and *transverse magnetic* (TM) waves. The *plane of incidence* of an incoming ray (such as those in Fig. A.2 or Fig. A.3) is defined as the plane common to the incident wave-vector $\mathbf{k}_i$ and a vector normal to the interface (*e.g.*, the x-direction $\hat{\mathbf{x}}$ in Fig. A.2 or the dashed line in Fig. A.3). This makes the plane of incidence equivalent to the plane of the page for Figures A.2 and A.3. Figure A.3 demonstrates the relationship between the incident and reflected and/or transmitted plane wave fields. An incident wave is termed TE if the electric field is normal to the plane of incidence (and hence lies in a plane parallel to the interface). Likewise, a wave is termed TM if its magnetic field is normal to the plane of incidence[8]. Now, electromagnetic boundary conditions assert that, in the absence of surface currents, the electric and magnetic fields tangential to

[8]The TE and TM polarisations are often called s and p polarisations in electromagnetic theory, standing for the German *senkrecht* (perpendicular) and *parallel* (parallel) [178], respectively, referring to the orientation of solely the electric field with respect to the plane of incidence.

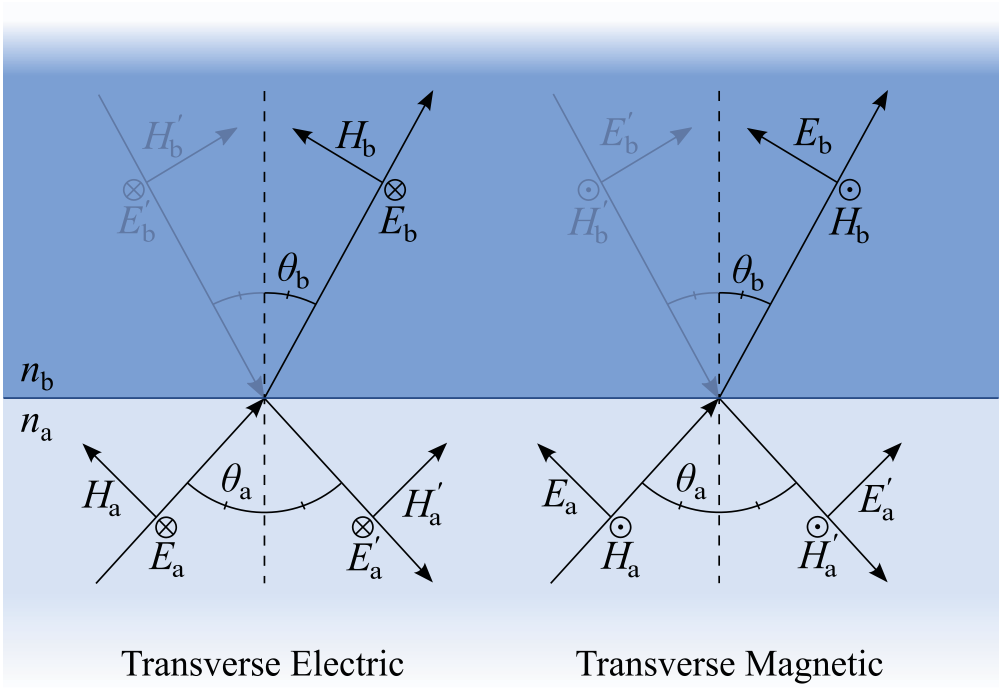

FIGURE A.3: Electric and magnetic fields of a plane wave before and after transmission and reflection at an interface. *Left*: A vector diagram representing an incoming *transverse electric* (TE) plane wave. *Right* A similar diagram representing an incoming *transverse magnetic* (TM) plane wave. Dark arrows represent propagation from a low- to a high-index medium ($n_\mathrm{a} < n_\mathrm{b}$), with incident, reflected and transmitted fields A_a, A_a' and A_b, respectively. The faint arrows represent high- to low-index propagation with incident, reflected and transmitted fields A_b', A_b and A_a', respectively.

an interface must be continuous across that interface[9] [14, 212]. This means that an incident TE wave will be transmitted or reflected as a TE wave and similarly for the TM equivalent; if this weren't the case, reflected or transmitted waves would contain field components that don't exist in the incident wave, breaking the field continuity at the interface. Arbitrary polarisation directions can be constructed from a superposition of TE and TM polarisations.

Using the field components as shown in Fig. A.3, the continuity boundary condition implies that at the interface (*i.e.*, $x = 0$ in Fig. A.2) [14, 178]:

$$E_\mathrm{at} + E'_\mathrm{at} = E_\mathrm{bt}, \tag{A.49}$$

$$H_\mathrm{at} + H'_\mathrm{at} = H_\mathrm{bt}, \tag{A.50}$$

where the subscript $_\mathrm{t}$ denotes the component of the vector tangential to the interface, *i.e.*, for field components not purely normal to the plane of incidence, the projection upon the interface plane of the component in question must be taken (*e.g.*, $\mathbf{H}_\mathrm{a}$ for the

[9]Such boundary conditions are derivable directly from Maxwell's equations [14, 212].

TE case in Fig. A.3 projects onto the interface plane as $-H_a cos\theta_a$ and simply as H_a for the TM).

Using the wave-vectors as shown in Fig. A.2 and the spatio-temporal expression for the fields as in Eq. A.48, these transmitted and reflected waves are expressed as, for TE polarisation:

$$\begin{aligned} E_\mathrm{a} &= E_{\mathrm{a}0}e^{i(\omega t-\mathbf{k}_\mathrm{a}\cdot\mathbf{r})}, && \text{(A.51)}\\ E'_\mathrm{a} &= E'_{\mathrm{a}0}e^{i(\omega t-\mathbf{k}'_\mathrm{a}\cdot\mathbf{r})}, && \text{(A.52)}\\ E_\mathrm{b} &= E_{\mathrm{b}0}e^{i(\omega t-\mathbf{k}_\mathrm{b}\cdot\mathbf{r})}, && \text{(A.53)} \end{aligned}$$

and for TM polarisation:

$$\begin{aligned} H_\mathrm{a} &= H_{\mathrm{a}0}e^{i(\omega t-\mathbf{k}_\mathrm{a}\cdot\mathbf{r})}, && \text{(A.54)}\\ H'_\mathrm{a} &= H'_{\mathrm{a}0}e^{i(\omega t-\mathbf{k}'_\mathrm{a}\cdot\mathbf{r})}, && \text{(A.55)}\\ H_\mathrm{b} &= H_{\mathrm{b}0}e^{i(\omega t-\mathbf{k}_\mathrm{b}\cdot\mathbf{r})}. && \text{(A.56)} \end{aligned}$$

Applying the Cartesian wave-vector expression of Eq. A.47 to these waves:

$$\begin{aligned} \mathbf{k}_\mathrm{a} &= n_\mathrm{a}k\left[\cos\theta_\mathrm{a}\hat{\mathbf{x}}+\sin\theta_\mathrm{a}\hat{\mathbf{z}}\right], && \text{(A.57)}\\ \mathbf{k}'_\mathrm{a} &= n_\mathrm{a}k\left[-\cos\theta'_\mathrm{a}\hat{\mathbf{x}}+\sin(\theta'_\mathrm{a})\hat{\mathbf{z}}\right], && \text{(A.58)}\\ \mathbf{k}_\mathrm{b} &= n_\mathrm{b}k\left[\cos\theta_\mathrm{b}\hat{\mathbf{x}}+\sin\theta_\mathrm{b}\hat{\mathbf{z}}\right]. && \text{(A.59)} \end{aligned}$$

By substituting Eqs. A.51 to A.53 into Eq. A.49 (and similarly for the H equivalents), enforcing the continuity boundary conditions on the incident, reflected and transmitted plane waves, one finds:

$$\begin{aligned} E_{\mathrm{a}0}e^{i(\omega t-\mathbf{k}_\mathrm{a}\cdot\mathbf{r})}+E'_{\mathrm{a}0}e^{i(\omega t-\mathbf{k}'_\mathrm{a}\cdot\mathbf{r})} &= E_{\mathrm{b}0}e^{i(\omega t-\mathbf{k}_\mathrm{b}\cdot\mathbf{r})}, && \text{(A.60)}\\ H_{\mathrm{a}0}e^{i(\omega t-\mathbf{k}_\mathrm{a}\cdot\mathbf{r})}+H'_{\mathrm{a}0}e^{i(\omega t-\mathbf{k}'_\mathrm{a}\cdot\mathbf{r})} &= H_{\mathrm{b}0}e^{i(\omega t-\mathbf{k}_\mathrm{b}\cdot\mathbf{r})}. && \text{(A.61)} \end{aligned}$$

In order for each of these two conditions to hold at a particular time for all points on the interface, *all three waves* (incident, reflected and transmitted) *must accumulate the same phase shift per unit distance across the interface.* In other words, the only way to incorporate a spatially evolving phase into these explicit boundary conditions is to add the same phase term to the arguments of each wavefunction. To see this, arbitrarily setting the instantaneous time to be $t = 0$ and adding a spatial phase of ϕ to the wavefunctions' argument ($\mathbf{k}_\mathrm{i}\cdot\mathbf{r} \to \mathbf{k}_\mathrm{i}\cdot\mathbf{r}+\phi$ with $i \in \{\mathrm{a,b}\}$), all terms in Eqs. A.60 and A.61 can factor out a common term of $e^{-i\phi}$, which cancels directly, preserving the continuity boundary conditions Eqs. A.49 and A.50. Specifically considering the z-direction along the interface, the accumulated spatial phase for a wave with wave-vector $\mathbf{k}$ over some distance Δz is thus $\mathbf{k} \cdot \hat{\mathbf{z}}\Delta z = k_z \Delta z$ (see Section A.1.2). For this phase term to be equal for all three waves, all waves' wave-vector components in the interface plane (k_z) must all be equal. Thus, *k_z is equal for the incident, reflected and transmitted waves*, *i.e.*, the transverse component of the incident wavenumber is conserved during reflection and transmission. Because of this, one can set the transverse components to a common value $k_{\mathrm{a}z} = k'_{\mathrm{a}z} = k_{\mathrm{b}z} = \beta$, as shown in Figs. A.1 and A.2. This conservation of longitudinal wavenumber becomes very important when considering more complicated plane wave behaviour, such as multilayer optical structures.

Conservation of k_z also leads to some vital relationships between the waves. By equating z-component of Eqs. A.57 and A.58, one finds:

$$\theta_{\mathrm{a}} = \theta'_{\mathrm{a}}, \tag{A.62}$$

which is known as the *Law of Reflection*. By equating the z-component of Eqs. A.57 and A.59, one also finds:

$$n_{\mathrm{a}} \sin\theta_{\mathrm{a}} = n_{\mathrm{b}} \sin\theta_{\mathrm{b}}, \tag{A.63}$$

which is the well known *Law of Refraction*, also known as *Snell's Law* or *Descarte's Law*[10]. An important corollary of Eq. A.63 is that rays traversing the interface for the case $n_{\mathrm{a}} < n_{\mathrm{b}}$ transmit with smaller angles to the normal, whereas they transmit with greater angles to the normal for $n_{\mathrm{a}} > n_{\mathrm{b}}$, as depicted in Fig. A.2. This has important consequences for the behaviour of modes within layer waveguides, discussed later.

The continuity boundary conditions can be used to also determine the amplitude of the incident, reflected and transmitted fields. By substituting the waves' transverse field components of Fig. A.2 into Eqs. A.49 and A.50:

$$\begin{aligned} E_{\mathrm{a}} + E'_{\mathrm{a}} &= E_{\mathrm{b}}, && \text{(A.64)}\\ -H_{\mathrm{a}}\cos\theta_{\mathrm{a}} + H'_{\mathrm{a}}\cos\theta_{\mathrm{a}} &= -H_{\mathrm{b}}\cos\theta_{\mathrm{b}}, && \text{(A.65)} \end{aligned}$$

for TE polarised waves, and:

$$\begin{aligned} -E_{\mathrm{a}}\cos\theta_{\mathrm{a}} + E'_{\mathrm{a}}\cos\theta_{\mathrm{a}} &= -E_{\mathrm{b}}\cos\theta_{\mathrm{b}}, && \text{(A.66)}\\ H_{\mathrm{a}} + H'_{\mathrm{a}} &= H_{\mathrm{b}}, && \text{(A.67)} \end{aligned}$$

for TM polarised waves.

[10] It is now often recognised that the relation was first discovered by Ibn Sahl in the late 10^{th} century.

Recall that the electric and magnetic field ratios are $\frac{E_{\text{a}}}{H_{\text{a}}} = \frac{E'_{\text{a}}}{H'_{\text{a}}} = \frac{\eta_0}{n_{\text{a}}}$ and $\frac{E_{\text{b}}}{H_{\text{b}}} = \frac{\eta_0}{n_{\text{a}}}$. Substituting them into Eq. A.65 produces:

$$-E_{\text{a}}n_{\text{a}}cos\theta_{\text{a}} + E'_{\text{a}}n_{\text{a}}cos\theta_{\text{a}} = -E_{\text{b}}n_{\text{b}}cos\theta_{\text{b}}, \tag{A.68}$$

for the TE waves, and substituting them into Eq. A.66 produces:

$$-H_{\text{a}}n_{\text{a}}cos\theta_{\text{a}} + H'_{\text{a}}n_{\text{a}}cos\theta_{\text{a}} = -H_{\text{b}}n_{\text{b}}cos\theta_{\text{b}}, \tag{A.69}$$

for the TM waves. Solving Eqs. A.64 and A.68 simultaneously leads to the reflection (Γ) and transmission (T) coefficients for the TE waves:

$$\Gamma_{\text{TE}} \equiv \frac{E'_{\text{a}}}{E_{\text{a}}} = \frac{n_{\text{a}}\cos\theta_{\text{a}} - n_{\text{b}}\cos\theta_{\text{b}}}{n_{\text{a}}\cos\theta_{\text{a}} + n_{\text{b}}\cos\theta_{\text{b}}} = \frac{k_{\text{a}x} - k_{\text{b}x}}{k_{\text{a}x} + k_{\text{b}x}}, \tag{A.70}$$

$$T_{\text{TE}} \equiv \frac{E_{\text{b}}}{E_{\text{a}}} = \frac{2k_{\text{a}x}}{k_{\text{a}x} + k_{\text{b}x}} = 1 + \Gamma_{\text{TE}}, \tag{A.71}$$

and solving Eqs. A.67 and A.69 simultaneously leads to the reflection and transmission coefficients for the TM waves:

$$\Gamma_{\text{TM}} \equiv \frac{E'_{\text{a}}}{E_{\text{a}}} = \frac{n_{\text{b}}\cos\theta_{\text{a}} - n_{\text{a}}\cos\theta_{\text{b}}}{n_{\text{b}}\cos\theta_{\text{a}} + n_{\text{a}}\cos\theta_{\text{b}}} = \frac{n_{\text{b}}^2k_{\text{a}x} - n_{\text{a}}^2k_{\text{b}x}}{n_{\text{b}}^2k_{\text{a}x} + n_{\text{a}}^2k_{\text{b}x}}, \tag{A.72}$$

$$T_{\text{TM}} \equiv \frac{E_{\text{b}}}{E_{\text{a}}} = \frac{2n_{\text{a}}n_{\text{b}}k_{\text{a}x}}{n_{\text{b}}^2k_{\text{a}x} + n_{\text{a}}^2k_{\text{b}x}} = \frac{n_{\text{a}}}{n_{\text{b}}}\left(1 + \Gamma_{\text{TE}}\right). \tag{A.73}$$

Equations A.70 to A.73 describe the relative amplitudes of incident, reflected and transmitted plane waves at the interface of two dielectrics, and are known as the *Fresnel Formulae.* They can be expressed in a more compact form[11] by using the trigonometric identities Eqs. B.11 to B.13 and the Law of Refraction, Eq. A.63. For Γ_{TE}:

$$\begin{aligned}
\Gamma_{\text{TE}} &= \frac{n_{\text{a}}\cos\theta_{\text{a}} - n_{\text{b}}\cos\theta_{\text{b}}}{n_{\text{a}}\cos\theta_{\text{a}} + n_{\text{b}}\cos\theta_{\text{b}}} \\
(\div \text{ all by } -n_{\text{b}}) \quad &= -\frac{\cos\theta_{\text{b}} - \frac{n_{\text{a}}}{n_{\text{b}}}\cos\theta_{\text{a}}}{\cos\theta_{\text{b}} + \frac{n_{\text{a}}}{n_{\text{b}}}\cos\theta_{\text{a}}} \\
(\text{by Eq. A.63}) \quad &= -\frac{\cos\theta_{\text{b}} - \frac{\sin\theta_{\text{b}}}{\sin\theta_{\text{a}}}\cos\theta_{\text{a}}}{\cos\theta_{\text{b}} + \frac{\sin\theta_{\text{b}}}{\sin\theta_{\text{a}}}\cos\theta_{\text{a}}} \\
(\times \text{ all by } \sin\theta_{\text{a}}) \quad &= -\frac{\sin\theta_{\text{a}}\cos\theta_{\text{b}} - \sin\theta_{\text{b}}\cos\theta_{\text{a}}}{\sin\theta_{\text{a}}\cos\theta_{\text{b}} + \sin\theta_{\text{b}}\cos\theta_{\text{a}}} \\
(\text{simplify via } B.11) \quad &= -\frac{\sin(\theta_{\text{a}} - \theta_{\text{b}})}{\sin(\theta_{\text{a}} + \theta_{\text{b}})}.
\end{aligned}$$

[11] Although Eqs. A.70 and A.72 must be used for normal incidence $\theta_{\text{a}} = \theta_{\text{b}} = 0$.

Similarly for Γ_{TM}:

$$\begin{aligned}
\Gamma_{\mathrm{TM}} &= \frac{n_{\mathrm{b}}\cos\theta_{\mathrm{a}} - n_{\mathrm{a}}\cos\theta_{\mathrm{b}}}{n_{\mathrm{b}}\cos\theta_{\mathrm{a}} + n_{\mathrm{a}}\cos\theta_{\mathrm{b}}} \\
(\div \text{ all by } n_{\mathrm{b}}) \quad &= -\frac{\cos\theta_{\mathrm{a}} - \frac{n_{\mathrm{a}}}{n_{\mathrm{b}}}\cos\theta_{\mathrm{b}}}{\cos\theta_{\mathrm{a}} + \frac{n_{\mathrm{a}}}{n_{\mathrm{b}}}\cos\theta_{\mathrm{b}}} \\
(\text{by Eq. A.63}) \quad &= \frac{\cos\theta_{\mathrm{a}} - \frac{\sin\theta_{\mathrm{b}}}{\sin\theta_{\mathrm{a}}}\cos\theta_{\mathrm{b}}}{\cos\theta_{\mathrm{a}} + \frac{\sin\theta_{\mathrm{b}}}{\sin\theta_{\mathrm{a}}}\cos\theta_{\mathrm{b}}} \\
(\times \text{ all by } \sin\theta_{\mathrm{a}}) \quad &= \frac{\sin\theta_{\mathrm{a}}\cos\theta_{\mathrm{a}} - \sin\theta_{\mathrm{b}}\cos\theta_{\mathrm{b}}}{\sin\theta_{\mathrm{a}}\cos\theta_{\mathrm{a}} + \sin\theta_{\mathrm{b}}\cos\theta_{\mathrm{b}}} \\
(\text{simplify via } B.13) \quad &= \frac{\tan(\theta_{\mathrm{a}} - \theta_{\mathrm{b}})}{\tan(\theta_{\mathrm{a}} + \theta_{\mathrm{b}})}.
\end{aligned}$$

The wonderfully compact forms are thus:

$$\Gamma_{\mathrm{TE}} = -\frac{\sin(\theta_{\mathrm{a}} - \theta_{\mathrm{b}})}{\sin(\theta_{\mathrm{a}} + \theta_{\mathrm{b}})}, \tag{A.74}$$

$$\Gamma_{\mathrm{TM}} = \frac{\tan(\theta_{\mathrm{a}} - \theta_{\mathrm{b}})}{\tan(\theta_{\mathrm{a}} + \theta_{\mathrm{b}})}. \tag{A.75}$$

These are the forms given in [14]. While they don't appear explicitly in these expressions, the refractive indices have influence through θ_{a} and θ_{b} via the Law of Refraction, Eq. A.63.

Γ is often called the *reflectivity* and T the *transmissivity* of an optical system.

By considering the power of the incident, reflected and transmitted waves, it can be shown (*e.g.*, Ref. [14]-p. 43 and Ref. [153]-p. 65) that the Fresnel Formulae can be used to express *power reflection* ($\mathcal{R}$) and *power transmission* ($\mathcal{T}$) *coefficients*:

$$\mathcal{R}_{\mathrm{TE,TM}} = |\Gamma_{\mathrm{TE,TM}}|^2, \tag{A.76}$$

$$\mathcal{T}_{\mathrm{TE,TM}} = \frac{k_{\mathrm{b}x}}{k_{\mathrm{a}x}}|T_{\mathrm{TE,TM}}|^2. \tag{A.77}$$

$\mathcal{R}$ and $\mathcal{T}$ are often called the *reflectance* and *transmittance* of the waves, respectively, and represent the ratios of the power in the reflected or transmitted waves to that of the incident wave. As expected from the principle of conservation of energy, they sum to unity: $\mathcal{R}_{\mathrm{TE,TM}} + \mathcal{T}_{\mathrm{TE,TM}} = 1$. Figure A.4 shows $\mathcal{R}$ from normal to grazing incidence ($\theta = 0 \rightarrow \pi/2$, expressed in degrees $0^\circ \rightarrow 90^\circ$ for clarity).

The *Principle of Reciprocity* states that the behaviour of light in one direction must be identical when the direction of propagation is everywhere reversed (by reversing the direction of time, say). With this in mind, it is readily shown [153] that the Fresnel Coefficients Γ_{ab} and T_{ab} for propagation from medium a into medium b (for both TE

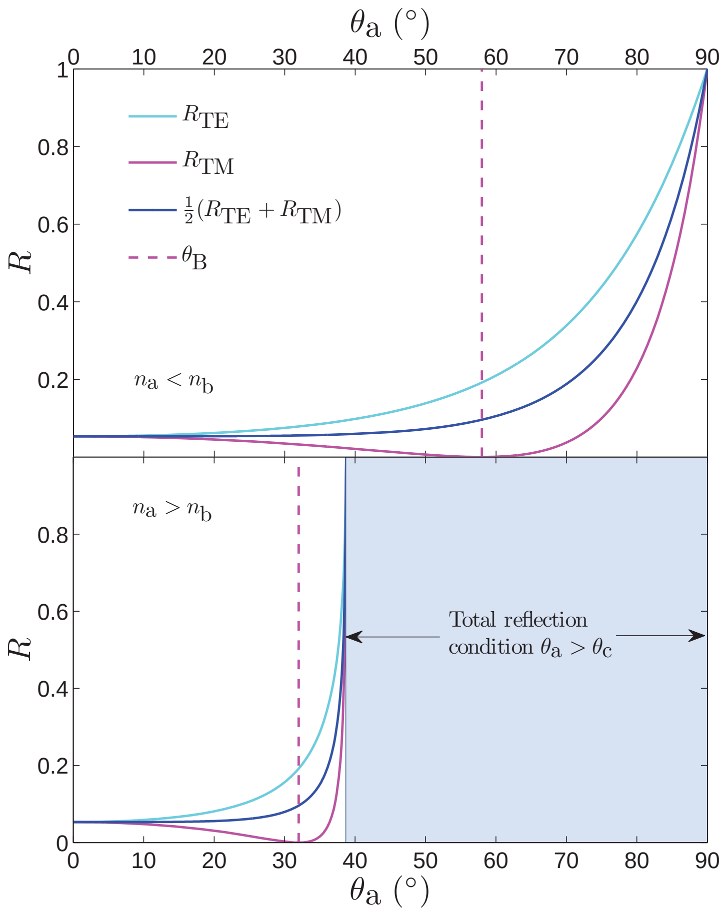

FIGURE A.4: Examples of TE and TM reflectance coefficients for a range of incidence angles. The fraction of power reflected for unpolarised light is the arithmetic mean of the reflectivities of the two orthogonal polarisations: $\frac{1}{2}(R_{TE} + R_{TM})$. *Top:* $n_a = 1$ and $n_b = 1.6 \Rightarrow n_a < n_b$. *Bottom:* $n_a = 1.6$ and $n_b = 1 \Rightarrow n_a > n_b$. Note how the reflected power falls to 0 for the TM polarisation at the Brewster condition $\theta = \theta_B$ in both cases.

and TM polarisations) are related to the coefficients Γ_{ba} and T_{ba} for propagation from medium b into medium a.

By definition, Eqs. A.70 to A.73 relate the incident to reflected and incident to transmitted fields respectively as:

$$E'_a = \Gamma_{ab} E_a, \tag{A.78}$$

$$E_b = T_{ab} E_a, \tag{A.79}$$

$$E'_b = 0, \tag{A.80}$$

where the nomenclature of Fig. A.3 has been used. The final condition (Eq. A.80) is due to the nature of propagation across an interface (E'_b could not be excited by the sole incident field E_a).

Consider now reversing the propagation directions of all rays by, say, a time-reversal. The ray arrows of Fig. A.3 thus reverse direction. The Principle of Reciprocity implies that the same laws of reflection and transmission hold for the time-reversed waves as for the original waves. In this case, the field E_a is excited by the reflection of E'_b and the transmission of E_b and the field E'_b is excited by the reflection of E_b and transmission of E'_a, such that:

$$E_a = \Gamma_{ab} E'_a + T_{ba} E_b, \tag{A.81}$$

$$E'_b = \Gamma_{ba} E_b + T_{ab} E'_a. \tag{A.82}$$

Section A.3.1 discusses this further in the context of superposed forward and backward propagating waves.

Eqs. A.78 to A.82 can be combined to produce the reflection and transmission reciprocity relations[12]:

$$\Gamma_{ba} = -\Gamma_{ab}, \tag{A.83}$$

$$T_{ab} T_{ba} = \Gamma_{ab} \Gamma_{ba} + 1. \tag{A.84}$$

Eq. A.83 is found by inserting Eq. A.79 into A.81, then inserting Eq. A.78. Eq. A.84 is found by inserting Eq. A.80 into A.82, then inserting Eq. A.79.

The Fresnel Formulae can be used to derive other important relationships between the rays. By setting $\Gamma_{\mathrm{TM}} = 0$, one finds that TM incident waves have no reflected wave when:

$$n_{\mathrm{b}} \cos\theta_{\mathrm{a}} = n_{\mathrm{a}} \cos\theta_{\mathrm{b}}. \tag{A.85}$$

Using the Law of Refraction (Eq. A.63) this can be solved for the incident angle as[13]:

$$\theta_{\mathrm{B}} \equiv \theta_{\mathrm{a}} = \tan^{-1}\left(\frac{n_{\mathrm{b}}}{n_{\mathrm{a}}}\right), \tag{A.86}$$

where θ_{B} is know as *Brewster's Angle*, representing the incident angle at which all TM-polarised light is transmitted across the interface; Figure A.4 shows an explicit example. Similarly, for $\Gamma_{\mathrm{TE}} = 0$ to hold, one requires a condition which will be shown to be unphysical for $n_{\mathrm{a}} \neq n_{\mathrm{b}}$:

$$n_{\mathrm{a}} \cos\theta_{\mathrm{a}} = n_{\mathrm{b}} \cos\theta_{\mathrm{b}}. \tag{A.87}$$

Dividing Eq. A.63 by Eq. A.87, one produces $\tan(\theta_{\mathrm{a}}) = \tan(\theta_{\mathrm{b}})$, which only has solutions $\theta_{\mathrm{a}} = \theta_{\mathrm{b}} \pm \pi/2$. Since only the domain $0 \leq \theta_{\mathrm{a}} < \pi/2$ is of interest here, then the solution

[12] A relation between T_{ab} and T_{ba} can also be derived [153]: $T_{ba}/[n_b \cos(\theta_b)] = T_{ab}/[n_a \cos(\theta_a)]$.

[13] Square Eqs. A.63 and A.85, add them, rearrange for $\cos^2(\theta_{\mathrm{a}})$, replace $\sin^2(\theta_{\mathrm{b}})$ with $1 - \cos^2(\theta_{\mathrm{b}})$, substitute for $\cos^2(\theta_{\mathrm{b}})$ using A.85, rearrange for $\cos\theta_{\mathrm{a}}$, then θ_{a}. Simple trigonometry gives $\tan^{-1}(y/x) = \cos^{-1}(\sqrt{x^2/(x^2+y^2)})$.

is $\theta_\mathrm{a} = \theta_\mathrm{b}$. The only solution satisfying Eq. A.63, $\theta_\mathrm{a} = \theta_\mathrm{b} = 0$, cannot simultaneously satisfy[14] Eq. A.87, implying that no incidence angle θ_a can produce $\Gamma_\mathrm{TE} = 0$. This gives the Brewster angle θ_B another unique property of behaving as a *polarising angle* at which only TE waves are reflected.

A specific range of the incidence angle can also produce another important phenomenon: *total reflection*. The Law of Refraction can be arranged as:

$$\cos\theta_\mathrm{b} = \sqrt{1 - \left(\frac{n_\mathrm{a}}{n_\mathrm{b}}\sin^2\theta_\mathrm{a}\right)^2}. \tag{A.88}$$

Recalling $k_{\mathrm{b}x} = k_\mathrm{b}\cos\theta_\mathrm{b}$, one finds $k_{\mathrm{b}x} = 0$ when $\cos\theta_\mathrm{b} = 0$, *i.e.*, the transmitted ray is directed along the interface. Equation A.88 implies this is the case when $\sin^2\theta_\mathrm{a} = \frac{n_\mathrm{b}}{n_\mathrm{a}}$. If the value of this term is increased, by increasing θ_a, then Eq. A.88 implies $k_{\mathrm{b}x} \in \mathbb{C}$; in fact, it's purely imaginary[15]: $k_{\mathrm{b}x} = -i|\mathrm{Im}(k_{\mathrm{b}x})|$. In this case, the oscillatory factor of the wavefunction Eq. A.48 adopts a real, negative, exponent, producing a decay term: $e^{i\omega t}e^{-i(k_{\mathrm{b}x}x + k_{\mathrm{b}y}y + k_{\mathrm{b}z}z)} \rightarrow e^{i\omega t}e^{-i(k_{\mathrm{b}y}y + k_{\mathrm{b}z}z)}e^{-|\mathrm{Im}(k_{\mathrm{b}x})|x}$. Thus, the transmitted wave is only allowed to propagate tangential to the interface (z-direction in Figs. A.1 and A.2) with a decaying field amplitude normal to the interface (x-direction in Figs. A.1 and A.2); this is known as an *evanescent wave*. This means there can be no net power transport away from the interface, implying all incident power must be transferred to the reflected wave. This is seen explicitly in that the power reflection coefficients are unity in this case:

$$\begin{aligned}
\mathcal{R} = |\Gamma_{\mathrm{TE,TM}}|^2 &= \Gamma_{\mathrm{TE,TM}}\Gamma^*_{\mathrm{TE,TM}} \\
&= \frac{(k_{\mathrm{a}x} - k_{\mathrm{b}x})(k_{\mathrm{a}x} - k_{\mathrm{b}x})^*}{(k_{\mathrm{a}x} + k_{\mathrm{b}x})(k_{\mathrm{a}x} + k_{\mathrm{b}x})^*} \\
&= \frac{[k_{\mathrm{a}x} + i\mathrm{Im}(k_{\mathrm{b}x})][k_{\mathrm{a}x} + i\mathrm{Im}(k_{\mathrm{b}x})]^*}{[k_{\mathrm{a}x} - i\mathrm{Im}(k_{\mathrm{b}x})][k_{\mathrm{a}x} - i\mathrm{Im}(k_{\mathrm{b}x})]^*} \\
&= \frac{[k_{\mathrm{a}x} + i\mathrm{Im}(k_{\mathrm{b}x})][k_{\mathrm{a}x} - i\mathrm{Im}(k_{\mathrm{b}x})]}{[k_{\mathrm{a}x} - i\mathrm{Im}(k_{\mathrm{b}x})][k_{\mathrm{a}x} + i\mathrm{Im}(k_{\mathrm{b}x})]} = 1.
\end{aligned}$$

[14] Which may seem strange as the two equations were solved simultaneously, until one recognises that $\theta_\mathrm{a} = \theta_\mathrm{b} = 0$ produces $\sin = 0$, removing the influence of Eq. A.87 on the condition. Eq. A.87 with $\theta_\mathrm{a} = \theta_\mathrm{b} = 0$ requires $n_\mathrm{a} = n_\mathrm{b}$ which is the trivial case of a plane wave in a homogeneous medium. This certainly produces no reflected wave, but the trivial scenario isn't of interest for these analyses of reflection and transmission.

[15] Since $\sqrt{-1} = \pm i$, the negative branch, $-i$, is taken here since $+i$ produces a *gain* term, resulting in an unphysical infinite field amplitude as $x \rightarrow \infty$; unphysical at least for a single reflection/transmission event as considered here—'leaky modes', discussed later, necessarily exhibit radially increasing field amplitudes, although these are due to a longitudinal accumulation of the field leaked along the prior length of a waveguide [178, 214] and [215] p.21.

From Eq. A.88, the range of incident angles producing an imaginary $k_{\mathbf{b}x}$, and hence total reflection, is thus:

$$\theta_{\mathrm{a}} \geq \theta_{\mathrm{c}} = \sin^{-1}\left(\frac{n_{\mathrm{b}}}{n_{\mathrm{a}}}\right), \tag{A.89}$$

where θ_{c} is known as the *critical angle* for total reflection. It is clear from Eq. A.89 that, to be physically meaningful, total reflection requires $n_{\mathrm{a}} > n_{\mathrm{b}}$. Total reflection cannot occur when $n_{\mathrm{a}} < n_{\mathrm{b}}$.

In this work, the transmission of light originating from a *lower* refractive index into a *higher* refractive index, $n_{\mathrm{a}} < n_{\mathrm{b}}$, is typically considered, *e.g.*, the guidance of light within a low-index layer. In this case, $\beta = n_{\mathrm{a}} k \sin\theta_{\mathrm{a}}$ satisfies the condition $\beta \leq n_{\mathrm{a}} k$. Exactly the same condition is required for the case of the transmission of light originating from a *higher* refractive index into a *lower* refractive index, $n_{\mathrm{a}} > n_{\mathrm{b}}$, except that total reflection occurs when $\sin\theta_{\mathrm{a}} \geq \frac{n_{\mathrm{b}}}{n_{\mathrm{a}}}$ (Eq. A.89). Total reflection thus occurs for the subset of propagation constants (incidence angles) satisfying $n_{\mathrm{b}} k < \beta \leq n_{\mathrm{a}} k$. A very important consequence of this is:

Corollary A.1. *Conservation of β implies that the transmitted component of an external ray incident on a high-index layer embedded in a low-index medium cannot satisfy the conditions for total reflection within the layer.*

Generalising this principle, Corollary A.1 implies:

Corollary A.2. *Light originating from a low-index medium will never succumb to total reflection at any subsequent parallel interface it may propagate across, provided the layers' refractive indices are equal to or greater than the initial medium's refractive index.*

Corollary A.2 is very important when considering multilayer structures, discussed later. These corollaries have been formulated specifically for this work, and are to the best of my knowledge unique (at the very least in the context of the current work).

It is useful here to define the *effective refractive index*:

$$\tilde{n}_i = \frac{\beta_i}{k} = n_{\mathrm{i}} \sin\theta_i, \tag{A.90}$$

Across any interface $\tilde{n}_{\mathrm{a}} = \tilde{n}_{\mathrm{b}}$, thanks to conservation of β. The permissible ranges of β leading to the above Corollaries become:

$$\text{Reflection \textit{and} transmission:} \quad \tilde{n}_{\mathrm{a}} \leq n_{\mathrm{a}} \quad \forall\, n_{\mathrm{a,b}}, \tag{A.91}$$

$$\text{\textit{Total} reflection:} \quad n_{\mathrm{b}} < \tilde{n}_{\mathrm{a}} \leq n_{\mathrm{a}} \quad \text{for } n_{\mathrm{a}} > n_{\mathrm{b}}. \tag{A.92}$$

In other words, a ray in a low-index medium can only ever take values $\tilde{n}_\mathrm{a} \leq n_\mathrm{a}$ and thus always transmits some power across the interface, whereas a ray in a high-index medium can also take higher $\tilde{n}_\mathrm{a}$ values (up to n_b) at which it undergoes total reflection.

The *phase* accumulated by a wave upon reflection can also be determined from the reflection and transmission coefficients Γ and T. The field amplitudes of an incident and reflected wave are related by $A_\mathrm{TE,TM} = \Gamma_\mathrm{TE,TM} A'_\mathrm{TE,TM}$. As well as describing the change in amplitude of the field components, Γ can also accommodate phase changes. Explicitly, one may decompose the reflection coefficient into amplitude and phase as $\Gamma = |\Gamma| e^{i\delta\phi}$, where $\delta\phi$ is the change in phase of the wave after reflection. The phase of a wave becomes critical when determining the waveguidance behaviour of a waveguide.

First consider the low- to high-index propagation case: $n_\mathrm{a} < n_\mathrm{b}$. As discussed above, $k_{\mathrm{a}x,\mathrm{b}x} \in \mathbb{R}$ in this case (no total reflection), so that $\theta_\mathrm{a,b} \in \mathbb{R}$. The Law of Refraction (Eq. A.63) then implies $\theta_\mathrm{a} > \theta_\mathrm{b}$. In this case, $\pi \geq \theta_\mathrm{a} - \theta_\mathrm{b} \geq 0$ and $\pi \geq \theta_\mathrm{a} + \theta_\mathrm{b} \geq 0$.

These conditions see $\sin(\theta_\mathrm{a} \pm \theta_\mathrm{b}) \geq 0$. Eq. A.74 then implies $\Gamma_\mathrm{TE} \in \mathbb{R}^-$. It must then be true that $\mathrm{sign}(A_\mathrm{TE}) = -\mathrm{sign}(A'_\mathrm{TE})$. This corresponds to a change in phase of $\delta\phi = \pi$ upon reflection for the TE wave.

The phase shift of a reflected TM wave is not as trivial since Eq. A.75 contains tan, not sin, terms. For $\pi/2 \geq \theta_\mathrm{a,b} \geq 0$ with $\theta_\mathrm{a} > \theta_\mathrm{b}$, $\tan(\theta_\mathrm{a} - \theta_\mathrm{b}) \geq 0$ but $\tan(\theta_\mathrm{a} + \theta_\mathrm{b}) < 0$ only for $\theta_\mathrm{a} + \theta_\mathrm{b} > \pi/2$. Thus, for $\theta_\mathrm{a} + \theta_\mathrm{b} \leq \pi/2$, $\Gamma_\mathrm{TM} \in \mathbb{R}^+ \Rightarrow \mathrm{sign}(A_\mathrm{TE}) = \mathrm{sign}(A'_\mathrm{TE}) \Rightarrow \delta\phi = 0$ (no phase shift occurs) but for $\theta_\mathrm{a} + \theta_\mathrm{b} > \pi/2$, $\Gamma_\mathrm{TM} \in \mathbb{R}^- \Rightarrow \mathrm{sign}(A_\mathrm{TM}) = -\mathrm{sign}(A'_\mathrm{TM}) \Rightarrow \delta\phi = \pi$ (a π phase shift occurs).

In summary:

$$\delta\phi_\mathrm{TE} = \quad \pi \qquad \text{for } \pi \geq \theta_\mathrm{a} \geq 0, \tag{A.93}$$

$$\delta\phi_\mathrm{TM} = \begin{cases} 0 & \text{for } \theta_\mathrm{a} + \theta_\mathrm{b} \leq \pi/2 \\ \pi & \text{for } \theta_\mathrm{a} + \theta_\mathrm{b} > \pi/2. \end{cases} \tag{A.94}$$

The incidence angle at which the TM phase jumps from 0 to π can be expressed solely in terms of the incident angle and refractive indices via Eq. A.63: $\theta_\mathrm{a} + \theta_\mathrm{b} = \pi/2 \rightarrow \theta_\mathrm{a} = \pi/2 - \sin^{-1}(\frac{n_\mathrm{a}}{n_\mathrm{b}} \sin\theta_\mathrm{a})$.

The case for high- to low-index index propagation, $n_\mathrm{a} > n_\mathrm{b}$, will not be discussed in as much detail as total reflection and the existence of θ_c makes the analysis quite complicated ($k_{\mathrm{a}x,\mathrm{b}x} \in \mathbb{C}$ and $\theta_\mathrm{a,b} \in \mathbb{C}$). Regardless, total reflection is not a focus of this work. However, it is very important to note that it can be shown [14] that both the TE and TM polarisations undergo nontrivial phase shifts upon reflection in this regime:

$$\tan\left(\frac{\delta\phi_{\mathrm{TE}}}{2}\right) = -\frac{\sqrt{\sin^2\theta_{\mathrm{a}} - n_{\mathrm{b}}^2/n_{\mathrm{a}}^2}}{\cos\theta_{\mathrm{a}}}, \tag{A.95}$$

$$\tan\left(\frac{\delta\phi_{\mathrm{TM}}}{2}\right) = -\frac{\sqrt{\sin^2\theta_{\mathrm{a}} - n_{\mathrm{b}}^2/n_{\mathrm{a}}^2}}{(n_{\mathrm{b}}^2/n_{\mathrm{a}}^2)\cos\theta_{\mathrm{a}}}, \tag{A.96}$$

sometimes called the *Goos-Hänchen phase shift*. Both phases continuously increase from 0 to π as θ_{a} goes from θ_{c} to $\pi/2$. The fact that this phase shift not only depends on the explicit values of n_{a}, n_{b} and θ_{a} but is also *transcendental* in form is critical for observing how its absence leads to the analytic nature of Eqs. A.93 and A.94 and hence to the establishment, and subsequent novel utility, of the SPARROW model constructed in Chapter 3.

A.2.1.3 Light Guidance in a Single Layer

The plane wave propagation, reflection and transmission behaviour presented in sections A.2.1.1 and A.2.1.2 is used here to describe the light guidance properties of a single dielectric layer. The basic principle is simple: a ray propagating within a layer will be partially or totally reflected from an interface with the bounding medium; this happens for each reflected ray on its opposing interface, essentially trapping the reflected rays within the layer. This is the fundamental premise of *waveguidance* and is represented schematically in Fig. A.1.

Hereon, two particular refractive indices will be discussed: n_1 and n_0 where $n_1 > n_0$. The local index n_{a} and adjacent index n_{b} (representing core and cladding indices of a waveguide, for example, respectively) can take either of these values. In other words, n_{a} and n_{b} are arbitrary but n_1 and n_0 are fixed to values in which $n_1 > n_0$.

Total reflection will not be considered here since, according to Corollary A.2, any ray originating from a low-index medium, as is the case for the majority of the present work, cannot undergo total reflection within any surrounding (parallel) layer. Thus, only *leaky* guidance within a given layer is of interest here.

More precisely, for a ray originating within a medium of lowest refractive index n_0, we are interested only in guided rays with effective indices $\tilde{n}_{\mathrm{a}}$ *below* the n_0-light-line ($\tilde{n}_{\mathrm{a}} < n_0$), which is strictly the full range of $\tilde{n}$ available to a ray incident from n_0 via Eq. A.90 over all incidence angles $0 \leq \theta_{\mathrm{a}} \leq \pi/2$.

Consider a homogeneous planar dielectric layer of refractive index n_{a} (the *core*) embedded in an infinite homogeneous dielectric medium of refractive index n_{b} (the *cladding*).

The bottom schematic of Fig. A.1 shows one such example. Following the conventions introduced in Fig. A.1, used in Sections A.2.1.1 and A.2.1.2, a given ray within the core will have wave-vector $\mathbf{k}_{\mathrm{a}}$ and will be reflected at the core-cladding interface at an angle θ_{a} to the interface normal. Rays transmitted across an interface have wave-vector $\mathbf{k}_{\mathrm{b}}$ and make an angle θ_b with the interface normal.

The phase accumulated by plane wave with oscillatory term $e^{i(\omega t-\mathbf{k}\cdot\mathbf{r})}$ (§ A.2.1.2) is:

$$\Delta\phi = \mathbf{k}\cdot\Delta\mathbf{r} = k_x\Delta x + \beta\Delta z. \tag{A.97}$$

Thus, the phase accumulated in the longitudinal dimension is $\beta\Delta z$ and the accumulated phase in the transverse dimension is $k_x\Delta x$.

The slab waveguides will only support modes, leaky or otherwise, if the accumulated transverse phase for one round-trip of the slab (traversing the slab twice due to reflection from each interface) is an integer multiple of 2π. For both slabs, the transverse phase accumulated by traversing the slab region once is $k_{\mathrm{a}x}t_{\mathrm{a}}$. The forms of the low- and high-index slabs' phase relations thus differ only in their reflection terms which were just discussed above. Since only the $\tilde{n} \leq n_0$ is of interest here, restricting oneself to light originating from a low-index region (Corollaries A.1 and A.2), the phase shifts for each case are only integer multiples of π (avoiding the Goos-Hänchen phase shift). Equating the cumulative phase shifts to $m2\pi$ ($m \in \mathbb{Z}^+$), a dispersion relation for each waveguide is derived [178, 198]:

$$k_{\mathrm{ax}}t_{\mathrm{a}} = \begin{cases} m\pi & \text{for } n_{\mathrm{a}} > n_{\mathrm{b}} \text{ and } m \in \mathbb{N} \\ (m+1)\pi & \text{for } n_{\mathrm{a}} < n_{\mathrm{b}} \text{ and } m \in \mathbb{Z}^+ \end{cases} \tag{A.98}$$

where $m = 0$ is obviously not allowed for the high-index slab, implying that the $m = 0$ bound mode has no leaky counterpart [178]. By rearranging the phase relations and setting a $\rightarrow$ 1 and b $\rightarrow$ 0 for the high-index ($n_{\mathrm{a}} = n_1 > n_{\mathrm{b}} = n_0$) slab and a $\rightarrow$ 0 and b $\rightarrow$ 1 for the low-index ($n_{\mathrm{a}} = n_0 < n_{\mathrm{b}} = n_1$) slab, we find a unified dispersion relation:

$$\tilde{n}_{m_i} = \left[n_i^2 - \left(\frac{m_i\pi}{t_i k}\right)^2\right]^{\frac{1}{2}}, \quad m_i \in \mathbb{N} \tag{A.99}$$

such that $m_1 = m$ and $m_0 = m+1$. Groups of dispersion curves for a range of mode orders are plotted in Fig. 3.3 (bottom) and subsequently in Figs. 3.4, 3.7 and 3.8.

Here it is convenient to define that $m_1 = 0$ refers to the $\tilde{n}$-axis ($k = 0$) and $m_0 = 0$ to the n_0-light-line ($\tilde{n} = n_0$). It is easily shown that, while not representative of physical modes, these definitions still satisfy Eqs. A.98 and A.99. Hereon the 'SPARROW curves' will refer to both the physical slab dispersion curves ($m_{1,0} \in \mathbb{N}$) *and* these $m_{1,0} = 0$ lines, unless otherwise specified. The lower limit line $\tilde{n} = 0$ is also important but its inclusion in this set is not required, as will soon be evident.

Note that Eq. A.99 is truly analytic since the non-analytic Goos-Hänchen phase shift [198] that appears in the bound-mode ($\tilde{n}_{m_1} > n_0$) solution of the high-index slab does not appear in these phase relations due to the nature of the reflective phase shifts for $\tilde{n}_{m_i} < n_0$. Also note how Eq. A.99 depends only on n_i, implying that, below the n_0-light-line, the dispersion properties of each slab depend only on the slab refractive index, not that of the medium surrounding it.

Eq. A.99 can be arranged to give the k values of resonances of order m_i for arbitrary $\tilde{n}$ as:

$$k_{m_i} = \frac{m_i \pi}{t_i} \left[n_i^2 - \tilde{n}^2 \right]^{-\frac{1}{2}}, \tag{A.100}$$

where, once expressed in wavelength, it is obvious that the forms of the large-core Duguay-ARROW model (Eq. 3.2) and SPARROW model (Eq. A.100) are identical save for two important differences: the SPARROW model is valid for all $\tilde{n} \leq n_0$ and depends explicitly on t_0.

A.3 Multilayer Planar Systems

A.3.1 Matrix Analysis of a Finite Multilayer Structure

The propagation of electromagnetic waves through multilayer structures is now considered. I will refer to the technique as the *planar transfer matrix method* (pTMM). The basis of the analysis presented below is adopted from [153], although many expressions have been reformulated somewhat differently for consistency. Many of the results of Sections A.2.1.1 and A.2.1.2 are leveraged here.

Consider an arbitrary number of stratified dielectric layers producing a refractive index profile:

$$n(x) = \begin{cases} n_0, & x < x_0 \\ n_1, & x_0 < x < x_1 \\ n_2, & x_1 < x < x_2 \\ \vdots & \vdots \\ n_N, & x_{N-1} < x < x_N \\ n_{N+1}, & x_N < x \end{cases}, \tag{A.101}$$

where the interface between the m^{th} and $(m+1)^{\text{th}}$ layers sits at $x = x_m$. There are thus N layers (with indices $1 \to N$) surrounded by two infinite homogeneous regions (of indices 0 and $N+1$). Figure A.5 shows a schematic of such a structure. Each layer of refractive index n_m has thickness $t_m = x_m - x_{m-1}$.

Across each interface, electric fields will behave according to the Fresnel Formulae, Eqs. A.70 to A.73. As discussed in Section A.2.1.2, the Principle of Reciprocity allows one to easily consider waves approaching an interface from either side. Since a multilayer structure doesn't just transmit but also partially reflects light at each and every interface, one must indeed consider waves propagating in both directions. To this end, one can define an arbitrary field in the m^{th} layer as:

$$E = \left[A_m e^{-ik_{mx}(x-x_m)} + B_m e^{+ik_{mx}(x-x_m)}\right] e^{i(\omega t - \beta z)} \tag{A.102}$$

where the amplitude A_m corresponds to a wave propagating in the $+x$ direction and B_m to a wave in the $-x$ direction. Figure A.5 demonstrates the field amplitude nomenclature explicitly; where they must be distinguished, fields within a layer close to the $+x$ side will be designated with a prime (*e.g.*, A'_m), whereas those close to the $-x$ side will be unprimed (*e.g.*, A_m). As will be shown presently, the primed and unprimed fields in a layer have the same magnitude and are related only by a phase term. Every wave within all layers has the same value of β, due to conservation of longitudinal wavenumber (Eq. A.63), *i.e.*, β is independent of m. k_{mx} is the transverse wavenumber, as defined

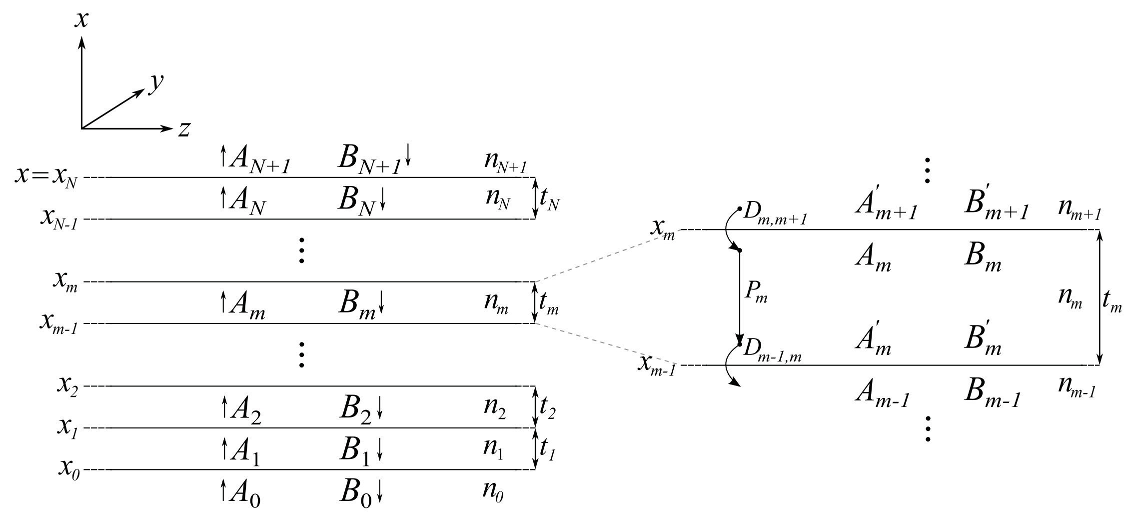

FIGURE A.5: *Left:* A schematic of a general finite planar multilayer optical structure, Eq. A.101. As per Eq. A.102, waves of amplitude A_m travel in the $+x$ direction while waves of amplitude B_m travel in the $-x$ direction. *Right:* A zoom-in of an arbitrary layer, defining the nomenclature for fields about either side of its interfaces.

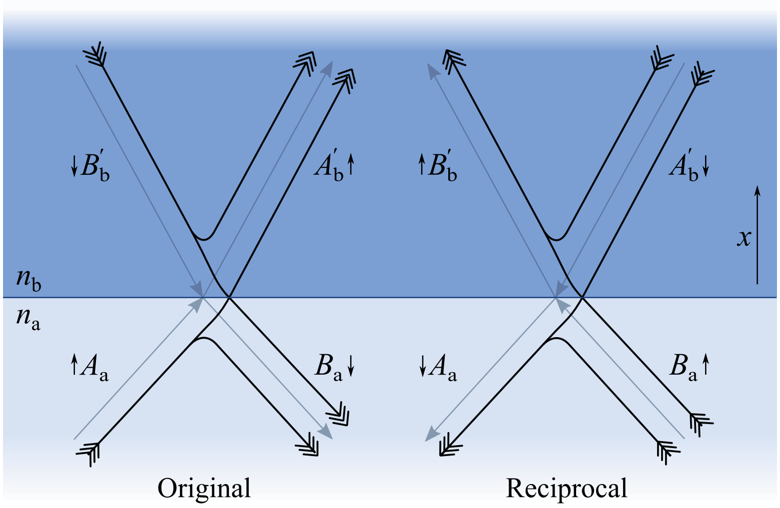

FIGURE A.6: A qualitative a representation of the incident, reflected and transmitted waves related through the principle of reciprocity. As per Eq. A.102, waves of amplitude A_m travel in the $+x$ direction while waves of amplitude B_m travel in the $-x$ direction. The reciprocal (time reversed) versions of the waves travel in the inverse direction. The bold curved lines indicate which waves are involved in interactions for the original (1 wave generates 2) and reciprocal (2 waves generate 1) cases.

in Section A.2.1.2. The x-dependence of the fields across the layers is thus:

$$E(x) = \begin{cases} A_0 e^{-ik_{0x}(x-x_0)} + B_0 e^{ik_{0x}(x-x_0)}, & x < x_0 \\ A_m e^{-ik_{mx}(x-x_m)} + B_m e^{ik_{mx}(x-x_m)}, & x_{m-1} < x < x_m \\ A_{N+1} e^{-ik_{(N+1)x}(x-x_N)} + B_{N+1} e^{ik_{(N+1)x}(x-x_N)}, & x > x_N. \end{cases} \tag{A.103}$$

It is possible to formulate a matrix equation relating the inner field amplitudes A_0 and B_0 to the outer field amplitudes[16] A_{N+1} and B_{N+1}:

$$\begin{pmatrix} A_0 \\ B_0 \end{pmatrix} = M \begin{pmatrix} A_{N+1} \\ B_{N+1} \end{pmatrix}. \tag{A.104}$$

This section will predominantly be devoted to deriving the form of M and its subsequent properties.

First consider how the fields change across an arbitrary interface as represented by Fig. A.6. By the Principle of Reciprocity, time-reversed waves are related as (Eqs. A.81

[16]The prime can be dropped from the $N+1$ region's fields since the primed and unprimed distinction becomes redundant in such an infinite homogeneous region.

and A.82):

$$A_{\rm a} = \Gamma_{\rm ab} B_{\rm a} + T_{\rm ba} A'_{\rm b}, \tag{A.105}$$

$$B'_{\rm b} = \Gamma_{\rm ba} A'_{\rm b} + T_{\rm ab} B_{\rm a}. \tag{A.106}$$

where Γ and T are the reflection and transmission coefficients defined in Section A.2.1.2. Figure A.6 gives a qualitative representation of the original and reciprocal interactions. Using these relations, one can construct a matrix relation between the fields on either side of the interface:

$$\begin{pmatrix} A_{\rm a} \\ B_{\rm a} \end{pmatrix} = D_{\rm ab} \begin{pmatrix} A'_{\rm b} \\ B'_{\rm b} \end{pmatrix}. \tag{A.107}$$

$D_{\rm ab}$ can be expressed in terms of Γ and T. Rearranging Eq. A.105 and using Eq. A.83:

$$B_{\rm a} = \frac{\Gamma_{\rm ab}}{T_{\rm ab}} A'_{\rm b} + \frac{B'_{\rm b}}{T_{\rm ab}}. \tag{A.108}$$

Inserting this into Eq. A.106 and using Eq. A.83 then Eq. A.84, one finds:

$$A_{\rm a} = \frac{A'_{\rm b}}{T_{\rm ab}} + \frac{\Gamma_{\rm ab}}{T_{\rm ab}} B'_{\rm b}, \tag{A.109}$$

producing:

$$D_{\rm ab} = \frac{1}{T_{\rm ab}} \begin{pmatrix} 1 & \Gamma_{\rm ab} \\ \Gamma_{\rm ab} & 1 \end{pmatrix}. \tag{A.110}$$

All other interfaces require the fields to also be propagated across the layer defined by adjacent interfaces, not just transmitted or reflected at the first interface. Since each wave simply accumulates a phase of $\phi_m = k_{mx} t_m$ in the x-dimension between the m and the $(m+1)^{\rm th}$ interfaces, the field amplitudes between these two points (see Fig. A.5) are thus related by:

$$\begin{pmatrix} A'_{\rm m} \\ B'_{\rm m} \end{pmatrix} = P_m \begin{pmatrix} A_{\rm m} \\ B_{\rm m} \end{pmatrix}. \tag{A.111}$$

where:

$$P_m = \begin{pmatrix} e^{i\phi_m} & 0 \\ 0 & e^{-i\phi_m} \end{pmatrix}. \tag{A.112}$$

such that for propagation across and between interfaces at x_m and x_{m+1}:

$$\begin{pmatrix} A_{m-1} \\ B_{m-1} \end{pmatrix} = D_{m-1,m} P_m \begin{pmatrix} A_m \\ B_m \end{pmatrix}. \tag{A.113}$$

This then allows one to express the evolution of the reciprocal fields from the outermost interface ($x = x_{N+1}$) to the innermost ($x = x_0$). With this in mind, it is clear that propagation across the first interface ($x = x_{N+1}$) needn't consider initial phase accumulation since the bounding medium is infinite, and the phase term becomes redundant. The propagation of fields across the total system can thus be embodied in the M matrix from Eq. A.104 as:

$$M = \begin{pmatrix} M_{11} & M_{12} \\ M_{21} & M_{22} \end{pmatrix} = \left(\prod_{m=1}^{N} D_{m-1,m} P_m \right) D_{N,N+1}. \tag{A.114}$$

Directly from this, one can express the reflection and transmission coefficients for the entire system. For propagation from the n_0 region through to the n_{N+1} region, $\Gamma_{0\mathrm{s}}$ and $T_{0\mathrm{s}}$ are found to be:

$$\Gamma_{0s} = \frac{B_0}{A_0} = \frac{M_{21}}{M_{11}}, \tag{A.115}$$

$$T_{0s} = \frac{A_{N+1}}{A_0} = \frac{1}{M_{11}}. \tag{A.116}$$

where $s \equiv N + 1$ is defined for convenience. These expressions are derived from simultaneous equations provided by Eq. A.104 with $B_{N+1} = 0$ (physically required: no incoming waves from infinity; B_{N+1} has nothing to have been reflected from, hence can't exist).

Just as for the single interface versions, Eqs. A.76 and A.77, from $\Gamma_{0,N+1}$ and $T_{0,\mathrm{N+1}}$ one can define the reflectance ($\mathcal{R}_{0s}$) and transmittance ($\mathcal{T}_{0s}$) coefficients for the whole system[17]:

$$\mathcal{R}_{0s} = |\Gamma_{0s}|^2 = \left| \frac{M_{21}}{M_{11}} \right|^2, \tag{A.117}$$

$$\mathcal{T}_{0s} = \frac{k_{sx}}{k_{0x}} |T_{0s}|^2 = \frac{k_{sx}}{k_{0x}} \left| \frac{1}{M_{11}} \right|^2. \tag{A.118}$$

These coefficients can be evaluated for TE and TM waves for any conceivable stratified planar system and are used explicitly in Chapter 3.

A.3.2 Bandgap Analysis of an Infinitely Periodic Multilayer Structure

While the matrix analysis of Section A.3.1 can be implemented for an arbitrary number of layers N, the calculations become increasingly cumbersome as $N \to \infty$; $N \geq 3$ becomes essentially prohibitive analytically and numerical calculations take longer for increasing

[17] This expression for $\mathcal{T}_{0s}$ requires that the bounding media be dielectrics and the incident waves have real k_{0x}. The latter is satisfied when n_0 is the lowest or equal-lowest refractive index in the system, discussed in Section A.2.1.2, which is the case throughout this work.

values of N. There is a more elegant way to describe the optical behaviour of an infinite multilayer stack, involving mathematical techniques exploited predominantly in solid-state physics. In fact, much of the following analysis is isomorphic to the Kronig-Penney model used in solid-state physics to describe the energy levels of atomic lattices [181]. The treatment given here is similar to that from [153] but has been significantly reworked in order to make it make clear, to simplify and to highlight the underlying physics of certain theoretical forms in the current context (any results that appear quite different in form to their equivalents in the cited references are described as such in the text).

An infinitely periodic multilayer structure is a essentially a one-dimensional lattice that is invariant under lattice translation. For a lattice pitch Λ, Fig. 2.3 of Chapter 2, the refractive index distribution must then satisfy:

$$n(x + \Lambda) = n(x). \tag{A.119}$$

The most general one dimensional structure satisfying this condition is that of Eq. A.101, but where the pattern repeats indefinitely for $x < x_0$ and $x > x_N$, *i.e.*, a lattice unit cell is then represented by a sub-section of the structure within some range $x = x_m \rightarrow x_m + \Lambda$ for any m. Of course, it naturally follows that the sum of the unit cell's layers' thicknesses sum to the pitch $\Lambda = \sum_{m=0}^{N} t_m$.

The Bloch-Floquet theorem states that solutions for the appropriate wave equations over this structure must be of the form [34]:

$$E_K(x, z) = E_K(x)e^{-i\beta z}e^{\pm iKx}, \tag{A.120}$$

where $E_k(x)$ has the same periodicity as the supporting lattice:

$$E_K(x + \Lambda) = E_K(x), \tag{A.121}$$

and K is called the *Bloch wave number*. The ambiguity in the sign of the exponential argument comes from the fact that the Bloch wave can propagate either direction over the one dimensional lattice. The fields between unit cells of the lattice thus differ by a phase of $K\Lambda$, *i.e.*, since the field amplitude E_K at two points separated along the x-dimension by a distance Λ must be the same, via Eq. A.120, the fields must differ by a unitary factor expressing the accumulated phase $E_K \rightarrow E_K e^{-iK\Lambda}$ (for propagation in the positive x direction). In other words, the fields propagating across the unit cell are related as:

$$\begin{pmatrix} A_m \\ B_m \end{pmatrix} = e^{\pm iK\Lambda} \begin{pmatrix} A_{m-N} \\ B_{m-N} \end{pmatrix}. \tag{A.122}$$

Similar to the treatment in Section A.3.1, the propagation of fields across a unit cell (Fig. A.5) can be described via a transfer matrix formulation:

$$\begin{pmatrix} A_{m-N} \\ B_{m-N} \end{pmatrix} = M \begin{pmatrix} A_m \\ B_m \end{pmatrix}, \tag{A.123}$$

much like Eq. A.104. Indeed, the decomposition of M from Eq. A.114 also holds here, where the relevant layers are only those of a unit cell and not of the entire (infinite) system at hand.

Equations A.122 and A.123 both represent propagation of fields across the entire unit cell. Combining them gives:

$$\begin{pmatrix} M_{11} M_{12} \\ M_{21} M_{22} \end{pmatrix} \begin{pmatrix} A_m \\ B_m \end{pmatrix} = e^{\mp iK\Lambda} \begin{pmatrix} A_m \\ B_m \end{pmatrix}, \tag{A.124}$$

which is clearly an eigenvalue equation with eigenvalue $e^{iK\Lambda}$. According to general result of Eq. B.9, this unit cell transfer matrix has eigenvalues:

$$e^{\mp iK\Lambda} = \mathrm{Tr}(M/2) \pm \sqrt{\mathrm{Tr}^2(M/2) - \det(M)}, \tag{A.125}$$

where the $\mp$ and $\pm$ aren't necessarily correlated.

The $N = 2$ special case is now focused on, the above results being valid for any number of unit cell layers. The refractive index profile of a unit cell is thus:

$$n(x) = \begin{cases} n_1, & x_{m-2} < x < x_{m-1} \\ n_2, & x_{m-1} < x < x_m, \end{cases}, \tag{A.126}$$

where $n_{m+2} = n_m$ by the periodic construction. The thickness of the unit cell is equal to the lattice pitch $\Lambda = t_m + t_{m-1} = x_m - x_{m-2}$.

The transfer matrix can thus be decomposed as per Eq. A.114:

$$M = D_{12} P_2 D_{21} P_1. \tag{A.127}$$

Terms from right to left (also Fig. A.5): propagation across layer with refractive index n_1, propagation across interface of refractive index n_1 to n_2, propagation across layer with refractive index n_2, propagation across interface of refractive index n_2 to n_1. The end terms are different (P and D matrices), not both D matrices as in Eq. A.114, since the unit cell repeats indefinitely (there is no final infinite homogeneous medium to propagate into); the expression for M must begin with a D and finish with a P, or vice verca, in order to represent the periodicity of the system.

The details of the following deviate quite a bit from the treatment of [153] in that I consider Γ and T explicitly in the matrices here. I feel this makes the analysis simpler and more intuitive and also makes derivations based on the results easier to construct.

Expanding Eq. A.127 using Eqs. A.110 and A.112:

$$\begin{aligned}
M &= D_{12}P_2D_{21}P_1 \\
&= \frac{1}{T_{12}T_{21}}\begin{pmatrix} 1 & \Gamma_{12} \\ \Gamma_{12} & 1 \end{pmatrix}\begin{pmatrix} e^{i\phi_2} & 0 \\ 0 & e^{-i\phi_2} \end{pmatrix}\begin{pmatrix} 1 & \Gamma_{21} \\ \Gamma_{21} & 1 \end{pmatrix}\begin{pmatrix} e^{i\phi_1} & 0 \\ 0 & e^{-i\phi_1} \end{pmatrix} \\
&= \frac{1}{T_{12}T_{21}}\begin{pmatrix} e^{i\phi_2} & e^{-i\phi_2}\Gamma_{12} \\ e^{i\phi_2}\Gamma_{12} & e^{-i\phi_2} \end{pmatrix}\begin{pmatrix} e^{i\phi_1} & e^{-i\phi_1}\Gamma_{21} \\ e^{i\phi_1}\Gamma_{21} & e^{-i\phi_1} \end{pmatrix} \\
&= \frac{1}{T_{12}T_{21}}\begin{pmatrix} e^{i\phi_1}e^{i\phi_2} + e^{i\phi_1}e^{-i\phi_2}\Gamma_{12}\Gamma_{21} & e^{-i\phi_1}e^{-i\phi_2}\Gamma_{12} + e^{-i\phi_1}e^{i\phi_2}\Gamma_{21} \\ e^{i\phi_1}e^{i\phi_2}\Gamma_{12} + e^{i\phi_1}e^{-i\phi_2}\Gamma_{21} & e^{-i\phi_1}e^{-i\phi_2} + e^{-i\phi_1}e^{i\phi_2}\Gamma_{12}\Gamma_{21} \end{pmatrix}, \qquad \text{(A.128)}
\end{aligned}$$

implying (Eq. A.114):

$$\begin{aligned}
M_{11} &= \frac{1}{T_{12}T_{21}}\left(e^{i\phi_1}e^{i\phi_2} + e^{i\phi_1}e^{-i\phi_2}\Gamma_{12}\Gamma_{21}\right) \\
&= \frac{e^{i\phi_1}}{T_{12}T_{21}}\left(e^{i\phi_2} + e^{-i\phi_2}\Gamma_{12}\Gamma_{21}\right) \\
\text{(by Eq. } B.14) \quad &= \frac{e^{i\phi_1}}{T_{12}T_{21}}\left[(1+\Gamma_{12}\Gamma_{21})\cos\phi_2 + (1-\Gamma_{12}\Gamma_{21})i\sin\phi_2\right] \\
\text{(by Eq. } A.84) \quad &= e^{i\phi_1}\left[\cos\phi_2 + \left(\frac{2}{T_{12}T_{21}} - 1\right)i\sin\phi_2\right], \qquad \text{(A.129)}
\end{aligned}$$

$$\begin{aligned}
M_{12} &= \frac{1}{T_{12}T_{21}}\left(e^{-i\phi_1}e^{i\phi_2}\Gamma_{21} + e^{-i\phi_1}e^{-i\phi_2}\Gamma_{12}\right) \\
&= \frac{e^{-i\phi_1}}{T_{12}T_{21}}\left(e^{i\phi_2}\Gamma_{21} + e^{-i\phi_2}\Gamma_{12}\right) \\
\text{(by Eq. } A.83) &= e^{-i\phi_1}\frac{\Gamma_{21}}{T_{12}T_{21}}\left(e^{i\phi_2} - e^{-i\phi_2}\right) \\
&= e^{-i\phi_1}\frac{\Gamma_{21}}{T_{12}T_{21}}2i\sin\phi_2, \qquad \text{(A.130)}
\end{aligned}$$

$$\begin{aligned}
M_{21} &= \frac{1}{T_{12}T_{21}}\left(e^{i\phi_1}e^{i\phi_2}\Gamma_{12} + e^{i\phi_1}e^{-i\phi_2}\Gamma_{21}\right) \\
&= \frac{e^{i\phi_1}}{T_{12}T_{21}}\left(e^{i\phi_2}\Gamma_{12} + e^{-i\phi_2}\Gamma_{21}\right) \\
\text{(by Eq. } A.83) &= -e^{i\phi_1}\frac{\Gamma_{21}}{T_{12}T_{21}}\left(e^{i\phi_2} - e^{-i\phi_2}\right) \\
&= -e^{i\phi_1}\frac{\Gamma_{21}}{T_{12}T_{21}}2i\sin\phi_2,
\end{aligned} \tag{A.131}$$

$$\begin{aligned}
M_{22} &= \frac{1}{T_{12}T_{21}}\left(e^{-i\phi_1}e^{i\phi_2}\Gamma_{12}\Gamma_{21} + e^{-i\phi_1}e^{-i\phi_2}\right) \\
&= \frac{e^{-i\phi_1}}{T_{12}T_{21}}\left(e^{i\phi_2}\Gamma_{12}\Gamma_{21} + e^{-i\phi_2}\right) \\
\text{(by Eq. } B.14) \quad &= \frac{e^{-i\phi_1}}{T_{12}T_{21}}\left[(1+\Gamma_{12}\Gamma_{21})\cos\phi_2 - (1-\Gamma_{12}\Gamma_{21})i\sin\phi_2\right] \\
\text{(by Eq. } A.84) \quad &= e^{-i\phi_1}\left[\cos\phi_2 - \left(\frac{2}{T_{12}T_{21}} - 1\right)i\sin\phi_2\right].
\end{aligned} \tag{A.132}$$

More succinctly:

$$M_{11} = e^{i\phi_1}\left[\cos\phi_2 + \left(\frac{2}{T_{12}T_{21}} - 1\right)i\sin\phi_2\right] \tag{A.133}$$

$$M_{12} = e^{-i\phi_1}\frac{\Gamma_{21}}{T_{12}T_{21}}2i\sin\phi_2 \tag{A.134}$$

$$M_{21} = -e^{i\phi_1}\frac{\Gamma_{21}}{T_{12}T_{21}}2i\sin\phi_2 \tag{A.135}$$

$$M_{22} = e^{-i\phi_1}\left[\cos\phi_2 - \left(\frac{2}{T_{12}T_{21}} - 1\right)i\sin\phi_2\right]. \tag{A.136}$$

which holds for both TE and TM polarisations, taking the correct $\Gamma_{\mathrm{TE,TM}}$ and $T_{\mathrm{TE,TM}}$ for each case. This formulation, and its derivation, is unique to this Thesis and is more general than that typically shown in the literature [36, 153], as only Γ and T themselves are used, an explicit form of them not being required.

The form of the transfer matrix in [36, 153] can be deduced from this by explicitly expanding Γ and T via Eqs.A.70 to A.73. For TE polarisation:

$$\left(\frac{2}{T_{12}T_{21}} - 1\right) = \frac{(k_{1x}+k_{2x})^2}{2k_{1x}k_{2x}} - 1 = \frac{k_{1x}^2+k_{2x}^2}{2k_{1x}k_{2x}} = \frac{1}{2}\left(\frac{k_{1x}}{k_{2x}} + \frac{k_{2x}}{k_{1x}}\right), \tag{A.137}$$

and:

$$\frac{\Gamma_{21}}{T_{12}T_{21}} = \frac{\left(\frac{k_{2x}-k_{1x}}{k_{1x}+k_{2x}}\right)}{\left(\frac{2k_{1x}}{k_{1x}+k_{2x}}\frac{2k_{2x}}{k_{1x}+k_{2x}}\right)} = \frac{(k_{2x}-k_{1x})(k_{1x}+k_{2x})}{4k_{1x}k_{2x}} = \frac{1}{4}\left(\frac{k_{2x}}{k_{1x}} - \frac{k_{1x}}{k_{2x}}\right), \tag{A.138}$$

The expansions for the TM polarisation produces exactly the same forms but with $k_{lx} \rightarrow n_l^2 k_{lx}$ (as per Eqs. A.70 to A.73). Substituting Eqs. A.137 and A.138 into Eqs. A.133 to A.136, for TE waves:

$$M_{11}^{\mathrm{TE}} = e^{ik_{1x}t_1}\left[\cos(k_{2x}t_2) + \frac{i}{2}\left(\frac{k_{1x}}{k_{2x}} + \frac{k_{2x}}{k_{1x}}\right)\sin(k_{2x}t_2)\right] \tag{A.139}$$

$$M_{12}^{\mathrm{TE}} = \frac{ie^{-ik_{1x}t_1}}{2}\left(\frac{k_{2x}}{k_{1x}} - \frac{k_{1x}}{k_{2x}}\right)\sin(k_{2x}t_2) \tag{A.140}$$

$$M_{21}^{\mathrm{TE}} = \frac{-ie^{ik_{1x}t_1}}{2}\left(\frac{k_{2x}}{k_{1x}} - \frac{k_{1x}}{k_{2x}}\right)\sin(k_{2x}t_2) \tag{A.141}$$

$$M_{22}^{\mathrm{TE}} = e^{-ik_{1x}t_1}\left[\cos(k_{2x}t_2) - \frac{i}{2}\left(\frac{k_{1x}}{k_{2x}} + \frac{k_{2x}}{k_{1x}}\right)\sin(k_{2x}t_2)\right]. \tag{A.142}$$

and for TM waves (instead using the $k_{lx} \rightarrow n_l^2 k_{lx}$ forms of Eqs. A.137 and A.138):

$$M_{11}^{\mathrm{TM}} = e^{ik_{1x}t_1}\left[\cos(k_{2x}t_2) + \frac{i}{2}\left(\frac{n_1^2 k_{1x}}{n_2^2 k_{2x}} + \frac{n_2^2 k_{2x}}{n_1^2 k_{1x}}\right)\sin(k_{2x}t_2)\right] \tag{A.143}$$

$$M_{12}^{\mathrm{TM}} = \frac{ie^{-ik_{1x}t_1}}{2}\left(\frac{n_2^2 k_{2x}}{n_1^2 k_{1x}} - \frac{n_1^2 k_{1x}}{n_2^2 k_{2x}}\right)\sin(k_{2x}t_2) \tag{A.144}$$

$$M_{21}^{\mathrm{TM}} = \frac{-ie^{ik_{1x}t_1}}{2}\left(\frac{n_2^2 k_{2x}}{n_1^2 k_{1x}} - \frac{n_1^2 k_{1x}}{n_2^2 k_{2x}}\right)\sin(k_{2x}t_2) \tag{A.145}$$

$$M_{22}^{\mathrm{TM}} = e^{-ik_{1x}t_1}\left[\cos(k_{2x}t_2) - \frac{i}{2}\left(\frac{n_1^2 k_{1x}}{n_2^2 k_{2x}} + \frac{n_2^2 k_{2x}}{n_1^2 k_{1x}}\right)\sin(k_{2x}t_2)\right]. \tag{A.146}$$

These explicit forms of M for the TE and TM waves are identical to those given in [36, 153] but they were arrived at here through a more general route here.

In either formulation, one can readily see that:

$$M_{22} = M_{11}^*, \tag{A.147}$$

$$M_{21} = M_{12}^*. \tag{A.148}$$

Indeed, from the precursor (Eq. A.128) of the general form of M (Eqs. A.133→ A.136), and with the knowledge that $\Gamma, T \in \mathbb{R}$ in the absence of total reflection ($\theta \in \mathbb{R}$), as is the case for the work at hand, one finds:

$$\begin{aligned} M_{11}M_{22} = |M_{11}|^2 &= \frac{1}{(T_{12}T_{21})^2}(e^{i\phi_1}e^{i\phi_2} + e^{i\phi_1}e^{-i\phi_2}\Gamma_{12}\Gamma_{21})(e^{-i\phi_1}e^{-i\phi_2} + e^{-i\phi_1}e^{i\phi_2}\Gamma_{12}\Gamma_{21}) \\ &= \frac{1}{(T_{12}T_{21})^2}[(\Gamma_{12}\Gamma_{21})^2 + (e^{2i\phi_2} + e^{-2i\phi_2})\Gamma_{12}\Gamma_{21} + 1], \end{aligned} \tag{A.149}$$

$$\begin{aligned}
M_{12}M_{21} = |M_{12}|^2 &= \frac{1}{(T_{12}T_{21})^2}(e^{-i\phi_1}e^{i\phi_2}\Gamma_{21} + e^{-i\phi_1}e^{-i\phi_2}\Gamma_{12})(e^{i\phi_1}e^{-i\phi_2}\Gamma_{21} + e^{i\phi_1}e^{i\phi_2}\Gamma_{12}) \\
&= \frac{1}{(T_{12}T_{21})^2}[\Gamma_{21}^2 + \Gamma_{12}^2 + (e^{2i\phi_2} + e^{-2i\phi_2})\Gamma_{12}\Gamma_{21}] \\
\text{(by Eq. } A.83) \quad &= \frac{(e^{2i\phi_2} + e^{-2i\phi_2} - 2)\Gamma_{12}\Gamma_{21}}{(T_{12}T_{21})^2}.
\end{aligned} \tag{A.150}$$

The matrix M is then found to be *unitary* (its determinant is unity):

$$\begin{aligned}
\det(M) &= M_{11}M_{22} - M_{12}M_{21} = |M_{11}|^2 - |M_{12}|^2 \\
&= \frac{[(\Gamma_{12}\Gamma_{21})^2 + (e^{2i\phi_2} + e^{-2i\phi_2})\Gamma_{12}\Gamma_{21} + 1] - (e^{2i\phi_2} + e^{-2i\phi_2} - 2)\Gamma_{12}\Gamma_{21}}{(T_{12}T_{21})^2} \\
&= \frac{(\Gamma_{12}\Gamma_{21})^2 + 2\Gamma_{12}\Gamma_{21} + 1}{(T_{12}T_{21})^2} \\
&= \frac{(\Gamma_{12}\Gamma_{21} + 1)^2}{(T_{12}T_{21})^2} \\
\text{(by Eq. } A.84) \quad &= 1.
\end{aligned} \tag{A.151}$$

Since M is unitary, by Section B.2, its two eigenvalues must be the *inverse* of each other. From Eq. A.124, the eigenvalues $e^{\mp iK\lambda}$ satisfy this requirement. These eigenvalues must then satisfy [using Eq. A.125 with $\det(M) = 1$]:

$$e^{\mp iK\Lambda} = \frac{M_{11} + M_{22}}{2} \pm \sqrt{\left(\frac{M_{11} + M_{22}}{2}\right)^2 - 1}. \tag{A.152}$$

The $\mp$ and $\pm$ aren't necessarily correlated.

By adding the two eigenvalues together, one can then solve for the Bloch wavenumber itself:

$$K(\tilde{n}, \omega) = \frac{1}{\Lambda}\cos^{-1}[\mathrm{Re}(M_{11})] \tag{A.153}$$

where Eq. A.147 has been used, producing $M_{11} + M_{22} = M_{11} + M_{11}^* = \mathrm{Re}(M_{11})$.

Immediately one can say that for waves with $\tilde{n}$ and ω producing $|\mathrm{Re}(M_{11})| \leq 1$, K will be real and hence, by the field expression of Eq. A.120, correspond to Bloch waves propagating in one or the other direction across the infinite structure without loss.

However, if a wave produces $|\mathrm{Re}(M_{11})| > 1$, then K will be complex and hence have an imaginary part: $K = \frac{m\pi}{\Lambda} \pm iK_i$, where $K_i \in \mathbb{R}^+$. More precisely, for $\mathrm{Re}(M_{11}) > 1$, $K = \frac{m\pi}{\Lambda} + iK_i$, and for $\mathrm{Re}(M_{11}) \leq -1$, $K = \frac{(m+1)\pi}{\Lambda} - iK_i$, due to the nature of the $\cos^{-1}$ function. By Eq. A.120, $\mathrm{Re}(M_{11}) > 1$ thus corresponds to a Bloch wave with exponential dependence e^{iKx}, in order to avoid an unphysical gain term. Similarly, $\mathrm{Re}(M_{11}) \leq -1$ corresponds to a Bloch wave with exponential dependence e^{-iKx}. This

Bandgap condition/region	$K(\tilde{n},\omega)$	**Bloch wave**
$\mathrm{Re}(M_{11}) > 1$	$K = m\pi + iK_i$	$E_K(x)e^{-i\beta z}e^{iKx}$
$\mathrm{Re}(M_{11}) \leq -1$	$K = (m+1)\pi - iK_i$	$E_K(x)e^{-i\beta z}e^{-iKx}$

TABLE A.1: Physically allowed Bloch wavenumbers and fields for the two fundamental bandgap conditions, arising from the general condition $|\mathrm{Re}(M_{11})| > 1$, which defines the bandgap regions on the $(\tilde{n},\omega)$ plane. $K_i \in \mathbb{R}^+$. The branches of the $\cos^{-1}$ function are unique to order $m \in \mathbb{Z}$.

analysis is summarised in Table A.1. These summarised points I have derived specifically for this Thesis since they are subtle but necessary for the proper treatment of this problem; to the best of my knowledge these relations are not discussed in the literature, possibly being implicitly assumed or simply for brevity.

Therefore, for $|\mathrm{Re}(M_{11})| > 1$, the physically permitted Bloch wave is *evanescent* and decays exponentially into the structure. Waves residing in this region of the $(\tilde{n},\omega)$ plane are said to be within the structure's *bandgaps*, *i.e.*, the regions in between the banded regions in which the Bloch waves are permitted to propagate.

The *edges* of the bandgaps are thus defined by the equality $|\mathrm{Re}(M_{11})| = 1$.

It is noteworthy that, via Eqs. A.133 to A.136, the expression can be expanded for both TE and TM polarisations as:

$$\begin{aligned}
\mathrm{Re}(M_{11}) =& \frac{e^{i\phi_1}}{2}\left[\cos\phi_2 + \left(\frac{2}{T_{12}T_{21}} - 1\right) i\sin\phi_2\right] \\
&+ \frac{e^{-i\phi_1}}{2}\left[\cos\phi_2 - \left(\frac{2}{T_{12}T_{21}} - 1\right) i\sin\phi_2\right] \\
=& \frac{e^{i\phi_1} + e^{-i\phi_1}}{2}\cos\phi_2 + \left(\frac{2}{T_{12}T_{21}} - 1\right)\frac{e^{i\phi_1} - e^{-i\phi_1}}{2} i\sin\phi_2 \\
=& \cos\phi_1\cos\phi_2 - \left(\frac{2}{T_{12}T_{21}} - 1\right)\sin\phi_1\sin\phi_2 \\
\text{(by Eq. } B.15) =& \frac{1 + \left(\frac{2}{T_{12}T_{21}} - 1\right)}{2}\cos(\phi_1+\phi_2) + \frac{1 - \left(\frac{2}{T_{12}T_{21}} - 1\right)}{2}\cos(\phi_1-\phi_2) \\
=& \frac{\cos(\phi_1+\phi_2)}{T_{12}T_{21}} + \left(1 - \frac{1}{T_{12}T_{21}}\right)\cos(\phi_1-\phi_2).
\end{aligned} \tag{A.154}$$

A.4 Homogeneous Cylindrical Waveguides

The asymptotic analyses below are not trivial and are not made as explicit in the literature as they could be. I have tried to expand on the analysis here to demonstrate the particulars of the derivations made in Ref. [5].

As will be shown later, physical insight can be drawn by considering the similarities between guidance within a Bragg fiber and a simple dielectric 'tube' (a circular air hole surrounded by a uniform dielectric, see Fig. A.7). The tube was one of the first structures considered for telecommunications [5, 7]. Marcatili et al. [5] describe the theory of propagation within tube structures using the general solution to the step-index waveguide of Stratton [6] where the core refractive index n_0 can be higher or lower than the cladding index n_1. The core diameter is $t_{\text{core}} = t_0 = 2a$ (a is the core radius).

The main difference between the two cases is that the truly bound modes of the $n_0 > n_1$ case are replaced by the fundamentally leaky modes of the $n_0 < n_1$ case (like the tube). We begin by considering the most general case of arbitrary fields and work towards the case of guided waves in a step-index waveguide for both $n_0 > n_1$ and, of most interest for this work, $n_0 < n_1$ (Fig. A.7).

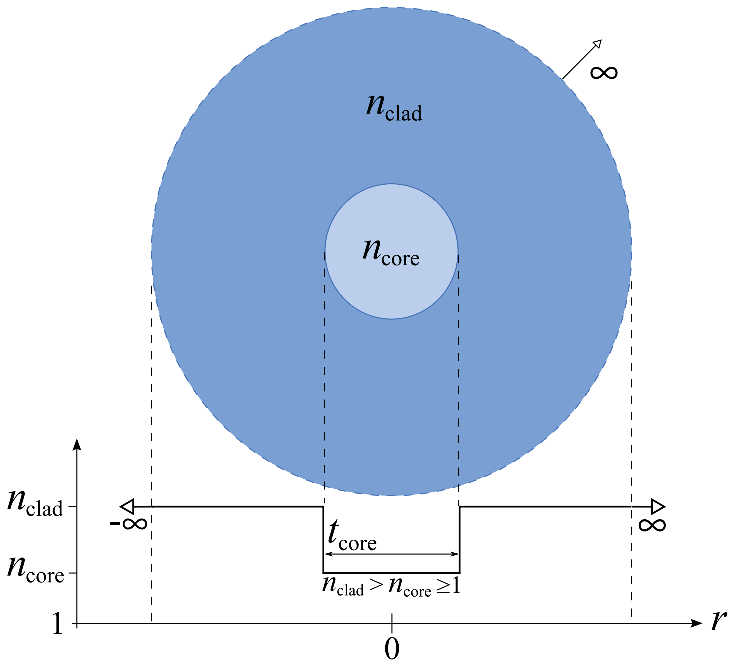

FIGURE A.7: Schematic of a cylindrical depressed-core dielectric waveguide (a tube) with infinite cladding extent. Here the notation is simplified as $n_0 = n_{\text{core}}$ and $n_1 = n_{\text{clad}}$, and $t_0 = t_{\text{core}} = 2a$ and $t_1 = t_{\text{clad}}$.

A.4.1 Arbitrary Fields from Cylindrical Wavefunctions

Any electromagnetic field within a homogeneous and isotropic domain can be represented, in cylindrical coordinates, by a linear combination of the elementary cylindrical wave functions [6]-§ 6.4:

$$\psi_{l\beta k_i} = e^{il\theta} J_l(\sqrt{k_i^2 - \beta^2} r) e^{\pm i\beta z - i\omega t}, \tag{A.155}$$

$$\psi_{l\beta k_i} = e^{il\theta} H_l^{(1)}(\sqrt{k_i^2 - \beta^2} r) e^{\pm i\beta z - i\omega t}. \tag{A.156}$$

Equation A.155 applies to propagation within spatially finite domains (including the $r = 0$ axis) since the Bessel function of the first kind $J_l(r)$ is finite at $r = 0$. For propagation in media far from such regions, though, the wavefunction must behave appropriately. The wavefunction of Eq. A.156 satisfies this since as $r \to \infty$, the spatial part reduces asymptotically to $\sqrt{\frac{2}{\pi r}} e^{-i\frac{\pi}{2}(l+\frac{1}{2})} e^{ir} e^{\pm i\beta z}$ (Eq. B.34), representing a sinusoidal wave propagating radially outward, as expected for a wave far from its source. Note that if the propagating mode has a propagation constant $\beta \in \mathbb{R}$ producing $\sqrt{k_i^2 - \beta^2} = i\mathrm{Im}\{\sqrt{k_i^2 - \beta^2}\}$, then, using the relation $K_n(z) \equiv \frac{\pi}{2} i^{n+1} H_n^{(1)}(iz)$, the cladding field becomes evanescent (exponentially decaying as $r \to \infty$), as expected for waveguides with $n_{\text{core}} > n_{\text{clad}}$ which produce such β. This behaviour explicitly demonstrates the main difference between bound- and leaky-mode guidance.

These cylindrical (scalar) wavefunctions can be used to find the values of the vectorial electric and magnetic fields. From a general consideration of the impedances of the individual field components, one can show that the field components can be expressed in terms of wavefunctions such as Eqs. A.155 and A.156 as ([6]-§ 6.6); for transverse electric (TE) components:

$$\begin{aligned} E_r &= \pm \frac{i\mu\omega}{r}\frac{\partial\psi}{\partial\theta}, & E_\theta &= \pm - i\mu\omega\frac{\partial\psi}{\partial r}, & E_z &= 0, \\ H_r &= \pm i\beta\frac{\partial\psi}{\partial r}, & H_\theta &= \pm\frac{i\beta}{r}\frac{\partial\psi}{\partial\theta}, & H_z &= \left(k_i^2 - \beta^2\right)\psi, \end{aligned}$$

and for transverse magnetic (TM) components:

$$\begin{aligned} E_r &= \pm i\beta\frac{\partial\psi}{\partial r}, & E_\theta &= \pm\frac{i\beta}{r}\frac{\partial\psi}{\partial\theta}, & E_z &= \left(k_i^2 - \beta^2\right)\psi, \\ H_r &= \pm\frac{ik_i^2}{\mu\omega}\frac{1}{r}\frac{\partial\psi}{\partial\theta}, & H_\theta &= \pm\frac{ik_i^2}{\mu\omega}\frac{\partial\psi}{\partial r}, & H_z &= 0. \end{aligned}$$

Here TE fields are defined in that the longitudinal electric field component is absent: $E_z = 0$, [6]-§ 6.1. In the same sense, transverse magnetic fields are defined by $H_z = 0$. While typically consistent, much care must be taken when interpreting the connection with the TE and TM fields of the ray picture discussed in Sections A.2.

When initial conditions are given over a plane or cylindrical surface, a solution may be constructed by a superposition of elementary wave functions such as those in Eqs. A.155 and A.156. For fixed values of k_i and β and a given set of elementary wavefunctions ψ_l, by superposing the above impedance-derived field components, an arbitrary solution would thus be:

$$\begin{aligned}
E_r &= i\beta \sum_{l=-\infty}^{\infty} a_l \frac{\partial \psi_l}{\partial r} - \frac{\mu\omega}{r} \sum_{l=-\infty}^{\infty} l b_l \psi_l, \\
E_\theta &= -\frac{\beta}{r} \sum_{l=-\infty}^{\infty} l a_l \psi_l - i\mu\omega \sum_{l=-\infty}^{\infty} b_l \frac{\partial \psi_l}{\partial r}, \\
E_z &= \left(k_i^2 - \beta^2\right) \sum_{l=-\infty}^{\infty} a_l \psi_l,
\end{aligned} \tag{A.157}$$

$$\begin{aligned}
H_r &= \frac{k_i^2}{\mu\omega} \frac{1}{r} \sum_{l=-\infty}^{\infty} l a_l \psi_l + i\beta \sum_{l=-\infty}^{\infty} b_l \frac{\partial \psi_l}{\partial r}, \\
H_\theta &= \frac{i k_i^2}{\mu\omega} \sum_{l=-\infty}^{\infty} a_l \frac{\partial \psi_l}{\partial r} - \frac{\beta}{r} \sum_{l=-\infty}^{\infty} l b_l \psi_l, \\
H_z &= \left(k_i^2 - \beta^2\right) \sum_{l=-\infty}^{\infty} b_l \psi_l,
\end{aligned} \tag{A.158}$$

where a_l and b_l are coefficients that can be determined from initial conditions.

A.4.2 Waveguidance Along a Cylinder

The general expressions above for an arbitrary field in cylindrical coordinates, Eqs. A.157 and A.158, can now be applied to the specific case of a cylindrical waveguide. No restrictions on the core or cladding material are made yet[18], except that the core has refractive index n_a and the cladding n_b. Let the core radius be a and the cladding be infinite.

Since guided waves must have finite amplitude within the guidance region, $r < a$, according to the previous section, Bessel functions of the first kind must be used (Eq. A.155). Outside of the guidance region, $r > a$, the wave fields must behave correctly at infinity. According to the previous section, Hankel functions must be used here. Indeed, the asymptotically sinusoidal behaviour of $H_l^{(1)}(r)$ (Section A.4.1 and Appendix B.4.2) as $r \to \infty$ is strictly required for the cladding fields of waveguide radiation modes [146, 178, 214], and so its requirement here is natural.

[18] Including the possibility of non-unity μ_r and complex n_i (*i.e.*, metals), although this isn't of as much interest as the dielectric case ($\mu_r = 1$, $n_i \in \mathbb{R}$) for this work.

Using this knowledge, we can now determine the forms of the fields inside and outside the cylinder. For all points $r < a$ (in the core):

$$
\begin{aligned}
E_r &= \sum_{l=-\infty}^{\infty} \left[\frac{i\beta a}{u} J_l'(ur/a) a_l - \frac{\mu_a \omega l a^2}{u^2 r} J_l(ur/a) b_l \right] F_l, \\
E_\theta &= -\sum_{l=-\infty}^{\infty} \left[\frac{l\beta a^2}{u^2 r} J_l(ur/a) a_l + \frac{i\mu_a a\omega}{u} J_l'(ur/a) b_l \right] F_l, \\
E_z &= \sum_{l=-\infty}^{\infty} \left[J_l(ur/a) a_l \right] F_l,
\end{aligned}
\tag{A.159}
$$

$$
\begin{aligned}
H_r &= -\sum_{l=-\infty}^{\infty} \left[\frac{l k_a a^2}{\mu_a \omega u^2 r} J_l(ur/a) a_l + \frac{i\beta a}{u} J_l'(ur/a) b_l \right] F_l, \\
H_\theta &= \sum_{l=-\infty}^{\infty} \left[\frac{i k_a^2 a}{\mu_a \omega u} J_l'(ur/a) a_l - \frac{l\beta a^2}{u^2 r} J_l(ur/a) b_l \right] F_l, \\
H_z &= \sum_{l=-\infty}^{\infty} \left[J_l(ur/a) b_l \right] F_l,
\end{aligned}
\tag{A.160}
$$

and for all points $r > a$ (in the cladding):

$$
\begin{aligned}
E_r &= \sum_{l=-\infty}^{\infty} \left[\frac{i\beta a}{v} H_l^{(1)\prime}(vr/a) c_l - \frac{\mu_b \omega l a^2}{v^2 r} H_l^{(1)}(vr/a) d_l \right] F_l, \\
E_\theta &= -\sum_{l=-\infty}^{\infty} \left[\frac{l\beta a^2}{v^2 r} H_l^{(1)}(vr/a) c_l + \frac{i\mu_b a\omega}{v} H_l^{(1)\prime}(vr/a) d_l \right] F_l, \\
E_z &= \sum_{l=-\infty}^{\infty} \left[H_l^{(1)}(vr/a) c_l \right] F_l,
\end{aligned}
\tag{A.161}
$$

$$
\begin{aligned}
H_r &= -\sum_{l=-\infty}^{\infty} \left[\frac{l k_a a^2}{\mu_b \omega v^2 r} H_l^{(1)}(vr/a) c_l + \frac{i\beta a}{v} H_l^{(1)\prime}(vr/a) d_l \right] F_l, \\
H_\theta &= \sum_{l=-\infty}^{\infty} \left[\frac{i k_a^2 a}{\mu_b \omega v} H_l^{(1)\prime}(vr/a) c_l - \frac{l\beta a^2}{v^2 r} H_l^{(1)}(vr/a) d_l \right] F_l, \\
H_z &= \sum_{l=-\infty}^{\infty} \left[H_l^{(1)}(vr/a) d_l \right] F_l,
\end{aligned}
\tag{A.162}
$$

where:

$$
u = a\sqrt{k^2 n_a^2 - \beta^2} = ak\sqrt{n_a^2 - \tilde{n}^2}, \tag{A.163}
$$

$$
v = a\sqrt{k^2 n_b^2 - \beta^2} = ak\sqrt{n_b^2 - \tilde{n}^2}, \tag{A.164}
$$

and the azimuthal periodicity and longitudinal and temporal oscillations are taken care of with:

$$
F_l = e^{il\theta + i\beta z - i\omega t}. \tag{A.165}
$$

The prime above the Bessel and Hankel functions implies differentiation with respect to the argument.

The coefficients a_l, b_l, c_l, and d_l are as yet undetermined. They can be related, however, by enforcing the required continuity boundary conditions at the interface; across $r = a$, the tangential components of the fields $(E_\theta, H_\theta, E_z, H_z)$ are continuous. By equating the i^{th} terms of the tangential components in Eqs. A.159 and A.160 with their counterparts in Eqs. A.161 and A.162, one finds, from the tangential components of $\mathbf{E}$:

$$\frac{l\beta}{u^2} J_l(u) a_l + \frac{i\mu_a\omega}{u} J_l'(u) b_l = \frac{l\beta}{v^2} H_l^{(1)}(v) c_l + \frac{i\mu_b\omega}{v} H_l^{(1)\prime}(v) d_l, \tag{A.166}$$

$$J_l(u) a_l = H_l^{(1)}(v) c_l, \tag{A.167}$$

and from the tangential components of $\mathbf{H}$:

$$\frac{ik_a^2}{\mu_a\omega u} J_l'(u) a_l - \frac{l\beta}{u^2} J_l(u) b_l = \frac{ik_b^2}{\mu_b\omega v} H_l^{(1)\prime}(v) c_l - \frac{l\beta}{v^2} H_l^{(1)}(v) d_l, \tag{A.168}$$

$$J_l(u) b_l = H_l^{(1)}(v) d_l. \tag{A.169}$$

Recasting as a matrix equation:

$$\begin{pmatrix} J_l(u) & 0 & -H_l^{(1)}(v) & 0 \\ 0 & J_l(u) & 0 & -H_l^{(1)}(v) \\ \frac{l\beta}{u^2} J_l(u) & \frac{i\mu_a\omega}{u} J_l'(u) & -\frac{l\beta}{v^2} H_l^{(1)}(v) & -\frac{i\mu_b\omega}{v} H_l^{(1)\prime}(v) \\ \frac{ik_a^2}{\mu_a\omega u} J_l'(u) & -\frac{l\beta}{u^2} J_l(u) & -\frac{ik_b^2}{\mu_b\omega v} H_l^{(1)\prime}(v) & \frac{l\beta}{v^2} H_l^{(1)}(v) \end{pmatrix} \begin{pmatrix} a_l \\ b_l \\ c_l \\ d_l \end{pmatrix} = A\boldsymbol{\alpha} = 0. \tag{A.170}$$

This set of equations represent a *homogeneous* system of linear equations ($A\boldsymbol{\alpha} = 0$) of the coefficients a_l, b_l, c_l, and d_l, which admits a nontrivial solution only when its determinant disappears: $\det(A) = 0$. Given this, *the propagation constant β can be determined by enforcing the condition* det(A)=0, which is independent of the value of the coefficients themselves.

Evaluating $\det(A)$ by expanding it into minors, and setting $J_l(u) \to J$ and $H_l^{(1)}(v) \to H$ for convenience, one finds:

$$
\begin{aligned}
\det(A) =& \begin{vmatrix} J & 0 & -H & 0 \\ 0 & J & 0 & -H \\ \frac{l\beta}{u^2}J & \frac{i\mu_a\omega}{u}J' & -\frac{l\beta}{v^2}H & -\frac{i\mu_b\omega}{v}H' \\ \frac{ik_a^2}{\mu_a\omega u}J' & -\frac{l\beta}{u^2}J & -\frac{ik_b^2}{\mu_b\omega v}H' & \frac{l\beta}{v^2}H \end{vmatrix} \\
=& J\begin{vmatrix} J & 0 & -H \\ \frac{i\mu_a\omega}{u}J' & -\frac{l\beta}{v^2}H & -\frac{i\mu_b\omega}{v}H' \\ \frac{l\beta}{u^2}J & -\frac{ik_b^2}{\mu_b\omega v}H' & \frac{l\beta}{v^2}H \end{vmatrix} - H\begin{vmatrix} 0 & J & -H \\ \frac{l\beta}{u^2}J & \frac{i\mu_a\omega}{u}J' & -\frac{i\mu_b\omega}{v}H' \\ \frac{ik_a^2}{\mu_a\omega u}J' & -\frac{l\beta}{u^2}J & \frac{l\beta}{v^2}H \end{vmatrix} \\
=& J\left\{J\begin{vmatrix} -\frac{l\beta}{v^2}H & -\frac{i\mu_b\omega}{v}H' \\ -\frac{ik_b^2}{\mu_b\omega v}H' & \frac{l\beta}{v^2}H \end{vmatrix} - H\begin{vmatrix} \frac{i\mu_a\omega}{u}J' & -\frac{l\beta}{v^2}H \\ \frac{l\beta}{u^2}J & -\frac{ik_b^2}{\mu_b\omega v}H' \end{vmatrix}\right\} \\
&- H\left\{-J\begin{vmatrix} \frac{l\beta}{u^2}J & -\frac{i\mu_b\omega}{v}H' \\ \frac{ik_a^2}{\mu_a\omega u}J' & \frac{l\beta}{v^2}H \end{vmatrix} - H\begin{vmatrix} \frac{l\beta}{u^2}J & \frac{i\mu_a\omega}{u}J' \\ \frac{ik_a^2}{\mu_a\omega u}J' & -\frac{l\beta}{u^2}J \end{vmatrix}\right\} \\
=& J^2\left[-\left(\frac{l\beta}{v^2}\right)^2 H^2 - \left(\frac{i\mu_b\omega}{v}\right)\left(\frac{ik_b^2}{\mu_b\omega v}\right)H'^2\right] \\
&- JH\left[-\left(\frac{i\mu_a\omega}{u}\right)\left(\frac{ik_b^2}{\mu_b\omega v}\right)J'H' - \left(\frac{l\beta}{u^2}\right)\left(\frac{l\beta}{v^2}\right)JH\right] \\
&+ JH\left[\left(\frac{l\beta}{u^2}\right)\left(\frac{l\beta}{v^2}\right)JH + \left(\frac{i\mu_b\omega}{v}\right)\left(\frac{ik_a^2}{\mu_a\omega u}\right)J'H'\right] \\
&+ H^2\left[-\left(\frac{l\beta}{u^2}\right)^2 J^2 - \left(\frac{i\mu_a\omega}{u}\right)\left(\frac{ik_a^2}{\mu_a\omega u}\right)J'^2\right] \\
=& J^2H^2\left[2\left(\frac{l\beta}{u^2}\right)\left(\frac{l\beta}{v^2}\right) - \left(\frac{l\beta}{u^2}\right)^2 - \left(\frac{l\beta}{v^2}\right)^2\right] \\
&+ JJ'HH'\left[\left(\frac{i\mu_\mathrm{a}\omega}{u}\right)\left(\frac{ik_\mathrm{b}^2}{\mu_\mathrm{b}\omega v}\right) + \left(\frac{i\mu_\mathrm{b}\omega}{v}\right)\left(\frac{ik_\mathrm{a}^2}{\mu_\mathrm{a}\omega u}\right)\right] \\
&- J^2H'^2\left(\frac{i\mu_\mathrm{b}\omega}{v}\right)\left(\frac{ik_\mathrm{b}^2}{\mu_\mathrm{b}\omega v}\right) \\
&- J'^2H^2\left(\frac{i\mu_\mathrm{a}\omega}{u}\right)\left(\frac{ik_\mathrm{a}^2}{\mu_\mathrm{a}\omega u}\right) \\
=& - J^2H^2l^2\beta^2(1/u^2 - 1/v^2)^2 \\
&- JJ'HH'[(\mu_\mathrm{b}/\mu_\mathrm{a})k_\mathrm{a}^2 + (\mu_\mathrm{a}/\mu_\mathrm{b})k_\mathrm{b}^2]/(uv) \\
&+ J^2H'^2(k_\mathrm{b}^2/v^2) \\
&+ J'^2H^2(k_\mathrm{a}^2/u^2).
\end{aligned} \tag{A.171}
$$

and then by enforcing $\det(A) = 0$ and dividing all by J^2H^2:

$$
\frac{J'^2}{u^2J^2}k_\mathrm{a}^2 + \frac{H'^2}{v^2H^2}k_\mathrm{b}^2 - \frac{J'H'}{uvJH}[(\mu_\mathrm{b}/\mu_\mathrm{a})k_\mathrm{a}^2 + (\mu_\mathrm{a}/\mu_\mathrm{b})k_\mathrm{b}^2] = l^2\beta^2(1/u^2 - 1/v^2)^2. \tag{A.172}
$$

Factorising this and replacing the indices and arguments of the functions, one gets:

$$\left[\frac{\mu_{\mathrm{a}}}{u}\frac{J_l'(u)}{J_l(u)} - \frac{\mu_{\mathrm{b}}}{v}\frac{H_l^{(1)'}(v)}{H_l^{(1)}(v)}\right]\left[\frac{k_{\mathrm{a}}^2}{\mu_{\mathrm{a}}u}\frac{J_l'(u)}{J_l(u)} - \frac{k_{\mathrm{b}}^2}{\mu_{\mathrm{b}}v}\frac{H_l^{(1)'}(v)}{H_l^{(1)}(v)}\right] = l^2\beta^2\left(\frac{1}{u^2}-\frac{1}{v^2}\right)^2 \quad \text{(A.173)}$$

which for purely dielectric media ($\mu_i \to 1$) becomes:

$$\left[\frac{J_l'(u)}{uJ_l(u)} + \frac{H_l^{(1)'}(v)}{vH_l^{(1)}(v)}\right]\left[n_0^2\frac{J_l'(u)}{uJ_l(u)} + n_1^2\frac{H_l^{(1)'}(v)}{vH_l^{(1)}(v)}\right] = l^2\frac{\beta^2}{k^2}\left(\frac{1}{u^2}+\frac{1}{v^2}\right)^2 \quad \text{(A.174)}$$

This is the *dispersion relation* or *characteristic equation* for the cylindrical waveguide. It can be used to determine the longitudinal phase accumulation per unit length, the propagation constant β, of an arbitrary supported mode. Since Eq. A.174 is transcendental, it must be solved numerically. Alternatively, one can enforce approximations to simplify its manipulation. Note that these days it is far more common for textbooks to cover the derivation of raised-core cylindrical waveguide where $n_0 > n_1$ (the 'step-index fibre') due to the overwhelming influence of the now indispensable silica step-index fibre used throughout modern telecommunications. Indeed, it can be shown that Eq. (A.174) reduces to the typical full-vector dispersion equation for this more familiar raised-core step index fiber when one enforces $n_a > \tilde{n} > n_b$, and noting the relation between the modified Bessel function of the second kind and the first order Hankel function $K_n(z) \equiv \frac{\pi}{2}i^{n+1}H_n^{(1)}(iz)$. A worked demonstration of this is given in Appendix B.4.1

A.4.3 Asymptotic Form of Dielectric Tube Modes

Consider now an air/vacuum-core ($n_0 = 1$), such as in Fig. 2.2. Making the reasonable assumptions [5]:

$$ka \gg |l|u_{lm}, \quad \text{(A.175)}$$

$$|(\beta/k) - 1| \ll 1, \quad \text{(A.176)}$$

the problem is simplified substantially. a is the core radius, as defined above. u_{lm} is the m^{th} zero of the Bessel function $J_{l-1}(u_{lm})$ where l and m are the azimuthal and radial quantum numbers of a given mode respectively; Table A.2 shows a selection of approximations to some low-order zeroes. Inequality (A.175) states that the wavelength of the guided light must be much smaller than the core and that only low-order modes be considered, while inequality (A.176) restricts accurate analysis to modes with β close to the air-line $\beta = k$. These assumptions are satisfied by most of the structures and modes considered here.

$l \downarrow$ $m \rightarrow$	1	2	3	4
1	2.405	5.52	8.654	11.796
2 or 0	3.832	7.016	10.173	13.324
3 or -1	5.136	8.417	11.62	14.796
4 or -2	6.380	9.761	13.015	16.223

TABLE A.2: Approximate values of low-order zeroes u_{lm} of $J_{l-1}(z)$ for $z \in \mathbb{R}$, *i.e.*, values producing $J_{l-1}(u_{lm}) = 0$. The degeneracy for values $|l| > 1$ arises from the Bessel function index symmetry property $J_{-l} = (-1)^l J_l$.

Using these assumptions, the dispersion relation can be manipulated to give the propagation constant analytically [5]:

$$\beta = \frac{2\pi}{\lambda}\left\{1 - \frac{1}{2}\left(\frac{u_{lm}\lambda}{2\pi R}\right)^2\right\} + i\left(\frac{u_{lm}}{2\pi}\right)^2 \frac{\lambda^2}{R^3}\nu_l, \tag{A.177}$$

$$\text{where} \quad \nu_l = \begin{cases} \frac{1}{\sqrt{n_1^2-1}} & \text{for TE}_{0m} \\ \frac{n_1^2}{\sqrt{n_1^2-1}} & \text{for TM}_{0m} \\ \frac{n_1^2+1}{2\sqrt{n_1^2-1}} & \text{for HE}_{lm}. \end{cases}$$

An important corollary of this is that all the mode types (TE,TM, and HE) of a given set (l, m) are degenerate in $\mathrm{Re}\{\beta\}$ under this approximation. $\mathrm{Im}\{\beta\}$, however, *is* polarization dependent. This is a result of the Brewster phenomenon mentioned in Section A.2.1.2, and for the same reasons, sees the TM mode always having a higher loss than the TE. The hybrid modes have a loss somewhere in between since their wavevectors are composed of both TE and TM components (*i.e.*, they correspond to skew rays in the plane-wave regime).

Note how modes lying close to the light-line have the lowest loss: as λ decreases, $\mathrm{Re}\{\beta\}$ approaches k_0 monotonically while $\mathrm{Im}\{\beta\}$ is proportional to λ^2 and hence decreases. From a ray picture, β approaching the light-line is equivalent to bound rays approach glancing incidence, thus confinement loss is reduced as the Fresnel reflectance is increased (Fig. A.4).

A.5 Periodic Multilayer Cylindrical Waveguides: Bragg Fibres

A.5.1 Transfer Matrix Solution of a Bragg Fibre

I will refer to the method shown here as the *cylindrical transfer matrix method* (cTMM) since it is conceptually identical to the pTMM from Section A.3.1 discussed above, except that here cylindrical waves, as discussed in Section A.4.1, are used to describe guidance within structures consisting of concentric cylindrical features (forming annular layers). As formulated here, the method is applied to the focus of this Thesis, Bragg fibres (two annular layer types), but the treatment can easily be generalised to arbitrarily many types of layers (layers of arbitrary thickness, refractive index and number). The technique shown here closely follows that of Yeh and Yariv [37] but here I have explicitly expanded many of the subtle derivation steps. It is noteworthy that the Bessel function basis treatment of [37] has been comprehensively reformulated in terms of Hankel functions[19] and analysed further by Street and de Sterke [39]. The use of the former formulation here is arbitrary.

A Bragg fibre typically consists of a central cylindrical core region of low refractive index enveloped by concentric, alternating, rings of two high-index dielectric materials. The refractive index distribution for an arbitrary number of layers is represented by:

$$n(x) = \begin{cases} n_{\text{core}}, & 0 \leq r < r_0 \\ n_1, & r_m \leq r < r_{m+1} \\ n_0, & r_{m+1} \leq r < r_{m+2}, \end{cases} \quad , \tag{A.178}$$

where $m \in \{0, 2, 4, \ldots\}$. $r_{\text{core}} \equiv r_0$ and n_{core} are the radius and refractive index of the core defect, respectively. The inner ring of a Bragg fibre typically has a higher refractive index than the second, such that $n_1 > n_0$. By definition, *the core has refractive index equal to or lower than the cladding layers'*: $n_{\text{core}} \leq n_0$.

[19]Since the first and second order Hankel functions naturally form a complete set; they are complex superpositions of J_l and Y_l, as per Section B.4.2.

More specifically, for N layers, one has the distribution:

$$n(x) = \begin{cases} n_{\text{core}}, & 0 \leq r < r_0 \\ n_1, & r_0 \leq r < r_1 \\ n_0, & r_1 \leq r < r_2 \\ n_1, & r_2 \leq r < r_3 \\ \vdots & \vdots \\ n_0, & r_{N-1} \leq r < r_N \\ n_1, & r \geq r_N \end{cases}, \tag{A.179}$$

where the terminating substrate is arbitrarily high-index, simply because this is often the case of concern for this work. The precise values of the refractive indices is of little concern for the derivation of the solution here.

The treatment here is similar to that for the homogeneous cladding case of Section A.4, but where the fields in each of the layers must be considered. The pioneering approach of [37] forms the basis of the method used here. As such, the dielectric assumption won't be enforced for this section, permitting arbitrary μ_r, noting that the dielectric case is trivially derived by setting $\mu_r \to 1$ in the results.

As per Section A.1.4, this longitudinally invariant waveguide will support longitudinally and temporally harmonic fields, Eqs. A.21 and A.22:

$$\begin{aligned} \mathbf{E}(\mathbf{r}_\perp, z) =& \mathbf{E}(\mathbf{r}_\perp) e^{i(\beta z - \omega t)}, \\ \mathbf{H}(\mathbf{r}_\perp, z) =& \mathbf{H}(\mathbf{r}_\perp) e^{i(\beta z - \omega t)}. \end{aligned}$$

The waveguide theory covered in Section A.1.3 shows that, within a given homogeneous region (such as the core or a layer), the transverse components of the fields may be expressed in terms of the longitudinal components via Eqs. A.40 to A.43. The problem thus reduces to one of solving for E_z and H_z only. These longitudinal components were shown to satisfy their own wave equations, Eqs. A.44 and A.44, which are explicit cylindrical formulations of the Helmholtz equation (Eq. A.46):

$$[\nabla_\perp^2 + k^2(n^2\mu_r - \tilde{n}^2)] \begin{Bmatrix} E_z \\ H_z \end{Bmatrix} = 0.$$

General solutions to this wave equation are [37]:

$$E_z = [A_m J_l(k_{lx}r) + B_m Y_l(k_{mx}r)] \cos(l\theta + \phi_m), \tag{A.180}$$

$$H_z = [C_m J_l(k_{lx}r) + D_m Y_l(k_{mx}r)] \cos(l\theta + \psi_m), \tag{A.181}$$

where J_l and Y_l are ordinary Bessel functions of the first and second kind (Section B.4), respectively, A_m, B_m, C_m and D_m are arbitrary weighting coefficients of the Bessel functions, ϕ and ψ account for an arbitrary azimuthal phase in the fields, $l \in \mathbb{Z}$ determines the order of the solutions, and $m \in \{\text{core}, 1, 2\}$ determines the homogeneous region the local fields are in. $k_{lx} = k\sqrt{n_l^2 - \tilde{n}^2}$ has the same form as per previous sections, but where μ terms are accommodated. The fields about an arbitrary cladding interface at $r = \rho$ are taken as:

$$\{E_z, H_z\} = \begin{cases} [\{A_1, C_1\} J_l(k_{1x}r) + \{B_1, D_1\} Y_l(k_{1x}r)] \cos(l\theta + \{\psi_1, \phi_1\}) & r < \rho \\ [\{A_2, C_2\} J_l(k_{2x}r) + \{B_2, D_2\} Y_l(k_{2x}r)] \cos(l\theta + \{\psi_2, \phi_2\}) & r > \rho \end{cases}. \tag{A.182}$$

Arbitrarily, this particular example has a type 1 layer for the small r side of the interface and a type 2 layer on the other side—the opposite will hold for an adjacent interface.

These two arbitrary solutions in adjoining regions can be related by enforcing continuity boundary conditions at the $r = \rho$ interface; the field components tangential to the interface $(E_z, H_z, E_\theta, H_\theta)$ must be continuous across $r = \rho$. The Bessel function amplitudes of Eqs. A.182 can thus be related as:

$$\begin{pmatrix} A_2 \\ B_2 \\ C_2 \\ D_2 \end{pmatrix} = M_{21}(\rho) \begin{pmatrix} A_1 \\ B_1 \\ C_1 \\ D_1 \end{pmatrix} \tag{A.183}$$

M_{21} thus represents a transfer matrix, relating the field amplitudes on one side of the interface to those on the other. In this sense, this treatment is very similar to the matrix approach for determining the fields of a multilayer planar system in Section A.3.1.

The form of M_{21} is now considered.

The continuity of E_z and H_z at $r = \rho$ implies the cos terms must be equal such that:

$$\phi_1 = \phi_2 = \phi, \tag{A.184}$$

$$\psi_1 = \psi_2 = \psi. \tag{A.185}$$

With this given, equating the Bessel terms for E_z and H_z gives, respectively:

$$A_1 J_l(k_{1x}\rho) + B_1 Y_l(k_{1x}\rho) = A_2 J_l(k_{2x}\rho) + B_2 Y_l(k_{2x}\rho), \tag{A.186}$$

$$C_1 J_l(k_{1x}\rho) + D_1 Y_l(k_{1x}\rho) = C_2 J_l(k_{2x}\rho) + D_2 Y_l(k_{2x}\rho). \tag{A.187}$$

Note that $\partial/\partial(k_{1x}\rho)$ of Eq. A.187 produces:

$$k_{1x}[C_1 J_l'(k_{1x}\rho) + D_1 Y_l'(k_{1x}\rho)] = k_{2x}[C_2 J_l'(k_{2x}\rho) + D_2 Y_l'(k_{2x}\rho)], \tag{A.188}$$

where, as in previous sections, the prime indicates derivation with respect to the argument, and it is noted that for some function $F(k_{2x}\rho)$:

$$\frac{\partial F(k_{2x}\rho)}{\partial(k_{1x}\rho)} = \frac{\partial F(k_{2x}\rho)}{\partial(k_{2x}\rho)}\frac{\partial(k_{2x}\rho)}{\partial(k_{1x}\rho)} = F'(k_{2x}\rho)\frac{\partial k_{2x}}{\partial k_{1x}} = F'(k_{2x}\rho)\frac{\partial k_{2x}}{\tilde{n}}\frac{\tilde{n}}{\partial k_{1x}} = F'(k_{2x}\rho)\frac{k_{2x}}{k_{1x}}.$$

Substituting Eqs. A.182 into Eq. A.40, the continuity of E_θ implies [37]:

$$\frac{1}{k_{1x}^2}\left\{\frac{l}{\rho}[A_1 J_l(k_{1x}\rho) + B_1 Y_l(k_{1x}\rho)]\sin(l\theta+\phi)\right.$$
$$\left. + \frac{\omega\mu_1 k_{1x}}{\beta}[C_1 J_l'(k_{1x}\rho) + D_1 Y_l'(k_{1x}\rho)]\cos(l\theta+\psi)\right\} = \{\mathrm{LHS}|1\to 2\}, \tag{A.189}$$

Where the right hand side implies it has the same functional form as the left hand side (LHS) but where the index 1 is replaced by 2. Factoring out the sin and cos terms from A.189, one finds:

$$\frac{l}{\rho}\left[\frac{A_1 J_l(k_{1x}\rho) + B_1 Y_l(k_{1x}\rho)}{k_{1x}^2} - \frac{A_2 J_l(k_{2x}\rho) + B_2 Y_l(k_{2x}\rho)}{k_{2x}^2}\right]\sin(l\theta+\phi)$$
$$= \frac{\omega\mu_1 k_{1x}}{\beta}\left\{\frac{\mu_1}{k_{1x}}[C_1 J_l'(k_{1x}\rho) + D_1 Y_l'(k_{1x}\rho)] - \frac{\mu_2}{k_{2x}}[C_2 J_l'(k_{2x}\rho) + D_2 Y_l'(k_{2x}\rho)]\right]\cos(l\theta+\phi). \tag{A.190}$$

From this result, Eqs. A.186 and A.188 imply that the grouped Bessel terms can not cancel out due to the factor of $1/k_{mx}$ for the A_m and B_m unprimed coefficient terms and the μ_m/k_{mx} factor for the C_m and D_m primed coefficient terms (the trivial case of $k_{1x} = k_{2x}$ being neglected). One can thus deduce the equivalence (up to a sign) of the *sin* and cos factors since they hold all the θ dependence, producing tighter restrictions on the azimuthal phase terms:

$$\sin(l\theta+\phi) = \pm\cos(l\theta+\psi) \tag{A.191}$$

$$\Rightarrow \phi = \psi \pm \frac{\pi}{2}. \tag{A.192}$$

Incidentally, similarly to Eq. A.189, the continuity of H_z implies:

$$\frac{1}{k_{1x}^2}\left\{\frac{l}{\rho}[C_1 J_l(k_{1x}\rho) + D_1 Y_l(k_{1x}\rho)]\sin(l\theta+\psi) + \frac{\omega\epsilon_1 k_{1x}}{\beta}[A_1 J_l'(k_{1x}\rho) + B_1 Y_l'(k_{1x}\rho)]\cos(l\theta+\phi)\right\} = \{\mathrm{LHS}|1\to 2\}. \tag{A.193}$$

With the knowledge that $\phi = \psi \pm \frac{\pi}{2}$, and arbitrarily setting $\phi = 0$, the ambiguity in the $\pm$ term allows the z-components to be classified into two categories, I and II:

$$E_z = [AJ_l(k_{mx}r) + BY_l(k_{mx}r)]\begin{cases}\cos(l\theta) & \text{Category I}\\ \sin(l\theta) & \text{Category II}\end{cases}, \tag{A.194}$$

$$H_z = [CJ_l(k_{mx}r) + DY_l(k_{mx}r)]\begin{cases}\sin(l\theta) & \text{Category I}\\ \cos(l\theta) & \text{Category II}\end{cases}. \tag{A.195}$$

Since only sin or cos terms appear (and hence can be factored out and cancelled) for the continuity conditions under a specific Category, the boundary conditions Eqs. A.186, A.187, A.189 and A.193 can be re-written in simpler forms. For Category I:

$$A_1 J_l(k_{1x}\rho) + B_1 Y_l(k_{1x}\rho) = \{\mathrm{LHS}|1\to 2\} \tag{A.196}$$

$$C_1 J_l'(k_{1x}\rho) + D_1 Y_l'(k_{1x}\rho) = \{\mathrm{LHS}|1\to 2\} \tag{A.197}$$

$$\frac{1}{k_{1x}^2}\left\{\frac{l}{\rho}[A_1 J_l(k_{1x}\rho) + B_1 Y_l(k_{1x}\rho)] + \frac{\omega\mu_1 k_{1x}}{\beta}[C_1 J_l'(k_{1x}\rho) + D_1 Y_l'(k_{1x}\rho)]\right\} = \{\mathrm{LHS}|1\to 2\}, \tag{A.198}$$

$$\frac{1}{k_{1x}^2}\left\{\frac{l}{\rho}[C_1 J_l(k_{1x}\rho) + D_1 Y_l(k_{1x}\rho)] + \frac{\omega\epsilon_1 k_{1x}}{\beta}[A_1 J_l'(k_{1x}\rho) + B_1 Y_l'(k_{1x}\rho)]\right\} = \{\mathrm{LHS}|1\to 2\}. \tag{A.199}$$

Category II bears the same results but with the coefficient $l/\rho \to -l/\rho$ (due to the difference in coefficient signs between Eqs. A.189 and A.193). These relations can be written as a matrix equation:

$$M_1(\rho)\begin{pmatrix}A_1\\B_1\\C_1\\D_1\end{pmatrix} = M_2(\rho)\begin{pmatrix}A_2\\B_2\\C_2\\D_2\end{pmatrix} \tag{A.200}$$

where:

$$M_m(\rho) = \begin{pmatrix} J_l(k_{mx}\rho) & Y_l(k_{mx}\rho) & 0 & 0 \\ \frac{\omega\epsilon_m}{\beta k_{mx}} J_l'(k_{mx}\rho) & \frac{\omega\epsilon_m}{\beta k_{mx}} Y_l'(k_{mx}\rho) & \frac{l}{k_{mx}^2\rho} J_l(k_{mx}\rho) & \frac{l}{k_{mx}^2\rho} Y_l(k_{mx}\rho) \\ 0 & 0 & J_l(k_{mx}\rho) & Y_l(k_{mx}\rho) \\ \frac{l}{k_{mx}^2\rho} J_l(k_{mx}\rho) & \frac{l}{k_{mx}^2\rho} Y_l(k_{mx}\rho) & \frac{\omega\epsilon_m}{\beta k_{mx}} J_l'(k_{mx}\rho) & \frac{\omega\epsilon_m}{\beta k_{mx}} Y_l'(k_{mx}\rho) \end{pmatrix}. \quad \text{(A.201)}$$

Note the very close similarity to the boundary condition matrix equation for the homogeneous cladding cylindrical waveguide, Eq. A.170, derived in the previous section. This is to be expected since the system is almost identical, save for the existence of a multiplicity of interfaces which permit both incoming and outgoing waves in a given domain. The treatment of the two cases is slightly different here for purely historical reasons. Indeed, one would expect to recover Eq. A.170 for the case of a single interface here.

The matrix M_{21} of Eq. A.183 can thus be re-written as:

$$M_{21} = M_2(\rho)^{-1} M_1(\rho), \quad \text{(A.202)}$$

where, after significant matrix manipulation, one can show [36] the form of M_{21} is explicitly:

$$M_{21} = \frac{\pi}{2} k_{2x}\rho \begin{pmatrix} m_{11} & m_{12} & m_{13} & m_{14} \\ m_{21} & m_{22} & m_{23} & m_{24} \\ m_{31} & m_{32} & m_{33} & m_{34} \\ m_{41} & m_{42} & m_{43} & m_{44} \end{pmatrix}, \quad \text{(A.203)}$$

where [37]:

$$
\begin{aligned}
m_{11} = \;& J_l(k_{1x}\rho)Y_l'(k_{2x}\rho) - (k_{2x}n_1^2/k_{1x}n_2^2)J_l'(k_{1x}\rho)Y_l(k_{2x}\rho),\\
m_{12} = \;& Y_l(k_{1x}\rho)Y_l'(k_{2x}\rho) - (k_{2x}n_1^2/k_{1x}n_2^2)Y_l'(k_{1x}\rho)Y_l(k_{2x}\rho),\\
m_{13} = \;& (\beta l/\omega n_2^2)(1/k_{2x}\rho - 1/k_{1x}\rho)J_l(k_{1x}\rho)Y_l(k_{2x}\rho),\\
m_{14} = \;& (\beta l/\omega n_2^2)(1/k_{2x}\rho - 1/k_{1x}\rho)Y_l(k_{1x}\rho)Y_l(k_{2x}\rho),\\
m_{21} = \;& (k_{2x}n_1^2/k_{1x}n_2^2)J_l'(k_{1x}\rho)J_l(k_{2x}\rho) - J_l(k_{1x}\rho)J_l'(k_{2x}\rho),\\
m_{22} = \;& (k_{2x}n_1^2/k_{1x}n_2^2)Y_l'(k_{1x}\rho)J_l(k_{2x}\rho) - Y_l(k_{1x}\rho)J_l'(k_{2x}\rho),\\
m_{23} = \;& (\beta l/\omega n_2^2)(1/k_{1x}\rho - 1/k_{2x}\rho)J_l(k_{1x}\rho)J_l(k_{2x}\rho),\\
m_{24} = \;& (\beta l/\omega n_2^2)(1/k_{1x}\rho - 1/k_{2x}\rho)Y_l(k_{1x}\rho)J_l(k_{2x}\rho),\\
m_{31} = \;& (\beta l/\omega \mu_2)(1/k_{2x}\rho - 1/k_{1x}\rho)J_l(k_{1x}\rho)Y_l(k_{2x}\rho),\\
m_{32} = \;& (\beta l/\omega \mu_2)(1/k_{2x}\rho - 1/k_{1x}\rho)Y_l(k_{1x}\rho)Y_l(k_{2x}\rho),\\
m_{33} = \;& J_l(k_{1x}\rho)Y_l'(k_{2x}\rho) - (k_{2x}\mu_1/k_{1x}\mu_2)J_l'(k_{1x}\rho)Y_l(k_{2x}\rho),\\
m_{34} = \;& Y_l(k_{1x}\rho)Y_l'(k_{2x}\rho) - (k_{2x}\mu_1/k_{1x}\mu_2)Y_l'(k_{1x}\rho)Y_l(k_{2x}\rho),\\
m_{41} = \;& (\beta l/\omega \mu_2)(1/k_{1x}\rho - 1/k_{2x}\rho)J_l(k_{1x}\rho)J_l(k_{2x}\rho),\\
m_{42} = \;& (\beta l/\omega \mu_2)(1/k_{1x}\rho - 1/k_{2x}\rho)Y_l(k_{1x}\rho)J_l(k_{2x}\rho),\\
m_{43} = \;& (k_{2x}\mu_1/k_{1x}\mu_2)J_l'(k_{1x}\rho)J_l(k_{2x}\rho) - J_l(k_{1x}\rho)J_l'(k_{2x}\rho),\\
m_{44} = \;& (k_{2x}\mu_1/k_{1x}\mu_2)Y_l'(k_{1x}\rho)J_l(k_{2x}\rho) - Y_l(k_{1x}\rho)J_l'(k_{2x}\rho),
\end{aligned}
\tag{A.204}
$$

The characteristic equation for the waveguide can be determined by constructing a global matrix M satisfying:

$$
\begin{pmatrix} A_{N+1} \\ B_{N+1} \\ C_{N+1} \\ D_{N+1} \end{pmatrix} = M \begin{pmatrix} A_0 \\ B_0 \\ C_0 \\ D_0 \end{pmatrix}, \tag{A.205}
$$

where:

$$
M = \prod_{m=N}^{0} M_{m+1,m} \tag{A.206}
$$

Given this formulation, as for the tube waveguide and multilayer stack analyses above, one must enforce the condition that there are no incoming waves on the outermost interface [39]. Finally, one can then solve the composite system by finding the roots of the condition $\det(M) = 0$, again as for the tube case earlier. The roots, the eigenvalues of the system, are the propagation constants $\beta \in \mathbb{C}$ of the supported eigenmodes.

In practice, one must use a numerical root-finding technique to solve for these β eigenvalues. For this work, the robust numerical root-finding function *fsolve* of the commercial program Matlab was employed, from which a precision beyond the values presented in this work was obtained.

Note that one can reduce this 4×4 matrix formulation down to a 2×2 when considering only TE or TM mode solutions [39], which can increase the numerical computation efficiency significantly.

Appendix B

Mathematical Miscellany

As the literature often leaves derivations and logical steps up to the reader to make explicit, I have made an effort here to describe some fundamental mathematical concepts and results that would otherwise be difficult to derive in the context they are referenced. While the content in this Appendix cites the work of others where appropriate, it has been adapted so as to adequately fit the nomenclature and structure of this Thesis.

B.1 Differential Calculus

These vectorial calculus identities (*e.g.*, see the appendices of Ref. [146]) are indispensable for some derivations shown within:

$$\nabla \times (\nabla \times \mathbf{A}) = \nabla (\nabla \cdot \mathbf{A}) - \nabla^2 \mathbf{A}, \tag{B.1}$$

$$\nabla \times (\psi \mathbf{A}) = \psi \nabla \times \mathbf{A} + (\nabla \psi) \times \mathbf{A}, \tag{B.2}$$

for some vector field $\mathbf{A}$ and scalar field ψ.

By evaluating the curl of an arbitrary vector field $\mathbf{A} = A_r \hat{\mathbf{r}} + A_\theta \hat{\theta} + A_z \hat{\mathbf{z}}$ in cylindrical coordinates, one derives the 'rotation formula':

$$\nabla \times \mathbf{A} = \left[\frac{1}{r} \frac{\partial A_z}{\partial \theta} - \frac{\partial A_\theta}{\partial z} \right] \hat{\mathbf{r}} + \left[\frac{\partial A_r}{\partial z} - \frac{\partial A_z}{\partial r} \right] \hat{\theta} + \left[\frac{1}{r} \frac{\partial}{\partial r} (r A_\theta) - \frac{1}{r} \frac{\partial A_r}{\partial \theta} \right] \hat{\mathbf{z}}, \tag{B.3}$$

B.2 Matrix Eigenvalues

Consider the eigenvalue equation:

$$A\mathbf{x} = \lambda \mathbf{x} \tag{B.4}$$

with 2x2 matrix:

$$A = \begin{bmatrix} a & b \\ c & d \end{bmatrix}. \tag{B.5}$$

For the eigenvalue equation to have nonzero solutions, one requires $\det(A - \lambda I) = 0$ producing the characteristic equation:

$$\begin{aligned} \det(A - \lambda I) &= (a-\lambda)(d-\lambda) - bc & \text{(B.6)} \\ &= \lambda^2 - \lambda(a+d) + ad - bc & \text{(B.7)} \\ &= \lambda^2 - \lambda \mathrm{Tr}(A) + \det(A). & \text{(B.8)} \end{aligned}$$

Being a quadratic equation, it has general solutions:

$$\lambda^{\pm} = \mathrm{Tr}(A/2) \pm \sqrt{\mathrm{Tr}^2(A/2) - \det(A)}. \tag{B.9}$$

recalling that in general $\mathrm{Tr}(xA) = x\mathrm{Tr}(A)$. These solutions are only valid for a 2x2 matrix system.

The product of the two eigenvalues is:

$$\begin{aligned} \lambda^+\lambda^- &= \left[\mathrm{Tr}(A/2) + \sqrt{\mathrm{Tr}^2(A/2) - \det(A)}\right]\left[\mathrm{Tr}(A/2) - \sqrt{\mathrm{Tr}^2(A/2) - \det(A)}\right] \\ &= \mathrm{Tr}^2(A/2) - \left[\mathrm{Tr}^2(A/2) - \det(A)\right] \\ &= \det(A). & \text{(B.10)} \end{aligned}$$

A unitary matrix has unit determinant: $\det(A) = 1$. The eigenvalues of a unitary matrix are thus the inverse of one another since Eq. B.10 implies $\lambda^+\lambda^- = 1$.

B.3 Trigonometric Functions

Many derivations of ray optics relations require frequent use of trigonometric identities. Those used in this work are:

$$\begin{aligned} \sin(\alpha \pm \beta) &= \sin\alpha\cos\beta \pm \sin\beta\cos\alpha, & \text{(B.11)} \\ \cos(\alpha \pm \beta) &= \sin\alpha\cos\alpha \mp \sin\beta\cos\beta, & \text{(B.12)} \end{aligned}$$

which can be readily derived via the Euler formula: $e^{\pm i\theta} = \sin\theta \pm i\cos\theta$.

A nontrivial tan identity can be derived from these:

$$\begin{aligned}
\frac{\tan(\alpha-\beta)}{\tan(\alpha+\beta)} &= \frac{\sin(\alpha-\beta)\cos(\alpha+\beta)}{\cos(\alpha-\beta)\sin(\alpha+\beta)} \\
&= \frac{(\sin\alpha\cos\beta-\sin\beta\cos\alpha)(\cos\alpha\cos\beta-\sin\beta\sin\alpha)}{(\cos\alpha\cos\beta+\sin\beta\sin\alpha)(\sin\alpha\cos\beta+\sin\beta\cos\alpha)} \\
&= \frac{\sin\alpha\cos\alpha(\sin^2\beta+\cos^2\beta)-\sin\beta\cos\beta(\sin^2\alpha+\cos^2\alpha)}{\sin\alpha\cos\alpha(\sin^2\beta+\cos^2\beta)+\sin\beta\cos\beta(\sin^2\alpha+\cos^2\alpha)} \\
&= \frac{\sin\alpha\cos\alpha-\sin\beta\cos\beta}{\sin\alpha\cos\alpha+\sin\beta\cos\beta},
\end{aligned} \tag{B.13}$$

where $\sin^2+\cos^2=1$ has been used.

The Euler formula can be used to also find:

$$\alpha e^{i\theta}\pm\beta e^{-i\theta}=(\alpha\pm\beta)\cos\theta+(\alpha\mp\beta)i\sin\theta, \tag{B.14}$$

and

$$\alpha\cos\theta\cos\phi\pm\beta\sin\theta\sin\phi=\frac{\alpha\mp\beta}{2}\cos(\theta+\phi)+\frac{\alpha\pm\beta}{2}\cos(\theta-\phi). \tag{B.15}$$

B.4 Bessel Functions

Bessel's differential equation:

$$z^2\frac{d^2y}{dz^2}+z\frac{dy}{dz}+\left(z^2-n^2\right)y=0 \tag{B.16}$$

has solutions which are linear combinations of the *Bessel functions* of the *first* and *second* types $J_\nu(z)$ and $Y_\nu(z)$, respectively. The *modified Bessel's equation*:

$$z^2\frac{d^2y}{dz^2}+z\frac{dy}{dz}-\left(z^2+n^2\right)y=0 \tag{B.17}$$

has solutions which are linear combinations of the *modified Bessel functions* of the *first* and *second* types $I_\nu(z)$ and $K_\nu(z)$, respectively.

The properties of these functions are well known and can be found in most elementary text books on differential calculus. Here we consider properties of these functions which are nontrivial but vital to analysis within the main body of this work.

B.4.1 Reduction of General Step-Index Dispersion Equation to the Well-Known $n_{\mathbf{core}} > n_{\mathbf{clad}}$ Case

It is easily shown that Eq. (A.174) reduces to the typical full-vector dispersion equation for the more familiar raised-core step index fiber [146, 178, 179] when one enforces $n_{\text{core}} > n_{\text{eff}} \geq n_{\text{clad}}$, and noting the relation between the modified Bessel function of the second kind and the first order Hankel function [216]:

$$K_n(z) \equiv \frac{\pi}{2} i^{n+1} H_n^{(1)}(iz), \tag{B.18}$$

producing derivative:

$$K_n'(z) \equiv \frac{\pi}{2} i^{n+2} H_n^{(1)\prime}(iz), \tag{B.19}$$

and thus the ratio:

$$\frac{H_n^{(1)\prime}(iz)}{H_n^{(1)}(iz)} = -i\frac{K_n'(z)}{K_n(z)}. \tag{B.20}$$

For $n_{\text{core}} = n_1 > \tilde{n} \geq n_{\text{clad}} = n_0$, v becomes imaginary[1] as:

$$v = k\sqrt{n_{\text{clad}} - \tilde{n}} = ik\sqrt{\tilde{n} - n_{\text{clad}}}, \tag{B.21}$$

ensuring the argument is positive. Defining $W = iv$ and $U = u$ from Eqs. A.163 and A.164, the characteristic equation (Eq. A.174) becomes:

$$\left[\frac{J_l'(U)}{UJ_l(U)} - \frac{H_l^{(1)\prime}(iW)}{iWH_l^{(1)}(iW)}\right]\left[n_0^2\frac{J_l'(U)}{UJ_l(U)} - n_1^2\frac{H_l^{(1)\prime}(iW)}{iWH_l^{(1)}(iW)}\right] = l^2\frac{\beta^2}{k^2}\left(\frac{1}{U^2} - \frac{1}{(iW)^2}\right)^2. \tag{B.22}$$

Using Eq. B.20, this becomes:

$$\left[\frac{J_l'(U)}{UJ_l(U)} + \frac{K_l'(W)}{WK_l(W)}\right]\left[n_0^2\frac{J_l'(U)}{UJ_l(U)} + n_1^2\frac{K_l'(W)}{WK_l(W)}\right] = l^2\frac{\beta^2}{k^2}\left(\frac{1}{U^2} + \frac{1}{W^2}\right)^2. \tag{B.23}$$

Dividing through by n_0 and defining the so-called V-parameter as:

$$V^2 = U^2 + W^2 = ak\sqrt{n_1^2 - n_0^2}, \tag{B.24}$$

one arrives at:

$$\left[\frac{J_l'(U)}{UJ_l(U)} + \frac{K_l'(W)}{WK_l(W)}\right]\left[\frac{J_l'(U)}{UJ_l(U)} + \left(\frac{n_1}{n_0}\right)^2\frac{K_l'(W)}{WK_l(W)}\right] = \left(\frac{l\beta}{n_0 k}\right)^2\left(\frac{V}{UW}\right)^4; \tag{B.25}$$

precisely the form of the raised-core step-index fibre characteristic equation of Ref. [146].

[1] Taking the positive branch to maintain the functional form of the characteristic equation.

B.4.2 Asymptotic Form of $H_\nu^{(1)}(z)$

The first order Hankel function is typically defined as a complex linear combination of the Bessel function of the first kind $J_\nu(z)$ and the Bessel function of the second kind[2] $Y_\nu(z)$:

$$H_\nu^{(1)}(z) = J_\nu + iY_\nu(z), \tag{B.26}$$

where $z \in \mathbb{C}$ in general. Incidentally, the second order Hankel function is defined as:

$$H_\nu^{(2)}(z) = J_\nu - iY_\nu(z). \tag{B.27}$$

It is useful to determine the asymptotic form of the Hankel functions; here we are interested in $H^{(1)}(z)$ for $z \in \mathbb{R}$ as $z \to \infty$. Arfken [216] discusses Bessel functions and their asymptotic forms at length.

Following the treatment of Arfken [216][3], one considers first the modified Bessel function of the second kind $K_\nu(z)$, expressed in terms of $H_\nu^{(1)}(z)$ via Eq. B.18. $K_\nu(z)$ has an integral representation:

$$K_\nu(z) = \frac{\sqrt{\pi}}{(\nu - \frac{1}{2})!}\left(\frac{z}{2}\right)^\nu \int_1^\infty e^{-zx}\left(x^2 - 1\right)^{\nu - \frac{1}{2}} dx, \quad \text{for } \nu > -\frac{1}{2}. \tag{B.28}$$

Here only $z \in \mathbb{R}$ is of interest, but this expression holds for $\{z \in \mathbb{C} | -\frac{\pi}{2} < \arg(z) < \frac{\pi}{2}\}$. It can be shown that this integral representation of $K_\nu(z)$ satisfies the modified Bessel equation Eq. B.17 (as it should) and has the proper normalisation [216].

For large z, Eq. B.28 can be written as:

$$K_\nu(z) = \sqrt{\frac{2}{\pi z}} \frac{e^{-z}}{(\nu - \frac{1}{2})!} \int_1^\infty e^{-t} t^{\nu - \frac{1}{2}} \left(1 + \frac{t}{2z}\right)^{\nu - \frac{1}{2}} dt. \tag{B.29}$$

Using the binomial theorem [216]:

$$(x+1)^\nu = \sum_{j=0}^\infty \binom{\nu}{j} x^j. \tag{B.30}$$

to expand the integrand factor of $(1 + \frac{t}{2z})^{\nu - \frac{1}{2}}$, Eq. B.28 can be expressed as:

$$K_\nu(z) = \sqrt{\frac{2}{\pi z}} \frac{e^{-z}}{(\nu - \frac{1}{2})!} \sum_{r=0}^\infty \frac{(\nu - \frac{1}{2})!}{(\nu - r - \frac{1}{2})!} (2z)^{-r} \int_1^\infty e^{-t} t^{\nu - \frac{1}{2}} \left(1 + \frac{t}{2z}\right)^{\nu + r - \frac{1}{2}} dt. \tag{B.31}$$

[2] Often called Neumann functions and represented instead by $N_\nu(z)$

[3] Ref. [216], p. 398 and pp. 402-406

By integrating each term in the sum, Eq. B.31 produces the sought asymptotic expansion of $K_\nu(z)$:

$$K_\nu(z) = \sqrt{\frac{2}{\pi z}} e^{-z} \left[1 + \frac{4\nu^2 - 1^2}{1!8z} + \frac{(4\nu^2 - 1^2)(4\nu^2 - 3^2)}{2!(8z)^2} + \dots \right] \tag{B.32}$$

where the square and factorial symbols have not been evaluated for the terms 1^2 and $1!$ to indicate the recursive pattern for subsequent terms of the expansion.

Using this asymptotic expansion of $K_\nu(z)$ with the definition B.18, one finds the asymptotic expansion for $H_\nu^{(1)}(z)$:

$$H_\nu^{(1)}(z) = \sqrt{\frac{2}{\pi z}} e^{-i\frac{\pi}{2}(\nu+\frac{1}{2})} e^{iz} \left[1 + i\frac{4\nu^2 - 1^2}{1!8z} - \frac{(4\nu^2 - 1^2)(4\nu^2 - 3^2)}{2!(8z)^2} + \dots \right]. \tag{B.33}$$

Both Eqs. B.32 and B.33 are actually also valid for $\{z \in \mathbb{C} | -\pi < \arg(z) < \pi\}$, but again, only $z \in \mathbb{R}$ is of interest here.

Thus, due to the asymptotic nature of the series, for sufficiently large z, one can approximate the series by the truncation:

$$H_\nu^{(1)}(z) \approx \sqrt{\frac{2}{\pi z}} e^{-i\frac{\pi}{2}(\nu+\frac{1}{2})} e^{iz} \quad \text{for } z \gg \tfrac{1}{2} \left| \nu^2 - \tfrac{1}{4} \right|. \tag{B.34}$$

Bibliography

[1] B. E. A. Saleh and M. C. Teich. *Fundamentals of Photonics*. Wiley-Interscience (Wiley Series in Pure and Applied Optics), 2^{nd} edition, 2007.

[2] Jonathan C. Knight. Photonic crystal fibres. *Nature*, 424(6950):847–851, Aug. 2003.

[3] Philip St.J. Russell. Photonic-crystal fibers. *Journal of Lightwave Technology*, 24 (12):4729–4749, 2006.

[4] L. Rayleigh. On the passage of electric waves through tubes, or the vibrations of dielectric cylinders. *Philosophy Magazine*, 43:125–132, 1897.

[5] E. A. J. Marcatili and R. A. Schmeltzer. Hollow metallic and dielectric waveguides for long distance optical transmission and lasers (long distance optical transmission in hollow dielectric and metal circular waveguides, examining normal mode propagation). *Bell System Technical Journal*, 43:1783–1809, 1964.

[6] J. A. Stratton. *Electromagnetic Theory*. New York and London: McGraw-Hill, 1941.

[7] Jeff Hecht. *City of Light: the Story of Fiber Optics*. Oxford University Press, USA, 2004.

[8] Charles K. Kao. The Nobel prize in physics - Nobel Foundation, 2009.

[9] F. Benabid, P. J. Roberts, F. Couny, and P. S. Light. Light and gas confinement in hollow-core photonic crystal fibre based photonic microcells. *Journal of the European Optical Society*, 4:1–9, 2009.

[10] M Shurgalin and C Anastassiou. A new modality for minimally invasive CO_2 laser surgery: flexible hollow-core photonic bandgap fibers. *Biomedical Instrumentation and Technology*, 42(4):318–325, Jul.-Aug. 2008.

[11] OmniGuide. The BeamPath^{TM} Technology, 2008.

[12] Stanislav O Konorov, Vladimir P Mitrokhin, Andrei B Fedotov, Dmitrii A Sidorov-Biryukov, Valentin I Beloglazov, Nina B Skibina, Ernst Wintner, Michael Scalora,

and Aleksei M Zheltikov. Hollow-core photonic-crystal fibres for laser dentistry. *Physics in Medicine and Biology*, 49(7):1359–1368, 2004.

[13] Stanislav O. Konorov, Vladimir P. Mitrokhin, Andrei B. Fedotov, Dmitrii A. Sidorov-Biryukov, Valentin I. Beloglazov, Nina B. Skibina, Andrei V. Shcherbakov, Ernst Wintner, Michael Scalora, and Aleksei M. Zheltikov. Laser ablation of dental tissues with picosecond pulses of 1.06μm radiation transmitted through a hollow-core photonic-crystal fiber. *Applied Optics*, 43(11):2251–2256, 2004.

[14] Max Born and Emil Wolf. *Principles of Optics: Electromagnetic Theory of Propagation, Interference and Diffraction of Light*. Cambridge University Press, 7$^{\text{th}}$ edition, 1999.

[15] Brian Mangan, Lance Farr, Allen Langford, P. John. Roberts, David P. Williams, Francois Couny, Matthew Lawman, Matthew Mason, Sam Coupland, Randolf Flea, Hendrik Sabert, Tim A. Birks, Jonathan C. Knight, and Philip St. J. Russell. Low loss (1.7 dB/km) hollow core photonic bandgap fiber. In *Optical Fiber Communication Conference*, page PD24. Optical Society of America, 2004.

[16] P. Roberts, F. Couny, H. Sabert, B. Mangan, D. Williams, L. Farr, M. Mason, A. Tomlinson, T. Birks, J. Knight, and P. St. J. Russell. Ultimate low loss of hollow-core photonic crystal fibres. *Optics Express*, 13(1):236–244, 2005.

[17] P. Roberts, D. Williams, B. Mangan, H. Sabert, F. Couny, W. Wadsworth, T. Birks, J. Knight, and P. Russell. Realizing low loss air core photonic crystal fibers by exploiting an antiresonant core surround. *Optics Express*, 13(20): 8277–8285, 2005.

[18] http://www.nktphotonics.com. NKT Photonics, 2010.

[19] Maksim Skorobogatiy. Microstructured and photonic bandgap fibers for applications in the resonant bio- and chemical sensors. *Journal of Sensors*, 2009:1–20, 2009.

[20] Stanislav O. Konorov, Christopher J. Addison, H. Georg Schulze, Robin F. B. Turner, and Michael W. Blades. Hollow-core photonic crystal fiber-optic probes for Raman spectroscopy. *Optics Letters*, 31(12):1911–1913, 2006.

[21] S. O. Konorov, A. B. Fedotov, L. A. Melnikov, A. V. Shcherbakov, R. B. Miles, and A. M. Zheltikov. Coherent Raman protocol of biosensing with a hollow photonic-crystal fiber. *Journal of X-Ray Science and Technology*, 13(4):163–169, Jan. 2005.

[22] Stanislav O. Konorov, Andrei B. Fedotov, Aleksei M. Zheltikov, and Richard B. Miles. Phase-matched four-wave mixing and sensing of water molecules by coherent anti-Stokes Raman scattering in large-core-area hollow photonic-crystal fibers. *Journal of the Optical Society of America B*, 22(9):2049–2053, 2005.

[23] F. Benabid, J. Knight, and P. Russell. Particle levitation and guidance in hollow-core photonic crystal fiber. *Optics Express*, 10(21):1195–1203, 2002.

[24] T. G. Euser, M. K. Garbos, J. S. Y. Chen, and P. St.J. Russell. Precise balancing of viscous and radiation forces on a particle in liquid-filled photonic bandgap fiber. *Optics Letters*, 34(23):3674–3676, 2009.

[25] Runqin Liu, Qi Zhou, Yaling Yin, and Jianping Yin. Laser guiding of cold molecules in a hollow photonic bandgap fiber. *Journal of the Optical Society of America B*, 26(5):1076–1083, 2009.

[26] Dongliang Yin, Holger Schmidt, John P. Barber, Evan J. Lunt, and Aaron R. Hawkins. Optical characterization of arch-shaped ARROW waveguides with liquid cores. *Optics Express*, 13(26):10564–10570, 2005.

[27] S. Kuhn, P. Measor, E.J. Lunt, A.R. Hawkins, and H. Schmidt. Particle manipulation with integrated optofluidic traps. In *Digest of the IEEE/LEOS Summer Topical Meetings*, pages 187–188, July 2008.

[28] Holger Schmidt and Aaron Hawkins. Optofluidic waveguides: I. Concepts and implementations. *Microfluidics and Nanofluidics*, 4(1):3–16, Jan. 2008.

[29] Philip Measor, Sergei Kühn, Evan J. Lunt, Brian S. Phillips, Aaron R. Hawkins, and Holger Schmidt. Multi-mode mitigation in an optofluidic chip for particle manipulation and sensing. *Optics Express*, 17(26):24342–24348, 2009.

[30] Ofer Shapira, Ken Kuriki, Nicholas D. Orf, Ayman F. Abouraddy, Gilles Benoit, Jean F. Viens, Alejandro Rodriguez, Mihai Ibanescu, John D. Joannopoulos, Yoel Fink, and Megan M. Brewster. Surface-emitting fiber lasers. *Optics Express*, 14 (9):3929–3935, 2006.

[31] F. Couny, F. Benabid, and P. S. Light. Subwatt threshold CW Raman fiber-gas laser based on H_2-filled hollow-core photonic crystal fiber. *Physics Review Letters*, 99(14):143903, 2007.

[32] Christopher C. Gregory and James A. Harrington. High peak power CO_2 laser transmission by hollow sapphire waveguides. *Applied Optics*, 32(21):3978–3980, 1993.

[33] D. Mendlovic, E. Goldenberg, S. Ruschin, J. Dror, and N. Croitoru. Ray model for transmission of metallic-dielectric hollow bent cylindrical waveguides. *Applied Optics*, 28(4):708–712, 1989.

[34] John D. Joannopoulos, Steven G. Johnson, Joshua N. Winn, and Robert D. Meade. *Photonic Crystals: Molding the Flow of Light.* Princeton University Press, 2$^{\text{nd}}$ edition, 2008.

[35] V. N. Melekin and A. B. Manenkov. Dielectric tube as a low-loss waveguide. *Soviet Physics - Technical Physics*, 13(12):1698–1699, 1968.

[36] Pochi Yeh, Amnon Yariv, and Chi-Shain Hong. Electromagnetic propagation in periodic stratified media. I. General theory. *Journal of the Optical Society of America*, 67(4):423–437, 1977.

[37] Pochi Yeh, Amnon Yariv, and Emanuel Marom. Theory of Bragg fiber. *Journal of the Optical Society of America*, 68(9):1196–1201, 1978.

[38] N. Doran and K. Blow. Cylindrical bragg fibers: A design and feasibility study for optical communications. *Journal of Lightwave Technology*, 1(4):588–590, Dec. 1983.

[39] Arthur G. Street, I. M. Bassett, and C. Martijn de Sterke. Differential losses in Bragg fibers. *Journal of Applied Physics*, 76(2):680–688, 1994.

[40] Shangping Guo, Sacharia Albin, and Robert Rogowski. Comparative analysis of Bragg fibers. *Optics Express*, 12(1):198–207, 2004.

[41] Burak Temelkuran, Shandon D. Hart, Gilles Benoit, John D. Joannopoulos, and Yoel Fink. Wavelength-scalable hollow optical fibres with large photonic bandgaps for CO_2 laser transmission. *Nature*, 420(6916):650–653, Dec. 2002.

[42] Ken Kuriki, Ofer Shapira, Shandon Hart, Gilles Benoit, Yuka Kuriki, Jean Viens, Mehmet Bayindir, John Joannopoulos, and Yoel Fink. Hollow multilayer photonic bandgap fibers for NIR applications. *Optics Express*, 12(8):1510–1517, 2004.

[43] Guillaume Vienne, Yong Xu, Christian Jakobsen, Hans-Jurgen Deyerl, Jesper Jensen, Thorkild Sorensen, Theis Hansen, Yanyi Huang, Matthew Terrel, Reginald Lee, Niels Mortensen, Jes Broeng, Harald Simonsen, Anders Bjarklev, and Amnon Yariv. Ultra-large bandwidth hollow-core guiding in all-silica Bragg fibers with nano-supports. *Optics Express*, 12(15):3500–3508, 2004.

[44] Yoel Fink, Joshua N. Winn, Shanhui Fan, Chiping Chen, Jurgen Michel, John D. Joannopoulos, and Edwin L. Thomas. A dielectric omnidirectional reflector. *Science*, 282(5394):1679–1682, 1998.

[45] F. Brechet, J.L. Auguste, J. Marcou, P. Roy, D. Pagnoux, J.M. Blondy, G. Monnom, and B. Dussardier. Very first evidence of propagation in a modified chemical vapour deposition photonic-band-gap fibre (Bragg type). In *Digest of the Conference on Lasers and Electro-Optics Europe*, Sep. 2000.

[46] F. Brechet, P. Roy, J. Marcou, and D. Pagnoux. Single-mode propagation into depressed-core-index photonic-bandgap fibre designed for zero-dispersion propagation at short wavelengths. *Electronics Letters*, 36(6):514–515, Mar. 2000.

[47] F. Brechet, P. Leproux, P. Roy, J. Marcou, and D. Pagnoux. Analysis of bandpass filtering behaviour of single mode depressed-core-index photonic-bandgap fibre. *Electronics Letters*, 36(10):870–872, May 2000.

[48] Takashi Katagiri, Yuji Matsuura, and Mitsunobu Miyagi. Photonic bandgap fiber with a silica core and multilayer dielectric cladding. *Optics Letters*, 29(6):557–559, 2004.

[49] Takashi Katagiri, Yuji Matsuura, and Mitsunobu Miyagi. All-solid single-mode Bragg fibers for compact fiber devices. *Journal of Lightwave Technology*, 24(11): 4314–4318, 2006.

[50] Alexandre Dupuis, Ning Guo, Bertrand Gauvreau, Alireza Hassani, Elio Pone, Francis Boismenu, and Maksim Skorobogatiy. Guiding in the visible with "colorful" solid-core Bragg fibers. *Optics Letters*, 32(19):2882–2884, 2007.

[51] Elio Pone, Charles Dubois, Ning Gu, Yan Gao, Alexandre Dupuis, Francis Boismenu, Suzanne Lacroix, and Maksim Skorobogatiy. Drawing of the hollow all-polymer Bragg fibers. *Optics Express*, 14(13):5838–5852, 2006.

[52] B. Gauvreau, N. Guo, K. Schicker, K. Stoeffler, F. Boismenu, A. Ajji, R. Wingfield, C. Dubois, and M. Skorobogatiy. Color-changing and color-tunable photonic bandgap fiber textiles. *Optics Express*, 16(20):15677–15693, 2008.

[53] Henry T. Bookey, Sonali Dasgupta, Nagaraju Bezawada, Bishnu P. Pal, Alexey Sysoliatin, John E. McCarthy, Mikhail Salganskii, Vladimir Khopin, and Ajoy K. Kar. Experimental demonstration of spectral broadening in an all-silica Bragg fiber. *Optics Express*, 17(19):17130–17135, 2009.

[54] John M. Dudley, Goëry Genty, and Stéphane Coen. Supercontinuum generation in photonic crystal fiber. *Reviews of Modern Physics*, 78(4):1135–1184, Oct. 2006.

[55] K. J. Rowland, Shahraam Afshar V., A. Stolyarov, Y. Fink, and T. M. Monro. Spectral properties of liquid-core Bragg fibers. In *Conference on Lasers and Electro-Optics*, 2009.

[56] Aaron Hawkins and Holger Schmidt. Optofluidic waveguides: II. Fabrication and structures. *Microfluidics and Nanofluidics*, 4(1):17–32, Jan. 2008.

[57] D. Yin, Holger Schmidt, J. Barber, and A. Hawkins. Integrated ARROW waveguides with hollow cores. *Optics Express*, 12(12):2710–2715, 2004.

[58] Romeo Bernini, Stefania Campopiano, and Luigi Zeni. Design and analysis of an integrated antiresonant reflecting optical waveguide refractive-index sensor. *Applied Optics*, 41(1):70–73, 2002.

[59] Stefania Campopiano, Romeo Bernini, Luigi Zeni, and Pasqualina M. Sarro. Microfluidic sensor based on integrated optical hollow waveguides. *Optics Letters*, 29 (16):1894–1896, 2004.

[60] Steven M. Block. Making light work with optical tweezers. *Nature*, 360(6403): 493–495, Dec. 1992.

[61] Kristopher J. Rowland, Shahraam Afshar V., and Tanya M. Monro. Bandgaps and antiresonances in integrated-ARROWs and Bragg fibers; a simple model. *Optics Express*, 16(22):17935–17951, 2008.

[62] Alexander Argyros, Ian Bassett, Martijn van Eijkelenborg, Maryanne Large, Joseph Zagari, Nicolae A. Nicorovici, Ross McPhedran, and C. Martijn de Sterke. Ring structures in microstructured polymer optical fibres. *Optics Express*, 9(13): 813–820, 2001.

[63] Alexander Argyros. Guided modes and loss in Bragg fibres. *Optics Express*, 10 (24):1411–1417, 2002.

[64] Alexander Argyros, Ian Bassett, Martijn van Eijkelenborg, and Maryanne Large. Analysis of ring-structured Bragg fibres for single TE mode guidance. *Optics Express*, 12(12):2688–2698, 2004.

[65] A. Argyros, N. Issa, I. Bassett, and M. A. van Eijkelenborg. Microstructured optical fiber for single-polarization air guidance. *Optics Letters*, 29(1):20–22, 2004.

[66] Alexander Argyros, Martijn A. van Eijkelenborg, Maryanne C. Large, and Ian M. Bassett. Hollow-core microstructured polymer optical fiber. *Optics Letters*, 31(2): 172–174, 2006.

[67] F. M. Cox, A. Argyros, and M. C. J. Large. Liquid-filled hollow core microstructured polymer optical fiber. *Optics Express*, 14(9):4135–4140, 2006.

[68] G. Vienne, Y. Xu, C. Jakobsen, H.J. Deyerl, T.P. Hansen, B.H. Larsen, J.B. Jensen, T. Sorensen, M. Terrel, Y. Huang, R. Lee, N.A. Mortensen, J. Broeng,

H. Simonsen, A. Bjarklev, and A. Yariv. First demonstration of air-silica Bragg fiber. In *Optical Fiber Communication Conference*, volume 2, page 3, Feb. 2004.

[69] Henri Uranus and H. Hoekstra. Modelling of microstructured waveguides using a finite-element-based vectorial mode solver with transparent boundary conditions. *Optics Express*, 12(12):2795–2809, 2004.

[70] Federica Poli, Matteo Foroni, Daniele Giovanelli, Annamaria Cucinotta, Stefano Selleri, Jesper Bo Jensen, Jesper Lægsgaard, Anders Bjarklev, Guillaume Vienne, Christian Jakobsen, and Jes Broeng. Silica bridge impact on hollow-core Bragg fiber transmission properties. In *Optical Fiber Communication Conference and Exposition and The National Fiber Optic Engineers Conference*, page OML8. Optical Society of America, 2007.

[71] M. Foroni, D. Passaro, F. Poli, A. Cucinotta, S. Selleri, J. Lægsgaard, and A. Bjarklev. Confinement loss spectral behavior in hollow-core Bragg fibers. *Optics Letters*, 32(21):3164–3166, 2007.

[72] Matteo Foroni, Davide Passaro, Federica Poli, Annamaria Cucinotta, Stefano Selleri, Jesper Lægsgaard, and Anders O. Bjarklev. Guiding properties of silica/air hollow-core Bragg fibers. *Journal of Lightwave Technology*, 26(13):1877–1884, 2008.

[73] Matteo Foroni, Davide Passaro, Federica Poli, Annamaria Cucinotta, Stefano Selleri, Jesper Lægsgaard, and Anders Bjarklev. Tailoring of the transmission window in realistic hollow-core Bragg fibers. In *National Fiber Optic Engineers Conference*, page JWA7. Optical Society of America, 2008.

[74] A. A. Maradudin and A. R. McGurn. Out of plane propagation of electromagnetic waves in a two-dimensional periodic dielectric medium. *Journal of Modern Optics*, 41:275–284, 1994.

[75] T.A. Birks, P.J. Roberts, P.S.J. Russell, D.M. Atkin, and T.J. Shepherd. Full 2-D photonic bandgaps in silica/air structures. *Electronics Letters*, 31(22):1941–1943, Oct. 1995.

[76] Jonathan Hu and Curtis R. Menyuk. Leakage loss and bandgap analysis in air-core photonic bandgap fiber for nonsilica glasses. *Optics Express*, 15(2):339–349, 2007.

[77] Yong Xu and Amnon Yariv. Loss analysis of air-core photonic crystal fibers. *Optics Letters*, 28(20):1885–1887, 2003.

[78] K. Saitoh and M. Koshiba. Confinement losses in air-guiding photonic bandgap fibers. *Photonics Technology Letters*, 15(2):236–238, Feb. 2003.

[79] Phillip Russell. Photonic crystal fibers: A historical account, 2007.

[80] R. F. Cregan, B. J. Mangan, J. C. Knight, T. A. Birks, P. St. J. Russell, P. J. Roberts, and D. C. Allan. Single-mode photonic band gap guidance of light in air. *Science*, 285(5433):1537–1539, 1999.

[81] R. Amezcua-Correa, F. Gèrôme, S. G. Leon-Saval, N. G. R. Broderick, T. A. Birks, and J. C. Knight. Control of surface modes in low loss hollow-core photonic bandgap fibers. *Optics Express*, 16(2):1142–1149, 2008.

[82] J. Pottage, David Bird, T. Hedley, J. Knight, T. Birks, P. Russell, and P. Roberts. Robust photonic band gaps for hollow core guidance in PCF made from high index glass. *Optics Express*, 11(22):2854–2861, 2003.

[83] G. Pearce, J. Pottage, D. Bird, P. Roberts, J. Knight, and P. Russell. Hollow-core PCF for guidance in the mid to far infra-red. *Optics Express*, 13(18):6937–6946, 2005.

[84] T. M. Monro, Y. D. West, D. W. Hewak, N. G. R. Broderick, and D. J. Richardson. Chalcogenide holey fibres. *Electronics Letters*, 36(24):1998–2000, 2000.

[85] Julien Fatome, Coraline Fortier, Thanh Nam Nguyen, Thierry Chartier, Frederic Smektala, Khalida Messaad, Bertrand Kibler, Stephane Pitois, Gregory Gadret, Christophe Finot, Johann Troles, Frederic Desevedavy, Patrick Houizot, Gilles Renversez, Laurent Brilland, and Nicholas Traynor. Linear and nonlinear characterizations of chalcogenide photonic crystal fibers. *Journal of Lightwave Technology*, 27(11):1707–1715, 2009.

[86] T. N. Nguyen, T. Chartier, Q. Coulombier, P. Houizot, L. Brilland, F. Smektala, J. Troles, C. Fortier, J. Fatome, and M. Thual. Ultra highly nonlinear AsSe chalcogenide holey fiber for nonlinear application. In *European Conference on Optical Communication*, 2009.

[87] J. Le Person, F. Smektala, T. Chartier, L. Brilland, T. Jouan, J. Troles, and D. Bosc. Light guidance in new chalcogenide holey fibres from GeGaSbS glass. *Materials Research Bulletin*, 41(7):1303–1309, 2006.

[88] Frédéric Désévédavy, Gilles Renversez, Johann Troles, Laurent Brilland, Patrick Houizot, Quentin Coulombier, Frédéric Smektala, Nicholas Traynor, and Jean-Luc Adam. Te-As-Se glass microstructured optical fiber for the middle infrared. *Applied Optics*, 48(19):3860–3865, 2009.

[89] Tanya M. Monro and Heike Ebendorff-Heidepriem. Progress in microstructured optical fibers. *Annual Review of Materials Research*, 36(1):467–495, 2006.

[90] Heike Ebendorff-Heidepriem and Tanya M. Monro. Extrusion of complex preforms for microstructured optical fibers. *Optics Express*, 15(23):15086–15092, 2007.

[91] Quentin Coulombier, Laurent Brilland, Patrick Houizot, Thierry Chartier, Thanh Nam N'Guyen, Frédéric Smektala, Gilles Renversez, Achille Monteville, David Méchin, Thierry Pain, Hervé Orain, Jean-Christophe Sangleboeuf, and Johann Trolès. Casting method for producing low-loss chalcogenide microstructured optical fibers. *Optics Express*, 18(9):9107–9112, 2010.

[92] J. Troles, L. Brilland, F. Smektala, N. Traynor, P. Houizot, and F. Desevedavy. Chalcogenide photonic crystal fibers for near and middle infrared applications. In *International Conference on Transparent Optical Networks*, 2007.

[93] Frédéric Désévédavy, Gilles Renversez, Laurent Brilland, Patrick Houizot, Johann Troles, Quentin Coulombier, Frédéric Smektala, Nicholas Traynor, and Jean-Luc Adam. Small-core chalcogenide microstructured fibers for the infrared. *Applied Optics*, 47(32):6014–6021, 2008.

[94] M. El-Amraoui, J. Fatome, J. C. Jules, B. Kibler, G. Gadret, C. Fortier, F. Smektala, I. Skripatchev, C.F. Polacchini, Y. Messaddeq, J. Troles, L. Brilland, M. Szpulak, and G. Renversez. Strong infrared spectral broadening in low-loss As-S chalcogenide suspended core microstructured optical fibers. *Optics Express*, 18(5):4547–4556, 2010.

[95] Nader Issa, Alexander Argyros, Martijn van Eijkelenborg, and Joseph Zagari. Identifying hollow waveguide guidance in air-cored microstructured optical fibres. *Optics Express*, 11(9):996–1001, 2003.

[96] F. Luan, A. K. George, T. D. Hedley, G. J. Pearce, D. M. Bird, J. C. Knight, and P. St. J. Russell. All-solid photonic bandgap fiber. *Optics Letters*, 29(20): 2369–2371, 2004.

[97] Tadashi Murao, Kunimasa Saitoh, and Masanori Koshiba. Detailed theoretical investigation of bending properties in solid-core photonic bandgap fibers. *Optics Express*, 17(9):7615–7629, 2009.

[98] Juan Juan Hu, Guobin Ren, Ping Shum, Xia Yu, Guanghui Wang, and Chao Lu. Analytical method for band structure calculation of photonic crystal fibers filled with liquid crystal. *Optics Express*, 16(9):6668–6674, 2008.

[99] N. M. Litchinitser, A. K. Abeeluck, C. Headley, and B. J. Eggleton. Antiresonant reflecting photonic crystal optical waveguides. *Optics Letters*, 27(18):1592–1594, 2002.

[100] T. P. White, R. C. McPhedran, C. Martijn de Sterke, N. M. Litchinitser, and B. J. Eggleton. Resonance and scattering in microstructured optical fibers. *Optics Letters*, 27(22):1977–1979, 2002.

[101] Natalia M. Litchinitser, Steven C. Dunn, Brian Usner, Benjamin J. Eggleton, Thomas P. White, Ross C. McPhedran, and C. Martijn de Sterke. Resonances in microstructured optical waveguides. *Optics Express*, 11(10):1243–1251, 2003.

[102] Natalia Litchinitser, Steven Dunn, Paul Steinvurzel, Benjamin Eggleton, Thomas White, Ross McPhedran, and C. Martijn de Sterke. Application of an ARROW model for designing tunable photonic devices. *Optics Express*, 12(8):1540–1550, 2004.

[103] Jesper Lgsgaard. Gap formation and guided modes in photonic bandgap fibres with high-index rods. *Journal of Optics A: Pure and Applied Optics*, 6(8):798–804, 2004.

[104] Timothy A. Birks, Greg J. Pearce, and David M. Bird. Approximate band structure calculation for photonic bandgap fibres. *Optics Express*, 14(20):9483–9490, 2006.

[105] N. M. Litchinitser and E. Poliakov. Antiresonant guiding microstructured optical fibers for sensing applications. *Applied Physics B: Lasers and Optics*, 81(2):347–351, Jul. 2005.

[106] P. Steinvurzel, B. J. Eggleton, C. Martijn de Sterke, and M. J. Steel. Continuously tunable bandpass filtering using high-index inclusion microstructured optical fibre. *Electronics Letters*, 41(8):1–2, 2005.

[107] T. Tanggaard Alkeskjold, J. Lægsgaard, A. Bjarklev, D. Sparre Hermann, J. Broeng, J. Li, S. Gauza, and S. T. Wu. Highly tunable large-core single-mode liquid-crystal photonic bandgap fiber. *Applied Optics*, 45:2261–2264, Apr. 2006.

[108] Yiping Wang, Wei Jin, Long Jin, Xiaoling Tan, Hartmut Bartelt, Wolfgang Ecke, Klaus Moerl, Kerstin Schroeder, Ron Spittel, Reinhardt Willsch, Jens Kobelke, Manfred Rothhardt, Liye Shan, and Sven Brueckner. Optical switch based on a fluid-filled photonic crystal fiber Bragg grating. *Optics Letters*, 34(23):3683–3685, 2009.

[109] Wu Yuan, Lei Wei, Thomas Tanggaard Alkeskjold, Anders Bjarklev, and Ole Bang. Thermal tunability of photonic bandgaps in liquid crystal infiltrated microstructured polymer optical fibers. *Optics Express*, 17(22):19356–19364, 2009.

[110] B. Zou, Y. G. Liu, J. B. Du, Z. Wang, T. T. Han, J. B. Xu, Y. Li, and B. Liu. Transmission bandwidth tunability of a liquid-filled photonic bandgap fiber. *Chinese Physics Letters*, 26(4):044210, Apr. 2009.

[111] Alexander Lorenz, Rolf Schuhmann, and Heinz-Siegfried Kitzerow. Infiltrated photonic crystal fiber: experiments and liquid crystal scattering model. *Optics Express*, 18(4):3519–3530, 2010.

[112] Johannes Weirich, Jesper Laegsgaard, Lara Scolari, Lei Wei, Thomas Tanggaard Alkeskjold, and Anders Bjarklev. Biased liquid crystal infiltrated photonic bandgap fiber. *Optics Express*, 17(6):4442–4453, 2009.

[113] G. Bouwmans, L. Bigot, Y. Quiquempois, F. Lopez, L. Provino, and M. Douay. Fabrication and characterization of an all-solid 2D photonic bandgap fiber with a low-loss region ($\leq$ 20 dB/km) around 1550nm. *Optics Express*, 13(21):8452–8459, 2005.

[114] Markus A. Schmidt, Nicolai Granzow, Ning Da, Mingying Peng, Lothar Wondraczek, and Philip St. J. Russell. All-solid bandgap guiding in tellurite-filled silica photonic crystal fibers. *Optics Letters*, 34(13):1946–1948, 2009.

[115] Xiao-Hui Fang, Ming-Lie Hu, Yan-Feng Li, Lu Chai, Ching-Yue Wang, and Aleksei M. Zheltikov. Hybrid multicore photonic-crystal fiber for in-phase supermode selection. *Optics Letters*, 35(4):493–495, 2010.

[116] A. Argyros, T. Birks, S. Leon-Saval, C.M. Cordeiro, F. Luan, and P. St. J. Russell. Photonic bandgap with an index step of one percent. *Optics Express*, 13(1):309–314, 2005.

[117] A. Argyros, T. Birks, S. Leon-Saval, C. M. B. Cordeiro, and P. St. J. Russell. Guidance properties of low-contrast photonic bandgap fibres. *Optics Express*, 13 (7):2503–2511, 2005.

[118] A. Fuerbach, P. Steinvurzel, J. A. Bolger, A. Nulsen, and B. J. Eggleton. Nonlinear propagation effects in antiresonant high-index inclusion photonic crystal fibers. *Optics Letters*, 30(8):830–832, 2005.

[119] A. Fuerbach, P. Steinvurzel, J. Bolger, and B. Eggleton. Nonlinear pulse propagation at zero dispersion wavelength in anti-resonant photonic crystal fibers. *Optics Express*, 13(8):2977–2987, 2005.

[120] P. Steinvurzel, C. Martijn de Sterke, M. J. Steel, B. T. Kuhlmey, and B. J. Eggleton. Single scatterer Fano resonances in solid core photonic band gap fibers. *Optics Express*, 14(19):8797–8811, 2006.

[121] Gilles Renversez, Philippe Boyer, and Angelo Sagrini. Antiresonant reflecting optical waveguide microstructured fibers revisited: a new analysis based on leaky mode coupling. *Optics Express*, 14(12):5682–5687, 2006.

[122] F. Couny, F. Benabid, P. J. Roberts, M. T. Burnett, and S. A. Maier. Identification of Bloch-modes in hollow-core photonic crystal fiber cladding. *Optics Express*, 15 (2):325–338, 2007.

[123] J. A. West, J. C. Fajardo, M. T. Gallagher, K. W. Koch, N. F. Borrelli, and D. C. Allan. Demonstration of an IR-optimized air-core photonic bandgap fiber. In *European Conference on Optical Communication*, page ThA2, 2001.

[124] N. Venkataraman, MT Gallagher, CM Smith, D. Muller, JA West, KW Koch, and JC Fajardo. Low loss (13 dB/km) air core photonic band-gap fibre. In *ECOC*, volume 5, 2002.

[125] G. Bouwmans, F. Luan, Jonathan Knight, P. St. J. Russell, L. Farr, B. Mangan, and H. Sabert. Properties of a hollow-core photonic bandgap fiber at 850 nm wavelength. *Optics Express*, 11(14):1613–1620, 2003.

[126] Charlene M. Smith, Natesan Venkataraman, Michael T. Gallagher, Dirk Muller, James A. West, Nicholas F. Borrelli, Douglas C. Allan, and Karl W. Koch. Low-loss hollow-core silica/air photonic bandgap fibre. *Nature*, 424(6949):657–659, Aug. 2003.

[127] K. Saitoh, N. Mortensen, and M. Koshiba. Air-core photonic band-gap fibers: the impact of surface modes. *Optics Express*, 12(3):394–400, 2004.

[128] James West, Charlene Smith, Nicholas Borrelli, Douglas Allan, and Karl Koch. Surface modes in air-core photonic band-gap fibers. *Optics Express*, 12(8):1485–1496, 2004.

[129] Rodrigo Amezcua-Correa, N. G. Broderick, M. N. Petrovich, F. Poletti, and D. J. Richardson. Optimizing the usable bandwidth and loss through core design in realistic hollow-core photonic bandgap fibers. *Optics Express*, 14(17):7974–7985, 2006.

[130] Philip S. Light, François Couny, Ying Ying Wang, Natalie V. Wheeler, P. John Roberts, and Fetah Benabid. Double photonic bandgap hollow-core photonic crystal fiber. *Optics Express*, 17(18):16238–16243, 2009.

[131] F. Benabid, F. Couny, J. C. Knight, T. A. Birks, and P. St J. Russell. Compact, stable and efficient all-fibre gas cells using hollow-core photonic crystal fibres. *Nature*, 434(7032):488–491, Mar. 2005.

[132] Dimitre G. Ouzounov, Faisal R. Ahmad, Dirk Muller, Natesan Venkataraman, Michael T. Gallagher, Malcolm G. Thomas, John Silcox, Karl W. Koch, and Alexander L. Gaeta. Generation of megawatt optical solitons in hollow-core photonic band-gap fibers. *Science*, 301(5640):1702–1704, 2003.

[133] Amar R. Bhagwat and Alexander L. Gaeta. Nonlinear optics in hollow-core photonic bandgap fibers. *Optics Express*, 16(7):5035–5047, 2008.

[134] Saikat Ghosh, Amar R. Bhagwat, C. Kyle Renshaw, Shireen Goh, and Alexander L. Gaeta. Low-light-level optical interactions with rubidium vapor in a photonic band-gap fiber. *Physics Review A*, 97(2):023603, 2006.

[135] Saikat Ghosh, Jay E. Sharping, Dimitre G. Ouzounov, and Alexander L. Gaeta. Resonant optical interactions with molecules confined in photonic band-gap fibers. *Physics Review Letters*, 94(9):093902, 2005.

[136] F. Benabid, P. Light, F. Couny, and P. Russell. Electromagnetically-induced transparency grid in acetylene-filled hollow-core PCF. *Optics Express*, 13(15): 5694–5703, 2005.

[137] Rajesh Thapa, Kevin Knabe, Mohammed Faheem, Ahmer Naweed, Oliver L. Weaver, and Kristan L. Corwin. Saturated absorption spectroscopy of acetylene gas inside large-core photonic bandgap fiber. *Optics Letters*, 31(16):2489–2491, 2006.

[138] Jes Henningsen, Jan Hald, and Jan C. Peterson. Saturated absorption in acetylene and hydrogen cyanide in hollow-core photonic bandgap fibers. *Optics Express*, 13 (26):10475–10482, 2005.

[139] J. K. Lyngsø, B. J. Mangan, C. Jakobsen, and P. J. Roberts. 7-cell core hollow-core photonic crystal fibers with low loss in the spectral region around 2 μm. *Optics Express*, 17(26):23468–23473, 2009.

[140] M. N. Petrovich, F. Poletti, A. van Brakel, and D. J. Richardson. Robustly single mode hollow core photonic bandgap fiber. *Optics Express*, 16(6):4337–4346, 2008.

[141] F. Benabid, J. C. Knight, G. Antonopoulos, and P. St. J. Russell. Stimulated Raman scattering in hydrogen-filled hollow-core photonic crystal fiber. *Science*, 298(5592):399–402, 2002.

[142] F. Couny, F. Benabid, P. J. Roberts, P. S. Light, and M. G. Raymer. Generation and photonic guidance of multi-octave optical-frequency combs. *Science*, 318 (5853):1118–1121, 2007.

[143] F. Couny, F. Benabid, and P. S. Light. Large-pitch Kagomé-structured hollow-core photonic crystal fiber. *Optics Letters*, 31(24):3574–3576, 2006.

[144] Alexander Argyros and Jarryd Pla. Hollow-core polymer fibres with a Kagomé lattice: potential for transmission in the infrared. *Optics Express*, 15(12):7713–7719, 2007.

[145] G. J. Pearce, G. S. Wiederhecker, C. G. Poulton, S. Burger, and P. St. J. Russell. Models for guidance in kagome-structured hollow-core photonic crystal fibres. *Optics Express*, 15(20):12680–12685, 2007.

[146] A .W. Snyder and J. Love. *Optical Waveguide Theory*. Springer, 1st edition, 1983.

[147] Kristopher J. Rowland, Shahraam Afshar V., and Tanya M. Monro. Novel low-loss bandgaps in all-silica Bragg fibers. *Journal of Lightwave Technology*, 26(1):43–51, 2008.

[148] Martijn A. van Eijkelenborg, Alexander Argyros, and Sergio G. Leon-Saval. Polycarbonate hollow-core microstructured optical fiber. *Optics Letters*, 33(21):2446–2448, 2008.

[149] Frédéric Gérôme, Raphaël Jamier, Jean-Louis Auguste, Georges Humbert, and Jean-Marc Blondy. Simplified hollow-core photonic crystal fiber. *Optics Letters*, 35(8):1157–1159, 2010.

[150] J. Von Neumann and E.P. Wigner. Uber merkwrdige diskrete eigenwerte. *Zschr. Phys.*, 30:465–467, 1929.

[151] Frank H. Stillinger and David R. Herrick. Bound states in the continuum. *Physics Review A*, 11:446–454, 1975.

[152] Federico Capasso, Carlo Sirtori, Jerome Faist, Deborah L. Sivco, Sung-Nee G. Chu, and Alfred Y. Cho. Observation of an electronic bound state above a potential well. *Nature*, 358(6387):565–567, Aug. 1992.

[153] Pochi Yeh. *Optical Waves in Layered Media*. John Wiley & Sons Inc, 2005.

[154] Julia S. Skibina, Rumen Iliew, Jens Bethge, Martin Bock, Dorit Fischer, Valentin I. Beloglasov, Reiner Wedell, and Gunter Steinmeyer. A chirped photonic-crystal fibre. *Nature Photonics*, 2(11):679–683, Nov. 2008.

[155] Jens Bethge, Günter Steinmeyer, Sven Burger, Falk Lederer, and Rumen Iliew. Guiding properties of chirped photonic crystal fibers. *Journal of Lightwave Technology*, 27(11):1698–1706, 2009.

[156] S. Konorov, O. Kolevatova, A. Fedotov, E. Serebryannikov, D. Sidorov-Biryukov, J. Mikhailova, A. Naumov, V. Beloglazov, N. Skibina, L. Melnikov, A. Shcherbakov, and A. Zheltikov. Waveguide modes of electromagnetic radiation in hollow-core microstructure and photonic-crystal fibers. *Journal of Experimental and Theoretical Physics*, 96(5):857–869, May 2003.

[157] F. Couny, F. Benabid, and O. Carraz. Enhanced stimulated raman scattering in hollow core photonic crystal fiber by use of fiber Bragg grating. In *Lasers and Electro-Optics, and Quantum Electronics and Laser Science Conference*, May 2006.

[158] F. Poletti and D. J. Richardson. Hollow-core photonic bandgap fibers based on a square lattice cladding. *Optics Letters*, 32(16):2282–2284, 2007.

[159] Alexander Argyros, Sergio G. Leon-Saval, Jarryd Pla, and Andrew Docherty. Antiresonant reflection and inhibited coupling in hollow-core square lattice optical fibres. *Optics Express*, 16(8):5642–5648, 2008.

[160] F. Couny, P. J. Roberts, T. A. Birks, and F. Benabid. Square-lattice large-pitch hollow-core photonic crystal fiber. *Optics Express*, 16(25):20626–20636, 2008.

[161] G. S. Wiederhecker, C. M. B. Cordeiro, F. Couny, F. Benabid, S. A. Maier, J. C. Knight, C. H. B. Cruz, and H. L. Fragnito. Field enhancement within an optical fibre with a subwavelength air core. *Nature Photonics*, 1(2):115–118, Feb. 2007.

[162] Shaghik Atakaramians, Shahraam Afshar V., Bernd M. Fischer, Derek Abbott, and Tanya M. Monro. Porous fibers: a novel approach to low loss THz waveguides. *Optics Express*, 16(12):8845–8854, 2008.

[163] Shaghik Atakaramians, Shahraam Afshar V., Heike Ebendorff-Heidepriem, Michael Nagel, Bernd M. Fischer, Derek Abbott, and Tanya M. Monro. THz porous fibers: design, fabrication and experimental characterization. *Optics Express*, 17(16):14053–15062, 2009.

[164] Alireza Hassani, Alexandre Dupuis, and Maksim Skorobogatiy. Porous polymer fibers for low-loss terahertz guiding. *Optics Express*, 16(9):6340–6351, 2008.

[165] Alexandre Dupuis, Jean-François Allard, Denis Morris, Karen Stoeffler, Charles Dubois, and Maksim Skorobogatiy. Fabrication and THz loss measurements of porous subwavelength fibers using a directional coupler method. *Optics Express*, 17(10):8012–8028, 2009.

[166] Alexandre Dupuis, Anna Mazhorova, Frédéric Désévédavy, Mathieu Rozé, and Maksim Skorobogatiy. Spectral characterization of porous dielectric subwavelength

THz fibers fabricated using a microstructured molding technique. *Optics Express*, 18(13):13813–13828, 2010.

[167] Bora Ung and Maksim Skorobogatiy. Chalcogenide microporous fibers for linear and nonlinear applications in the mid-infrared. *Optics Express*, 18(8):8647–8659, 2010.

[168] James A. Harrington and Christopher C. Gregory. Hollow sapphire fibers for the delivery of CO_2 laser energy. *Optics Letters*, 15(10):541–543, 1990.

[169] J.Y. Zhou, D.J. Zhou, Z.Z. Huang, and Z.X. Yu. Dye laser transverse mode control using capillaries. *Optics Communications*, 74(1-2):75–78, 1989.

[170] A. Balakin, D. Kartashov, A. Kiselev, S. Skobelev, A. Stepanov, and G. Fraiman. Laser pulse amplification upon Raman backscattering in plasma produced in dielectric capillaries. *JETP Letters*, 80(1):12–16, July 2004.

[171] Steven Johnson, Mihai Ibanescu, M. Skorobogatiy, Ori Weisberg, Torkel Engeness, Marin Soljacic, Steven Jacobs, J. Joannopoulos, and Yoel Fink. Low-loss asymptotically single-mode propagation in large-core OmniGuide fibers. *Optics Express*, 9(13):748–779, 2001.

[172] Ian Bassett and Alexander Argyros. Elimination of polarization degeneracy in round waveguides. *Optics Express*, 10(23):1342–1346, 2002.

[173] M. A. Duguay, Y. Kokubun, T. L. Koch, and Loren Pfeiffer. Antiresonant reflecting optical waveguides in SiO_2-Si multilayer structures. *Applied Physics Letters*, 49 (1):13–15, 1986.

[174] J.-L. Archambault, R. J. Black, S. Lacroix, and J. Bures. Loss calculations for antiresonant waveguides. *Journal of Lightwave Technology*, 11(3):416–423, Mar. 1993.

[175] K. J. Rowland, H. Ebendorff-Heidepriem, S. Afshar V., and T. M. Monro. Extruded soft-glass hollow-core microstructured optical fibres; fabrication and light guidance properties. In *Australian Conference on Optical Fibre Technology*, 2009.

[176] Yong Xu, Amnon Yariv, James Fleming, and Shawn-Yu Lin. Asymptotic analysis of silicon based Bragg fibers. *Optics Express*, 11(9):1039–1049, 2003.

[177] Christopher J. Voyce, Alistair D. Fitt, John R. Hayes, and Tanya M. Monro. Mathematical modeling of the self-pressurizing mechanism for microstructured fiber drawing. *Journal of Lightwave Technology*, 27(7):871–878, 2009.

[178] John A. Buck. *Fundamentals of Optical Fibers.* Wiley-Interscience (Wiley Series in Pure and Applied Optics), 1995.

[179] Katsunari Okamoto. *Fundamentals of Optical Waveguides.* Academic Press, 2^{nd} edition, 2005.

[180] Yoel Fink, Daniel J. Ripin, Shanhui Fan, Chiping Chen, John D. Joannopoulos, and Edwin L. Thomas. Guiding optical light in air using an all-dielectric structure. *Journal of Lightwave Technology*, 17(11):2039–2041, Nov. 1999.

[181] C. Kittel. *Introduction to Solid State Physics.* Wiley New York, 1996.

[182] P. Viale, S. Fevrier, F. Gerome, and H. Vilard. Confinement loss computation in photonic crystal fibres using a novel perfectly matched layer design. In *Proceedings of the COMSOL Multiphysics users conference (Paris)*, 2005.

[183] J. Jin. *The Finite Element Method in Electromagnetics.* Wiley New York, 1993.

[184] P. McIsaac. Symmetry-induced modal characteristics of uniform waveguides - I: Summary of results. *IEEE Transactions on Microwave Theory and Techniques*, 23(5):421–429, May 1975.

[185] M. J. Steel, T. P. White, C. Martijn de Sterke, R. C. McPhedran, and L. C. Botten. Symmetry and degeneracy in microstructured optical fibers. *Optics Letters*, 26(8): 488–490, 2001.

[186] T. Birks, D. Bird, T. Hedley, J. Pottage, and P. Russell. Scaling laws and vector effects in bandgap-guiding fibres. *Optics Express*, 12(1):69–74, 2004.

[187] K. Saitoh and M. Koshiba. Full-vectorial imaginary-distance beam propagation method based on a finite element scheme: application to photonic crystal fibers. *IEEE Journal of Quantum Electronics*, 38(7):927–933, Jul. 2002.

[188] Federica Poli, Matteo Foroni, Annamaria Cucinotta, and Stefano Selleri. Spectral behavior of integrated antiresonant reflecting hollow-core waveguides. *Journal of Lightwave Technology*, 25(9):2599–2604, 2007.

[189] Francesco Poletti, Marco N. Petrovich, Rodrigo Amezcua-Correa, Neil G. Broderick, Tanya M. Monro, and David J. Richardson. Advances and limitations in the modeling of fabricated photonic bandgap fibers. In *Optical Fiber Communication Conference and Exposition and The National Fiber Optic Engineers Conference*, page OFC2. Optical Society of America, 2006.

[190] Guangyu Xu, Wei Zhang, Yidong Huang, and Jiangde Peng. Loss characteristics of single-HE_{11}-mode Bragg fiber. *Journal of Lightwave Technology*, 25(1):359–366, 2007.

[191] Yong Xu, Reginald K. Lee, and Amnon Yariv. Asymptotic analysis of Bragg fibers. *Optics Letters*, 25(24):1756–1758, 2000.

[192] Yong Xu, Reginald K. Lee, and Amnon Yariv. Asymptotic analysis of dielectric coaxial fibers. *Optics Letters*, 27(12):1019–1021, 2002.

[193] Rodrigo Amezcua-Correa, Neil G. Broderick, Marco N. Petrovich, Francesco Poletti, David J. Richardson, Vittoria Finazzi, and Tanya M. Monro. Realistic designs of silica hollow-core photonic bandgap fibers free of surface modes. In *Optical Fiber Communication Conference and Exposition and The National Fiber Optic Engineers Conference*, page OFC1. Optical Society of America, 2006.

[194] Toshihiko Baba and Yasuo Kokubun. High efficiency light coupling from antiresonant reflecting optical waveguide to integrated photodetector using an antireflecting layer. *Applied Optics*, 29(18):2781–2792, 1990.

[195] T. Baba and Y. Kokubun. Dispersion and radiation loss characteristics of antiresonant reflecting optical waveguides - numerical results and analytical expressions. *IEEE Journal of Quantum Electronics*, 28(7):1689–1700, July 1992.

[196] Akheelesh Abeeluck, N. Litchinitser, C. Headley, and B. Eggleton. Analysis of spectral characteristics of photonic bandgap waveguides. *Optics Express*, 10(23): 1320–1333, 2002.

[197] Dongliang Yin, John Barber, Aaron Hawkins, and Holger Schmidt. Waveguide loss optimization in hollow-core ARROW waveguides. *Optics Express*, 13(23): 9331–9336, 2005.

[198] P. K. Tien. Light waves in thin films and integrated optics. *Applied Optics*, 10 (11):2395–2413, 1971.

[199] O. S. Heavens. *Optical Properties of Thin Solid Films*. Dover Publications, 2^{nd} edition, 1991.

[200] Jonathan Knight, M. G. Welch, C. E. de Nobriga, and R. Amezcua. Correa. Controlled dispersion in photonic crystal fibres. In *Conference on Lasers and Electro-Optics/International Quantum Electronics Conference*, page CMW1. Optical Society of America, 2009.

[201] Jie Li and Kin Seng Chiang. Disappearance of modes in planar Bragg waveguides. *Optics Letters*, 32(16):2369–2371, 2007.

[202] W. J. Hsueh, S. J. Wun, and T. H. Yu. Characterization of omnidirectional bandgaps in multiple frequency ranges of one-dimensional photonic crystals. *Journal of the Optical Society of America B*, 27(5):1092–1098, 2010.

[203] Inna Nusinsky and Amos A. Hardy. Band-gap analysis of one-dimensional photonic crystals and conditions for gap closing. *Physics Review B*, 73(12):125104, Mar. 2006.

[204] Goëry Genty, Stéphane Coen, and John M. Dudley. Fiber supercontinuum sources (invited). *Journal of the Optical Society of America B*, 24(8):1771–1785, 2007.

[205] James A. Harrington. Infrared fiber optics, 2000.

[206] Bradley F. Bowden and James A. Harrington. Fabrication and characterization of chalcogenide glass for hollow Bragg fibers. *Applied Optics*, 48(16):3050–3054, 2009.

[207] Kimmo Paivasaari, Victor K. Tikhomirov, and Jari Turunen. High refractive index chalcogenide glass for photonic crystal applications. *Optics Express*, 15(5):2336–2340, 2007.

[208] Meisong Liao, Chitrarekha Chaudhari, Guanshi Qin, Xin Yan, Chihiro Kito, Takenobu Suzuki, Yasutake Ohishi, Morio Matsumoto, and Takashi Misumi. Fabrication and characterization of a chalcogenide-tellurite composite microstructure fiber with high nonlinearity. *Optics Express*, 17(24):21608–21614, 2009.

[209] J. C. Knight, T. A. Birks, P. St. J. Russell, and D. M. Atkin. All-silica single-mode optical fiber with photonic crystal cladding. *Optics Letters*, 21(19):1547–1549, 1996.

[210] Y. Zhang and ID Robertson. Analysis and design of bragg fibers using a novel confinement loss diagram approach. *Lightwave Technology, Journal of*, 28(22): 3197–3206, 2010.

[211] J. A. Stratton. *Electromagnetic Theory*. Wiley-IEEE Press, 2007.

[212] D.J. Griffiths. *Introduction to Electrodynamics*. Prentice Hall New Jersey;, 1999.

[213] Nader Issa. *Modes and Propagation in Microstructured Optical Fibres*. PhD thesis, Optical Fibre Technology Centre and School of Physics, University of Sydney, 2005.

[214] Jonathan Hu and Curtis R. Menyuk. Understanding leaky modes: slab waveguide revisited. *Advances in Optics and Photonics*, 1(1):58–106, 2009.

[215] Frederic Zolla, Gilles Renversez, Andr Nicolet, Boris Kuhlmey, Sebastien Guenneau, and Didier Felbacq. *Foundations Of Photonic Crystal Fibres*. World Scientific Publishing Company, 2005.

[216] G. Arfken. *Mathematical Methods for Physicists*. Academic Press, New York, 1966.